May 2024
Report No. 24-053

Maura Healey
Governor
Kim Driscoll
Lieutenant Governor
Monica Tibbits-Nutt
MassDOT Secretary & CEO

Smart Work Zone Control and Performance Evaluation Based on Trajectory Data

Principal Investigator (s)
Yuanchang Xie

University of Massachusetts Lowell

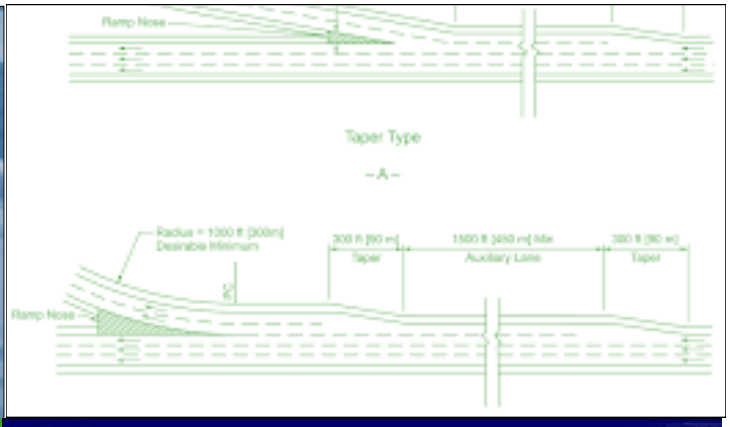

Research and Technology Transfer Section
MassDOT Office of Transportation Planning

U.S. Department of Transportation
Federal Highway Administration

[This blank, unnumbered page will be the back of your front cover]

Technical Report Document Page

1. Report No.	2. Government Accession No.	3. Recipient's Catalog No.
24-053	n/a	n/a

4. Title and Subtitle	5. Report Date
Smart Work Zone Control and Performance Evaluation Based on Trajectory Data	May 2024
	6. Performing Organization Code: n/a

7. Author(s)	8. Performing Organization Report No.
Yuanchang Xie, Zubin Bhuyan, Ruifeng Liu, and Benyuan (Ben) Liu	24-053

9. Performing Organization Name and Address	10. Work Unit No. (TRAIS)
University of Massachusetts Lowell 1 University Avenue Lowell, MA 01854	n/a
	11. Contract or Grant No.

12. Sponsoring Agency Name and Address	13. Type of Report and Period Covered
Massachusetts Department of Transportation Office of Transportation Planning 10 Park Plaza, Room 4150 Boston, MA 02116-3969	Final Report - May 2024 (March 2022- May 2024)
	14. Sponsoring Agency Code: n/a

15. Supplementary Notes
Project Champion - Corey O'Connor, MassDOT

16. Abstract

Work zone control strategies, such as taper length and transverse rumble strips, have the potential to significantly impact traffic operations and safety. The performance of these strategies is often evaluated based on traffic throughput, time headway, speed, and travel time measured at multiple locations or over a segment. Such metrics do not provide sufficient details regarding individual drivers' speed choices and lane-changing behaviors over the course of the entire work zone. To address this issue, this research utilizes ultrahigh-definition radar and thermal camera sensors to capture detailed driver behavior data. Specifically, the radar sensors provide individual vehicle speed profiles along the segment prior to a work zone, allowing us to study how drivers adjust speeds in response to various control strategies. From the thermal camera videos, last-minute lane-changing events at the beginning of lane closure taper are extracted, which are further correlated with work zone control settings. Two taper lengths, transverse rumble strips, portable changeable message sign, and flashing speed limit signs are field evaluated in this study. Both descriptive and regression analyses have been conducted. The results do not show consistent and statistically significant impacts of transverse rumble strips and taper length on approaching speed and vehicle merges. However, both flashing speed limit signs and portable changeable message signs can significantly encourage early merging and reduce approaching speed. Additionally, drivers tend to drive slower and merge later at nighttime than in daytime work zones.

17. Key Word	18. Distribution Statement
Work zone, speed, lane-changing, safety, thermal, radar, UAV, artificial intelligence, rumble strips, flashing speed limit sign, taper, changeable message sign	

19. Security Classif. (of this report)	20. Security Classif. (of this page)	21. No. of Pages	22. Price
Unclassified	Unclassified	112	n/a

Form DOT F 1700.7 (8-72) Reproduction of completed page authorized

This page left blank intentionally.

Smart Work Zone Control and Performance Evaluation Based on Trajectory Data

Final Report

Prepared By:

Yuanchang Xie, PhD, PE, Professor
Department of Civil and Environmental Engineering
University of Massachusetts Lowell

Zubin Bhuyan, Graduate Research Assistant
Ruifeng Liu, Graduate Research Assistant
Benyuan Liu, PhD, Professor
Department of Computer Science
University of Massachusetts Lowell

Prepared For:

Massachusetts Department of Transportation
Office of Transportation Planning
Ten Park Plaza, Suite 4150
Boston, MA 02116

May 2024

This page left blank intentionally.

Acknowledgments

Prepared in cooperation with the Massachusetts Department of Transportation, Office of Transportation Planning, and the United States Department of Transportation, Federal Highway Administration.

The project team would like to acknowledge Neil Boudreau, Carrie McInerney, Corey O'Connor, and Christopher Falcos for their support and guidance. We also extend our thanks to Ed Gomez, Bill Larned, and Robin Grace from the MassDOT Aeronautics Division for their drone support. Additionally, we appreciate the assistance from Northeast Traffic Control in deploying the traffic trailers for data collection.

Disclaimer

The contents of this report reflect the views of the authors, who are responsible for the facts and the accuracy of the data presented herein. The contents do not necessarily reflect the official view or policies of the Massachusetts Department of Transportation or the Federal Highway Administration. This report does not constitute a standard, specification, or regulation.

This page left blank intentionally.

Executive Summary

The number of fatalities due to work zone crashes has increased by 42% from 2013 to 2019. Also, approximately 24% of non-recurring congestion is attributed to work zones. Given the aging infrastructure in the United States and the recent $1.2 trillion infrastructure bill, it is anticipated that there will be more work zones in the coming years. How to improve work zone traffic safety and operations will become an increasingly important issue.

Many strategies can potentially affect work zone safety and traffic operations, including taper length and transverse rumble strips. The performance of these strategies is often evaluated based on traffic throughput, speed, and so forth, measured at selected locations. Such metrics do not provide sufficient detail regarding individual drivers' speed choice and lane-changing behavior over the course of the entire work zone, which are critical for understanding work zone safety and traffic operations under different traffic, control, and layout conditions.

This research aims to (1) develop artificial intelligence (AI) methods to extract vehicle trajectories from thermal videos; (2) utilize the trajectories to analyze driver behavior, particularly lane-changing behavior under different traffic conditions; (3) use the trajectories to quantify the effects of various merging taper lengths and rumble strip configurations on vehicle speed and lane-changing behavior; and (4) identify safety hazards and opportunities to improve work zone safety and operations based on the trajectory analysis results.

Specifically, this research utilizes ultrahigh-definition radar and thermal camera sensors to capture detailed driver behavior data. The radar sensors provide individual vehicle speed profiles along the segment prior to a work zone, allowing us to study how drivers adjust speeds in response to various control strategies. From the thermal camera videos, last-minute lane-changing events at the beginning of lane closure taper are extracted, which are further correlated with work zone control settings.

Two taper lengths, transverse rumble strips, portable changeable message sign, and flashing speed limit signs are field evaluated in this study. Both descriptive and regression analyses have been conducted. The results do not show consistent or statistically significant impacts of transverse rumble strips and taper length on approaching speed and vehicle merges. However, both flashing speed limit signs and portable changeable message signs can significantly encourage early merging and reduce approaching speed. Additionally, drivers tend to drive slower and merge later at nighttime than in daytime work zones.

This page left blank intentionally.

Table of Contents

List of Tables

This page left blank intentionally.

List of Figures

List of Acronyms

Acronym	Expansion
AI	Artificial Intelligence
AP	Average Precision
CAV	Connected and Autonomous Vehicles
CVAT	Computer Vision Annotation Tool
FN	False Negative
FP	False Positive
FSLS	Flashing Speed Limit Sign
IoU	Intersection over Union
MA	Massachusetts
mAP	Mean Average Precision
MassDOT	Massachusetts Department of Transportation
MGHPCC	Massachusetts Green High Performance Computing Center
NETC	New England Transportation Consortium
NH	New Hampshire
PCMS	Portable Changeable Message Signs
RGB	Red Green Blue
PAFPN	Path Aggregation Feature Pyramid Network
SHAI	Slicing-Aided Hyper Inference
SF	Slicing-Aided Fine-Tuning
SUV	Sports Utility Vehicle
TN	True Negative
TP	True Positive
UHD	Ultrahigh Definition
VIF	Variance Inflation Factor
YOLOv8	You Only Look Once version 8

This page left blank intentionally.

1.0 Introduction

The number of fatalities due to work zone crashes has increased by 42% from 2013 to 2019 [*1*]. Also, approximately 24% of non-recurring congestion is attributed to work zones [*2*]. Many control and design strategies can have significant impacts on work zone traffic operations, including taper length and rumble strips. The performance of these strategies is often evaluated based on traffic throughput, time headway, and speed (or travel time) measured at multiple locations or over a segment. Such metrics cannot fully reflect work zone safety and mobility performance. They do not provide sufficient details regarding individual drivers' speed choice and lane-changing behavior over the course of the entire work zone, which are critical for understanding the fundamental causes of work zone crashes under different traffic, control, and layout conditions.

Given the aging infrastructure in the United States and the recent $1.2 trillion infrastructure bill, it is anticipated that there will be more work zones in the next few years. How to improve work zone traffic safety and operations will become an increasingly important issue.

This study aims to do the following:

- Develop advanced computer vision technologies to extract trajectories of vehicles approaching nighttime work zones.

- Use the detailed continuous trajectory results to analyze driver behavior. Specifically, we would like to study drivers' lane-changing behaviors when approaching the lane closure taper under different traffic conditions.

- Use the detailed trajectory data to quantify the effects of various work zone control strategies and design features, including lane closure taper length (referred to as taper length for simplicity in the rest of this report) and transverse rumble strips (referred to as rumble strips in the rest of this report), on vehicle speed and lane-changing behavior.

- Use the results to identify safety hazards and opportunities to improve work zone safety and operations.

This research will demonstrate how work zone traffic operations can be evaluated by utilizing detailed vehicle trajectory data. It targets four popular control strategies affecting work zone mobility and safety: taper length, rumble strips, flashing speed limit sign, and portable changeable message sign. The findings can be used by MassDOT to improve work zone layout design, develop guidance for installing rumble strips, and enhance existing smart work zone dynamic merge control.

In addition, the developed computer vision approach is a general method for trajectory extraction, which has broad applications. For example, it can be applied to analyze and improve traffic operations at on-ramps and entrances of managed lane facilities.

This page left blank intentionally.

2.0 Data Collection

This research collected data from two highway work zones in Massachusetts. Also, data collected through another research project funded by the New England Transportation Consortium (NETC) was provided to the team and analyzed in this research. Our data collection was conducted using both ground sensors and sensors mounted on drones. Ground sensors included radar and thermal cameras, and the drone-mounted sensors consisted of RGB and thermal cameras. The rest of this section presents our data collection efforts in Massachusetts and briefly describes the NETC dataset collected in Campton, NH.

2.1 Site Selection and Control Strategies

Working with the MassDOT project champions, the team identified two work zones. The first work zone was located on I-93S in Medford, MA, and the second one was on I-95N in Danvers, MA. The exact locations are illustrated in Figure 2.1. The detailed site plans for each work zone are provided in Figure 2.2 and Figure 2.3.

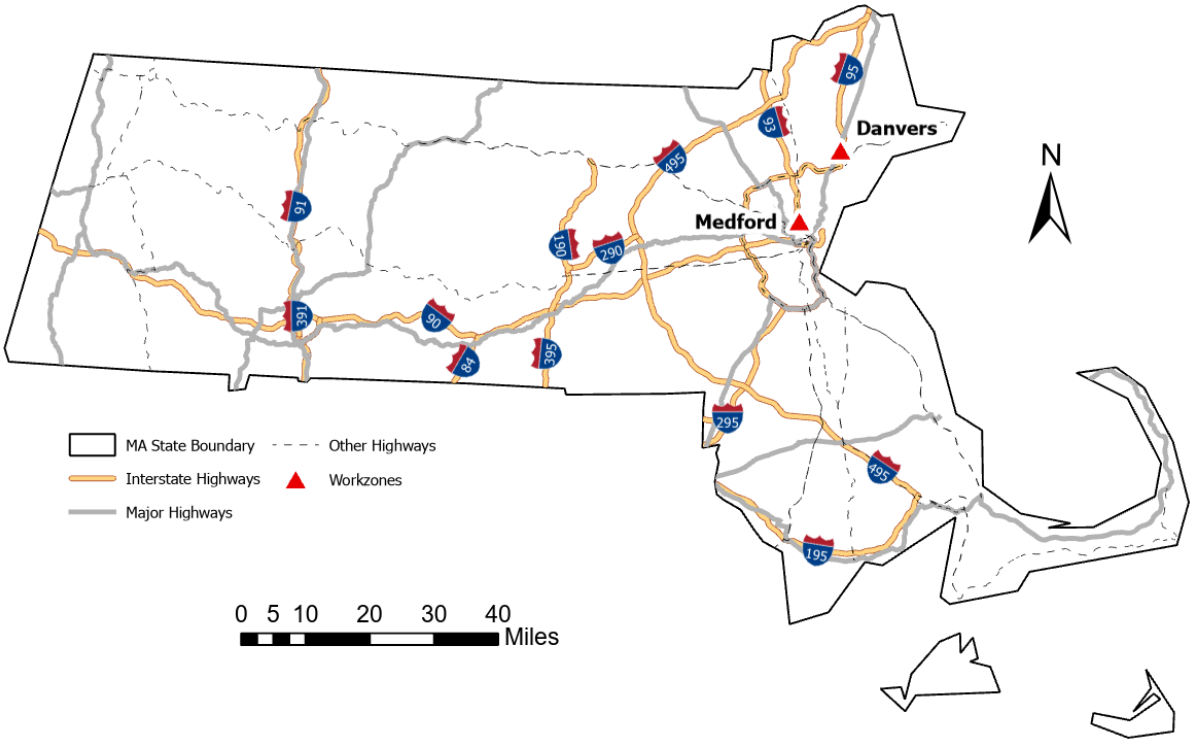

Figure 2.1. Work zone locations

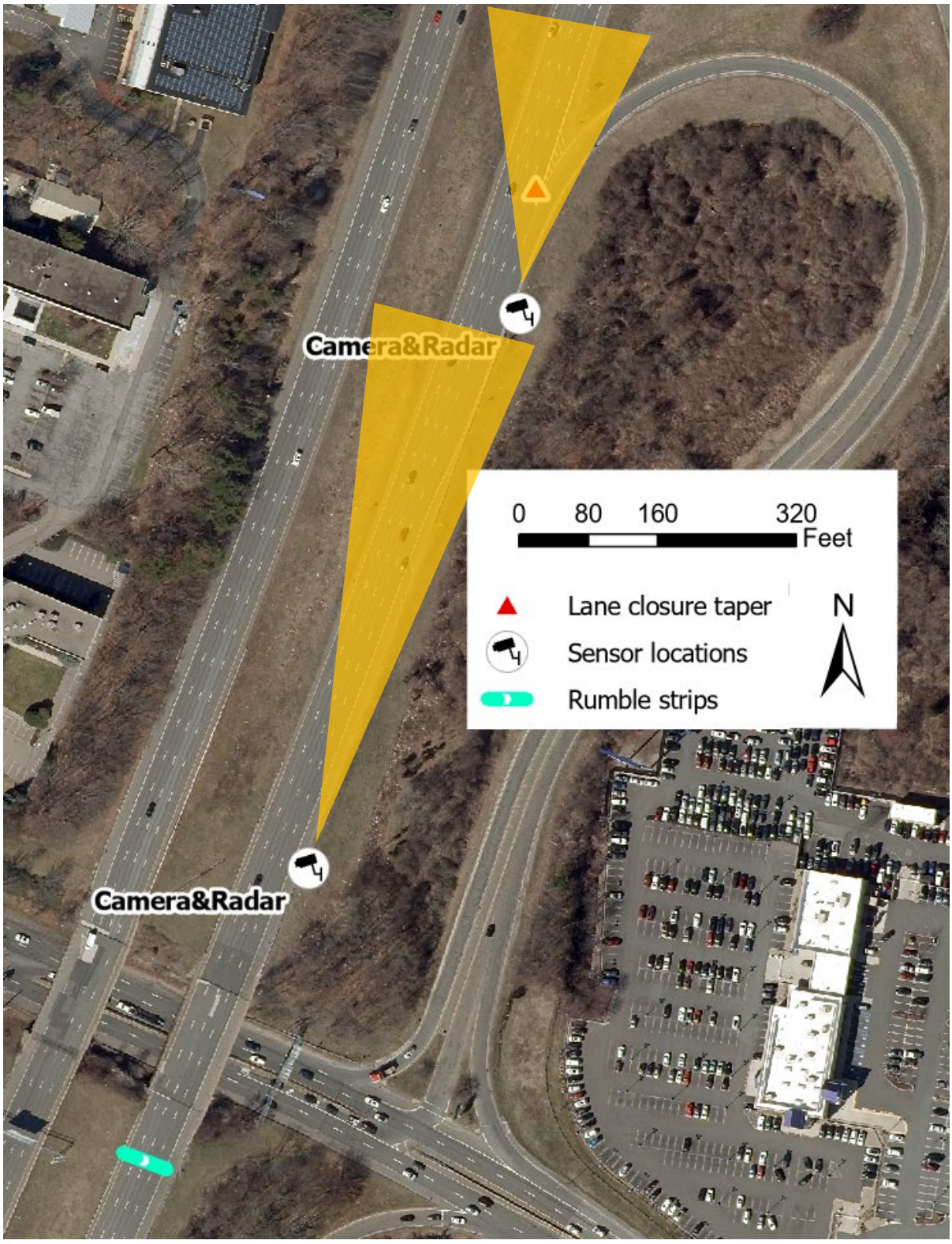

Figure 2.2. Work zone in Danvers, MA

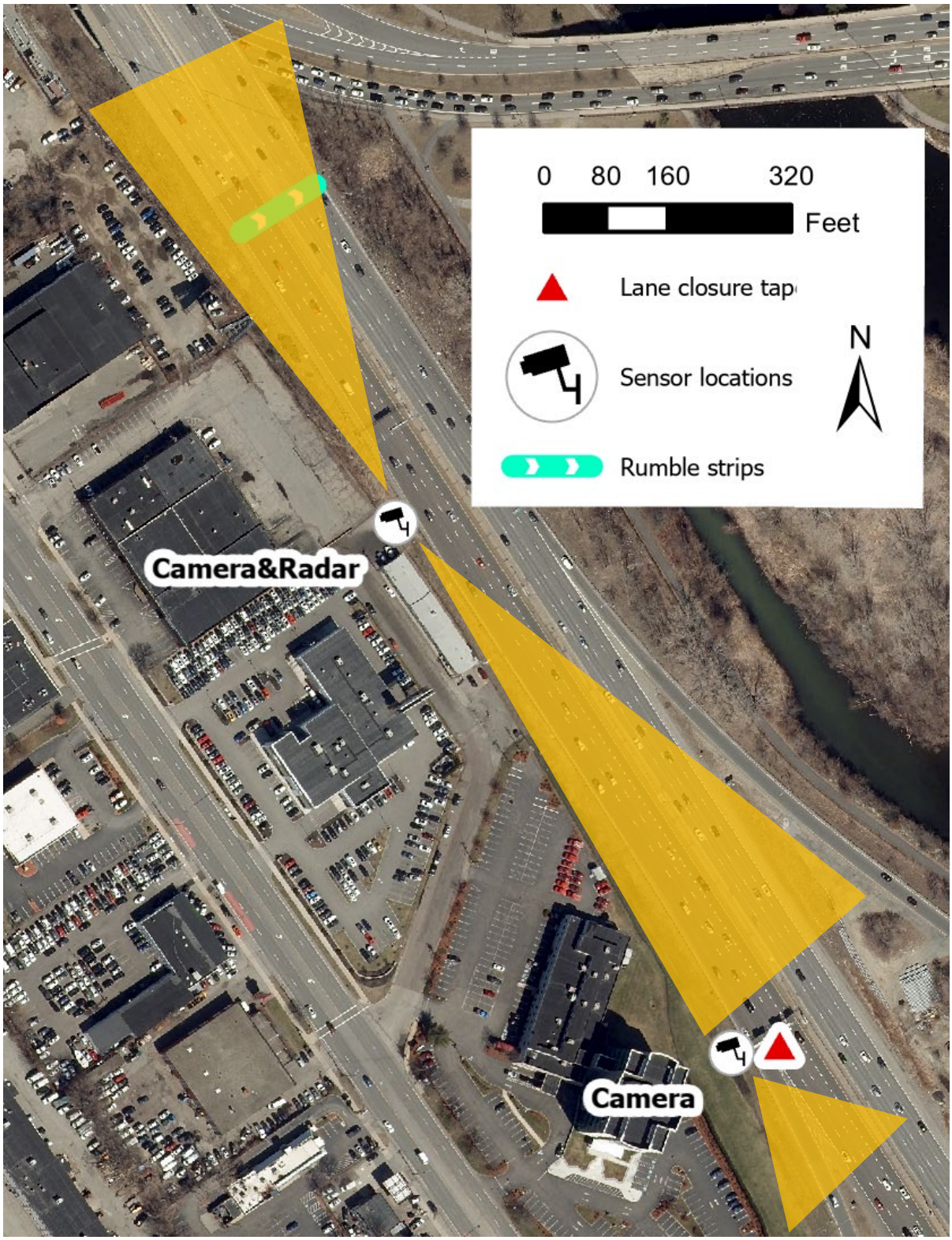

Figure 2.3. Work zone in Medford, MA

As shown in Figure 2.2 and Figure 2.3, both work zones were on a highway with four lanes in each direction. Also, the work zone lane closure taper was right next to an exit ramp. Both work zones had the right-most lane closed. A simplified view of these two work zones is illustrated in Figure 2.4, in which the circled dashed lines represent the position of the lane closure taper. Table 2.2 shows the coordinates of sensor locations and the start and end dates of those work zones. Location M1 in Figure 2.4 is not listed in Table 2.2, since data from this location was not utilized in the analysis.

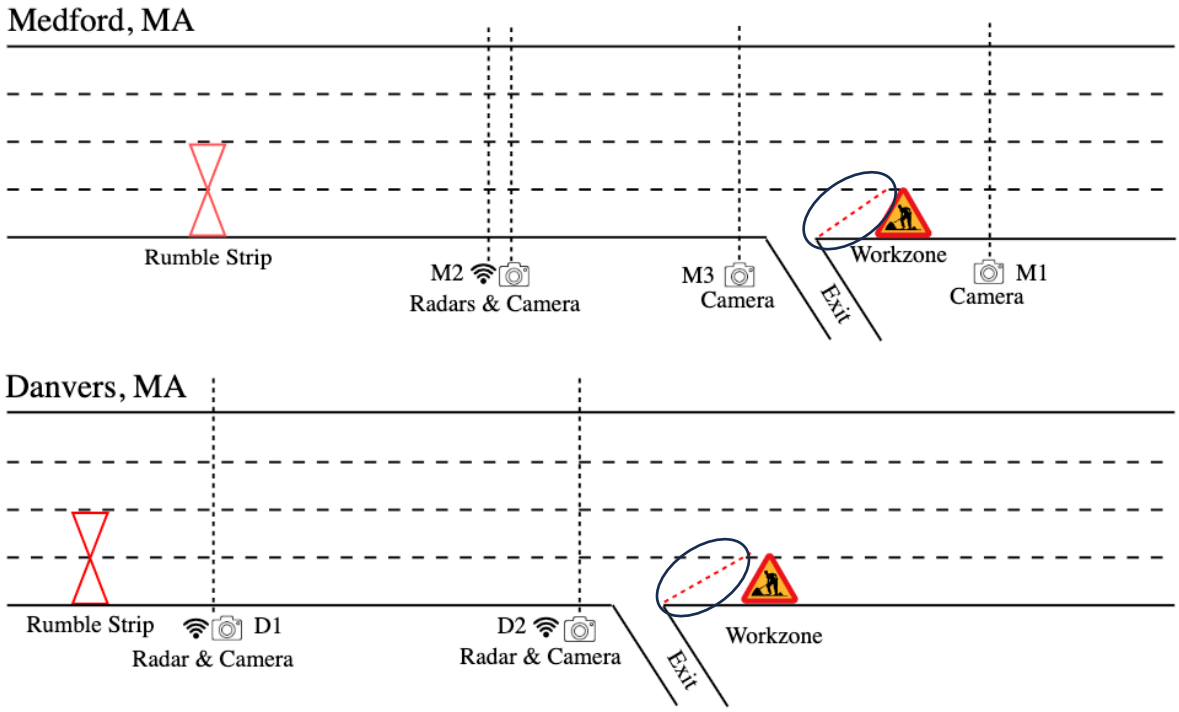

Figure 2.4. Medford and Danvers data collection sites

Table 2.1. General site information and sensor locations

Coordinate	Location Name (see definition in Figure 2.4)	Start date	End date
42.400244, −71.094581	M1	2023-05-08	2023-05-23
42.404189, −71.098262	M2	2023-05-08	2023-05-23
42.402282, −71.096515	M3	2023-05-08	2023-05-23
42.560039, −70.973476	D1	2023-05-31	2023-06-06
42.561895, −70.972527	D2	2023-05-31	2023-06-06

Transverse rumble strips and two different lane closure taper lengths were considered at the Medford and Danvers sites. The rumble strips were deployed following the requirements in the MassDOT Work Zone Safety Manual [*3*]. This manual also specifies the standard lane closure taper length (L), which is calculated as $L=WS$ for highways with a posted speed limit of ≥45 mph. W represents lane width in ft, and S is the posted speed limit measured in mph.

Therefore, the standard (normal) taper length for both Danvers and Medford was set to 780 ft (65 mph and 12 ft lane width). This study also collected speed data before the work zone started. The measured 85th percentile speed at the Danvers site was 71 mph. Given the discrepancy between the posted speed limit and the measured 85th percentile speed, this study also considered a longer taper length of 900 ft. Therefore, the following control strategy combinations were considered:

- No rumble strips and normal taper length (780 ft),
- Rumble strips and normal taper length (780 ft), and
- Rumble strips and longer taper length (900 ft).

2.2 Radar and Ground Camera Data Collection

Ultrahigh-definition (UHD) radar and thermal cameras were adopted for traffic data collection. The UHD radar sensor utilizes forward-firing technology, which is different from the widely used side-firing radar sensors. Although the side-firing radar sensors can cover multiple lanes and both travel directions, they only provide point detection results such as spot speed. The UHD radar used in this study can detect and track individual vehicles over a road segment of up to 1,000 feet. If mounted above the traffic, the radar sensor theoretically could directly differentiate vehicle trajectories by lanes to study lane-changing behavior. However, we were only able to mount the radar sensor on a trailer deployed on the roadside. Therefore, an algorithm was developed to separate data points into different lanes. The detailed speed data generated by the UHD radar allows us to study how drivers adjust their speed when approaching a highway work zone.

The thermal cameras were also mounted on roadside trailers. The resolution of the cameras is 640 × 480 pixels. Although higher-resolution thermal cameras are more desirable, they are much more expensive. The thermal cameras effectively address the challenges of nighttime data collection due to poor lighting and provide important data for understanding driver behavior during the night at highway work zones. Several key insights were learned throughout data collection for this study:

- The radar sensor should be mounted between 20 and 26 ft above the pavement.
- Ideally, both radar and camera sensors should be mounted on a stable structure (e.g., a sign gantry) directly above the traffic, although achieving this in many cases is difficult.
- Mounting radar and camera on the roadside made it challenging to separate trajectories by lane. To address this issue, an algorithm was developed to estimate the average speeds of each lane based on the radar data.
- The trailer's vibrations affected the quality of the collected video data. Algorithms were developed to correct the changes in the camera's field of view.
- The radar unit accurately detected and tracked small-sized vehicles. For heavy trucks, it sometimes generated phantom targets. This was likely caused by the radar's

mounting position. Mounting the radar directly above the traffic may well address this problem. These phantom targets were filtered out during our data processing.

To minimize the impact on traffic, work zones at the Medford and Danvers sites were mostly set up around 9 p.m. and removed before 5 a.m. Table 2.2 and Table 2.3 show the start and end times of temporary work zones at these two sites on different dates in summer 2023. Data from certain days were excluded due to major changes in traffic patterns, such as the closure of adjacent exit ramps. Data were gathered during the night at both the Medford and Danvers sites. Although there were streetlights at the Medford site, the overall light coverage of the road segments was poor, as seen in drone video footage in Figure 3.12 and Figure 8.43.

Table 2.2. Medford work zone schedule

Start date, time	End date, time	Selected?	Traffic Control
05/08/2023, 22:45	05/09/2023, 04:15	No	Rumble Strips + Normal Taper
05/09/2023, 21:00	05/10/2023, 03:00	Yes	Rumble Strips + Normal Taper
05/21/2023, 21:15	05/22/2023, 04:00	Yes	Rumble Strips + Normal Taper
05/14/2023, 22:30	05/15/2023, 03:45	Yes	No rumble strips + Normal Taper
05/15/2023, 20:15	05/16/2023, 04:15	Yes	No rumble strips + Normal Taper
05/17/2023, 21:30	05/18/2023, 03:45	No	No rumble strips + Normal Taper
05/22/2023, 21:15	05/23/2023, 03:45	Yes	Rumble strips + Longer Taper
05/23/2023, 23:45	05/24/2023, 03:30	No	Rumble strips + Longer Taper
05/24/2023, 22:45	05/25/2023, 03:45	Yes	Rumble strips + Longer Taper

Table 2.3. Danvers work zone schedule

Start date, time	End date, time	Selected?	Traffic Control
05/31/2023, 20:15	06/01/2023, 04:30	Yes	Rumble Strips + Normal Taper
06/01/2023, 20:15	06/02/2023, 04:00	Yes	No rumble Strips + Normal Taper
06/05/2023, 20:15	06/06/2023, 05:00	Yes	Rumble strips + Longer Taper
06/06/2023, 20:30	06/07/2023, 03:45	No	Rumble strips + Longer Taper

2.2.1 Ground Camera Data

Video data was collected using FLIR TrafiSense AI-632 thermal cameras, with the recorded data being stored on site. These cameras were mounted on roadside trailers and a boom lift, as shown in Figure 2.5. The average power consumption of the cameras is rated at 10.5W, with a peak of 15W.

Figure 2.5. Thermal cameras and radar systems at Medford

Table 2.4. Thermal video recording sessions at Medford

Camera Site	Phase	Start Date, Time	End Date, Time	Duration (hours)	Size (GB)
M1 Downstream	1	05/09/2023, 18:57	05/14/2023, 16:00	117	105.2
M1 Downstream	2	05/14/2023, 22:37	05/25/2023, 22:40	252	226.8
M2 Upstream	1	05/09/2023, 15:57	05/14/2023, 14:20	119	106.2
M2 Upstream	2	05/14/2023, 22:00	05/25/2023, 09:22	203	181.7
M2 Downstream	1	05/09/2023, 14:00	05/14/2023, 13:20	119	106.5
M2 Downstream	2	05/14/2023, 20:57	05/25/2023, 08:23	204	181.6
M3 Upstream	1	05/08/2023, 22:45	05/14/2023, 15:12	136	123.5
M3 Upstream	2	05/14/2023, 22:24	05/25/2023, 08:45	250	226.5
M3 Downstream	1	05/08/2023, 22:45	05/14/2023, 14:44	136	122.2
M3 Downstream	2	05/14/2023, 22:24	05/25/2023, 08:46	250	224.8

In Medford, the camera data collection started on May 9 and ended on May 25, using five cameras. Two cameras were located at Location M2 (Figure 2.4), one facing upstream (North) and one facing downstream (South). Similarly, two cameras were deployed at Location M3. Location M1 was further downstream of the lane closure taper. Due to data logger storage limitations, data collection was conducted in two phases. The retrieval of recorded videos in Phase I on May 14 was needed to accommodate the subsequent recording Phase II.

At the Danvers site, videos were recorded continuously from May 31 to June 7, 2023, employing four cameras without the need for interim data retrieval. Detailed accounts of the camera setups, recording periods, and specific configurations employed at the Danvers site are given in Table 2.5.

Table 2.5. Overview of thermal video recording sessions at the Danvers site

Camera Site	Start Date, Time	End Date, Time	Duration (hours)	Size (GB)
D1 Downstream	05/31/2023, 14:45	06/07/2023, 12:58	166	149.2
D1 Upstream	05/31/2023, 13:47	06/07/2023, 11:59	166	146.4
D2 Downstream	05/31/2023, 16:37	06/07/2023, 12:10	165	147.1
D2 Upstream	05/31/2023, 16:44	06/07/2023, 12:11	164	147.2

2.2.2 Radar Data

In Medford and Danvers, we utilized two radars at each site. Table 2.6 and Table 2.7 show the start and end time stamps of our radar installation.

Table 2.6. Overview of radar recording sessions at the Danvers site

Radar Site	Start Date, Time	End Date, Time	Duration (hours)	Size (MB)
D1 Downstream	05/31/2023, 14:40	06/01/2023, 19:54	29.2	107.90
	06/01/2023, 19:54	06/05/2023, 17:44	93.8	268.59
	06/05/2023, 18:32	06/07/2023, 12:57	42.4	121.27
D2 Downstream	05/31/2023, 16:49	06/01/2023, 19:57	27.1	113.97
	06/01/2023, 19:57	06/05/2023, 17:56	94.0	333.25
	06/05/2023, 17:56	06/07/2023, 12:12	42.3	148.87

Table 2.7. Overview of radar recording sessions at the Medford site

Radar Site	Start Date, Time	End Date, Time	Duration (hours)	Size (MB)
M2 Upstream	05/09/2023, 20:54	05/11/2023, 20:30	47.6	122.38
	05/11/2023, 20:58	05/14/2023, 16:51	67.9	184.25
	05/14/2023, 21:41	05/15/2023, 14:14	16.6	36.77
	05/15/2023, 22:46	05/16/2023, 10:40	11.9	15.72
	05/17/2023, 20:25	05/18/2023, 12:06	15.7	35.22
	05/21/2023, 20:24	05/22/2023, 20:05	23.7	65.99
	05/22/2023, 20:27	05/23/2023, 20:17	23.8	63.60
	05/24/2023, 20:31	05/25/2023, 05:33	9.0	29.08
M2 Downstream	05/09/2023, 20:53	05/10/2023, 06:27	9.6	36.50
	05/11/2023, 21:05	05/12/2023, 05:47	8.7	36.27
	05/14/2023, 21:39	05/15/2023, 06:24	8.8	31.29
	05/15/2023, 22:46	05/16/2023, 06:22	7.6	21.39
	05/17/2023, 20:25	05/18/2023, 06:35	10.2	43.77
	05/21/2023, 20:25	05/22/2023, 06:32	10.1	44.04
	05/22/2023, 20:27	05/23/2023, 06:23	9.9	40.05
	05/24/2023, 20:30	05/25/2023, 05:51	9.3	40.32

2.3 Drone Videos

Table 2.8. Aggregated drone video data recorded at Medford

Date	Flight Location	Start Time	Duration (min)	Video Type	No. of Video Clips	Size (GB)
05/08/2023	North	21:20	84	RGB	14	38.7
	Central	21:26	9	RGB	1	4.1
	South	21:35	107	RGB	14	48.9
05/09/2023	North	21:06	98	RGB	15	44.7
	South	21:02	121	RGB	15	54.3
05/15/2023	North	21:20	81	RGB + Thermal	5 + 5	11.1
	South	21:21	99	RGB	12	44.7
05/23/2023	North	21:23	90	RGB + Thermal	5 + 5	12.3
	South	21:25	100	RGB + Thermal	8 + 8	28

This research also collected videos using drones. Both RGB and thermal cameras were experimented with during the study. Drone cameras provided a much better view than ground cameras and minimized the impacts of occlusion. However, providing continuous monitoring covering multiple days is challenging. Table 2.8 and Table 2.9 summarize our drone video data collection efforts.

Table 2.9. Aggregated drone video data recorded at Danvers

Date	Flight Location	Start Time	Duration (min)	Video Type	No. of Video Clips	Uncompressed Size (GB)
05/31/2023	North	20:29	102	RGB + Thermal	8 + 8	28.7
	South	20:23	85	RGB + Thermal	5 + 5	11.7
06/01/2023	North	20:25	103	Thermal	4	4.8
	South	20:19	87	RGB + Thermal	5 + 5	12.0
06/06/2023	North	19:03	40	Thermal	2	1.86
	—	21:06	41	RGB + Thermal	4 + 4	11.6
	South	20:24	91	RGB + Thermal	6 + 6	12.6

2.4 Additional Data from Campton, NH

The team also obtained camera and radar data from another work zone in Campton, NH. This Campton dataset was collected through a study [*4*] funded by the NETC. At the Campton site, only radar and ground thermal cameras were utilized. This site was on the southbound of Interstate Highway 93 (I-93). The southbound direction had two lanes, and the left lane was closed from August 17 to August 31 in 2023.

The left lane closure taper started at mile marker 86.2. Two flashing speed limit signs (FSLS) were located at mile marker 86.4 on the two sides of the highway. The right-side FSLS coordinate was 43.845542, −71.646369, and the left-side FSLS coordinate was 43.845486, −71.646117. A portable changeable message sign (PCMS) was located in the median cross-over at mile marker 88.2, and the coordinate was 43.866556, −71.662878. The PCMS was two miles upstream of where the left lane closure taper started. The Campton site is illustrated in Figure 2.6. More details regarding this work zone can be found in the NETC study [*4*].

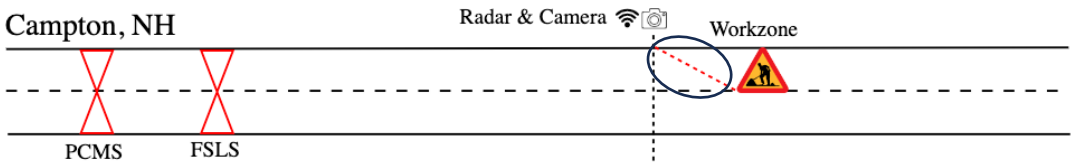

Figure 2.6. Campton data collection site

The FSLS had three different states as listed in Table 2.10, which are defined as follows:

- UP/ON: The sign was up, and its beacons were on.
- UP/OFF: The sign was up but the beacons were turned off.
- DOWN/OFF: The sign was taken down, and its beacons were also turned off.

Table 2.10. Campton traffic control schedule

Date	Flashing Speed Limit Signs (FSLS)			PCMS Message	
	UP/ON	UP/OFF	DOWN/OFF	LEFT LANE CLOSED/ MM 86.4 MERGE EARLY	POSSIBLE SLOW OR STOPPED/ TRAFFIC AHEAD BE AWARE
8/17/2023	06:00	13:30	NO	ALL DAY	NO
8/18/2023	06:00	NO	09:00	UNTIL 12:30	12:30
8/19/2023	NO	NO	ALL DAY	NO	ALL DAY
8/20/2023	NO	NO	ALL DAY	NO	ALL DAY
8/21/2023	06:00	13:30	UNTIL 06:00	13:00	UNTIL 13:00
8/22/2023	06:00	13:30	NO	ALL DAY	NO
8/23/2023	06:00	13:30	NO	ALL DAY	NO
8/24/2023	06:00	13:30	NO	ALL DAY	NO
8/25/2023	06:00	NO	13:00	UNTIL 15:00	15:00
8/26/2023	NO	NO	ALL DAY	NO	ALL DAY
8/27/2023	NO	NO	ALL DAY	NO	ALL DAY
8/28/2023	06:00	14:00	UNTIL 06:00	NO	ALL DAY
8/29/2023	06:00	13:00	NO	NO	ALL DAY
8/30/2023	06:00	13:00	NO	NO	ALL DAY
8/31/2023	06:00	17:30	NO	NO	ALL DAY

For the PCMS, there were two states represented by a variable ME. ME = 0 means each PCMS was displaying “POSSIBLE SLOW OR STOPPED” and “TRAFFIC AHEAD BE AWARE” alternately. When ME = 1, it means each PCMS was displaying “LEFT LANE CLOSED” and “MM 86.4 MERGE EARLY” alternately. At the Campton site, radar data

was collected from August 17 to August 23, 2023, while thermal video data was collected from August 17 to August 31, 2023. The radar sensor stopped working on August 23, 2023, probably due to a power supply issue.

3.0 Video Data Analysis

This section focuses on the methodologies and technologies applied to detect and track vehicles in thermal videos, starting with dataset curation and annotation, progressing to model training and validation. It details algorithm development for vehicle trajectory extraction, lane usage assessment, and detection of vehicle proximity to work zone lane closure tapers. Additionally, it discusses the analysis of drone video data, highlighting the advantages and disadvantages of using drone footage and how it can complement traditional data collection methods.

3.1 Introduction: Vehicle Detection in Thermal Videos

In contemporary transportation engineering and safety analysis, the significance of accurate vehicle detection cannot be overstated. The advent of deep learning has revolutionized the field of object detection across diverse domains. Among its numerous applications, vehicle detection and tracking has emerged as a critical area, particularly in the context of enhancing road safety and traffic management. This technology's ability to automate the monitoring and analysis of vehicle behavior presents a significant opportunity to enhance our understanding of driver behavior under different traffic management strategies.

One significant advantage of deep learning in vehicle detection is its ability to learn and recognize object features effectively, even without color information. This attribute is particularly beneficial when applied in conjunction with thermal imaging. Unlike traditional optical cameras, thermal cameras capture heat emitted by objects, making them highly effective under poor lighting conditions where optical cameras often struggle. This capability ensures that vehicle detection systems remain operational across various times of the day. Also, unlike conventional video feeds that can capture and potentially compromise personal privacy through identifiable features or license plates, thermal imagery abstracts these details into anonymous heat maps. This abstraction preserves individual privacy and allows for continuous monitoring of traffic flow and vehicle behavior without ethical concerns.

The integration of recent deep learning models such as YOLOv8 (You Only Look Once version 8) [*5*] and ByteTrack [*6*] is particularly effective for vehicle tracking in work zones, even in challenging scenarios involving occlusion. YOLOv8 represents the latest advancement in a series of robust, real-time object detection systems, which have been systematically enhanced to deliver superior accuracy and speed. ByteTrack complements YOLOv8's capabilities by offering an efficient solution for tracking vehicles through instances of partial or complete occlusion, enabling a detailed analysis of their trajectories, speeds, and lane-changing behaviors over time. Together, these technologies establish a comprehensive framework for the analysis of vehicle behavior in work zones, utilizing thermal videos to provide critical data without the constraints of lighting conditions or privacy issues.

This section discusses the video analytics facilitated by deep learning, with a focus on employing thermal imaging for vehicle detection and tracking within work zones. Our work is structured around several key methodologies that span the entire process from initial data collection to final analysis. We begin with the curation and annotation of a comprehensive dataset derived from thermal videos, ensuring a robust foundation for model training. Following this, we detail the process of model training, emphasizing the application of YOLOv8 and ByteTrack algorithms for accurate vehicle detection and tracking. The subsequent sections describe the specifics of algorithm development tailored for analyzing vehicle trajectories from thermal footage. We also outline the methods employed for validating the performance of our deep learning models, using precise metrics to assess their effectiveness in real-world scenarios. Through this systematic approach, we aim to offer a thorough understanding of vehicle dynamics in work zones.

3.2 Related Datasets

The development and refinement of algorithms for vehicle detection in thermal videos heavily relies on comprehensive and diverse datasets. A relatively popular dataset is the Boston University Thermal Infrared Video Benchmark [*7*]. This dataset serves as a critical benchmark for researchers in computer vision and machine learning, facilitating the advancement of visual analysis tasks in thermal infrared videos. The C3I dataset [*8*] is a comprehensive collection of thermal images that are instrumental in developing and testing algorithms for automotive applications, which covers a variety of vehicle types and scenarios. Similarly, the Teledyne FLIR Thermal Dataset, provided by a leading manufacturer of thermal imaging cameras, has high-quality thermal and RGB image pairs. The Oregon State University Thermal Pedestrian Dataset [*9*]. is a collection of thermal sequences. It includes both thermal and visible light image data captured from the rooftop of an 8-story building, providing aerial perspectives that are invaluable for developing algorithms capable of interpreting and analyzing scenes from elevated viewpoints.

Deep learning has emerged as a transformative force in vehicle detection, particularly in the domain of connected and autonomous vehicles (CAV), automated traffic analysis, and driver behavior modeling. This technology has shown outstanding capability in identifying and tracking vehicles from both ground-level cameras and drones [*10*,*11*,*12*,*13*], offering a level of precision and adaptability previously unattainable with traditional computer vision techniques. Despite the advancements in this domain, there remain significant gaps in research, particularly concerning the specific application of these technologies to work zone safety and operations. Most existing studies and datasets do not focus on the unique dynamics and challenges presented by highway work zones. Moreover, the datasets available predominantly comprise either general traffic scenarios or controlled environments, lacking the specificity required to address the complexities of work zones and traffic analytics.

This study aims to fill these gaps by collecting and analyzing thermal video data from cameras strategically placed next to highway work zones. This approach is novel in that no existing dataset specifically caters to the thermal imaging of vehicles in such a context. By focusing on thermal video data captured by fixed cameras, we provide unique insight into vehicle dynamics,

lane-changing behaviors, and speed variations near work zones. Our methodology is designed to be highly adaptable, allowing it to be replicated in other work zones or similar traffic environments to enhance traffic safety and operational efficiency.

3.3 Dataset Curation and Annotation

The foundation of any successful deep learning application lies in the quality and diversity of its training dataset. Recognizing this, a significant portion of our effort was dedicated to the curation and annotation of a comprehensive thermal vehicle dataset, tailored to the unique environmental and operational variables present in highway work zones. This dataset is critical not only for training our models but also for ensuring their applicability and effectiveness in real-world scenarios.

The dataset was compiled from thermal video footage recorded at locations in Medford and Danvers. From these videos, frames were extracted to create an image dataset. We ensure that the dataset includes a broad spectrum of vehicles, positions, and environmental conditions. Figure 3.1 shows some sample frames captured in Danvers and Medford. CVAT (Computer Vision Annotation Tool) is an open-source, web-based tool designed to facilitate the annotation of images and videos for training computer vision models, offering features like object detection, classification, and segmentation. CVAT streamlines the annotation process with its user-friendly interface and efficient task distribution capabilities among several annotators, significantly enhancing the management and annotation of large datasets for computer vision projects. Figure 3.2 shows a screenshot of the tool.

Vehicles within the dataset were categorized into three distinct classes based on their size and type: small, medium, and large. Small vehicles encompass sedans, motorbikes, SUVs, pickup trucks, and generally smaller cars. Medium vehicles include single-piece trucks such as garbage trucks, concrete mixer trucks, construction vehicles, and buses. Large vehicles are primarily comprised of tractor-trailers. This categorization not only reflects the diversity of vehicles encountered in highway work zones but also facilitates the nuanced analysis and understanding of different vehicle dynamics and their implications on traffic flow and safety.

Figure 3.1. Sample frames recorded in Medford and Danvers

Figure 3.2. CVAT annotation tool

The final dataset comprised 2,728 images, representing over 11,000 instances of vehicles. This significant instance count shows the dataset's diversity, with a wide range of vehicle types, sizes, and thermal signatures represented. Such diversity is critical for deep learning applications, ensuring that the trained models can accurately recognize and track vehicles under various conditions and in different traffic scenarios. To further enrich our dataset and enhance the robustness of our models, data augmentation was performed by creating copies of frames that contained only medium and large vehicle instances. This comparison is shown in Figure 3.3. These copies were subjected to minimal random rotation, along with small random cropping and translation, to simulate a broader range of angles and positions, thereby increasing the diversity and complexity of our training data without compromising the integrity of vehicle instances.

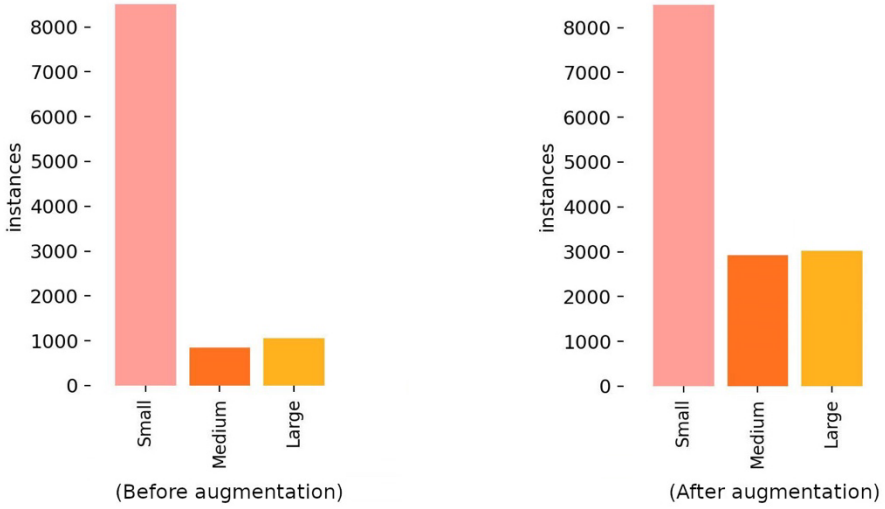

Figure 3.3. Instances before and after data augmentation

In addition to the vehicle dataset, a separate dataset was created for the segmentation of the roadway. This includes classifications for the highway, exit lanes, shoulders, gore areas, and channelizer drums.

By training our models on this rich dataset, we ensure that they can accurately detect and track vehicles across a spectrum of real-world conditions, from varying weather conditions to diverse traffic densities. Moreover, the inclusion of roadway segmentation data allows for a more nuanced analysis of vehicle trajectories, enabling us to understand not just how vehicles move, but how their movements relate to the surrounding infrastructure (e.g., lane boundary, channelizer drums). This comprehensive approach is critical for identifying potential safety hazards and inefficiencies in work zone layouts and traffic management strategies. The curation and annotation of this dataset represent a foundational step in our research, enabling the development of deep learning models that are both robust and relevant.

3.4 Model Training and Validation

The selection of YOLOv8 and ByteTrack for this study was primarily influenced by their state-of-the-art capabilities and their suitability for addressing the unique challenges posed by thermal video analysis. YOLOv8, recognized for its cutting-edge performance in object detection, is ideally suited to our project's requirements. Given that vehicle movements within our study context are predominantly unidirectional and not random, there was no necessity to develop a custom tracking algorithm. Instead, fine-tuning the hyperparameters of these existing, advanced models proved to be sufficient for achieving robust tracking results. This approach significantly reduced our implementation timeline, allowing us to focus on other critical aspects of the project. Moreover, ByteTrack's efficiency and accuracy are well aligned with the demands of our project, which involves processing hundreds of hours of video feeds. Its ability to track objects accurately in real-time is critical for analyzing the extensive amount of data collected, ensuring that our study benefits from both rapid processing and high-quality tracking outcomes. This strategic choice of technologies enables us to harness the full potential of deep learning for vehicle detection and tracking in thermal videos.

In the field of computer vision, particularly in object detection and segmentation tasks, several metrics are essential for evaluating the performance of models. Among these, classification accuracy, mean Average Precision (mAP), mAP(50), and mAP(50–95) stand out as key indicators of how well a model can identify and delineate objects within images. These metrics are used for both bounding box predictions (object detection) and segmentation (delineating the exact outline of objects). Validation involved comparing the models' performance against a subset of the dataset not used during training.

Classification accuracy, as defined in equation 1, is the simplest and most intuitive metric, representing the proportion of correct predictions (both true positives and true negatives) out of the total number of cases examined. Precision and Recall are also commonly used metrics used to compare model performance. In the following equations, TP, TN, FP, and FN, respectively, mean True Positive, True Negative, False Positive, and False Negative.

$$\text{Accuracy} = \frac{TP+TN}{TP+TN+FP+FN} \tag{1}$$

$$\text{Precision} = \frac{\text{TP}}{\text{TP+FP}} \tag{2}$$

$$\text{Recall} = \frac{TP}{TP+FN} \tag{3}$$

Mean Average Precision (mAP), shown in equation 4, is a comprehensive metric that combines precision and recall across all classes and prediction thresholds. Precision measures the correctness of the predictions (the percentage of your predictions that are correct), while recall measures the completeness (the percentage of total relevant instances that have been retrieved). mAP computes the average precision (AP) for each class at different recall levels,

then averages these APs across all classes. This metric provides a holistic view of the model's performance, balancing between precision and recall.

$$mAP = \frac{1}{|classes|} \sum_{c \in classes} \frac{|TP_c|}{|FP_c| + |TC_c|} \quad (4)$$

mAP(50) is a specific instance of mAP, where the model's predictions are considered correct if the Intersection over Union (IoU) between the predicted bounding box and the ground truth is greater than 50%. IoU is a measure of overlap between two boundaries, indicating how much the predicted boundary coincides with the ground truth. mAP(50) thus focuses on predictions that are reasonably accurate in terms of location and size, offering a lenient threshold for correctness. It is widely used due to its simplicity and the clear interpretability of its results. mAP(50–95) is a more stringent and detailed version of mAP, calculated by averaging the mAP values for IoU thresholds from 50% to 95%, in steps of 5%. Figure 3.4 shows how the various performance metrics improves over the training process, and Table 3.1 shows the metrics for different models after final epoch of training.

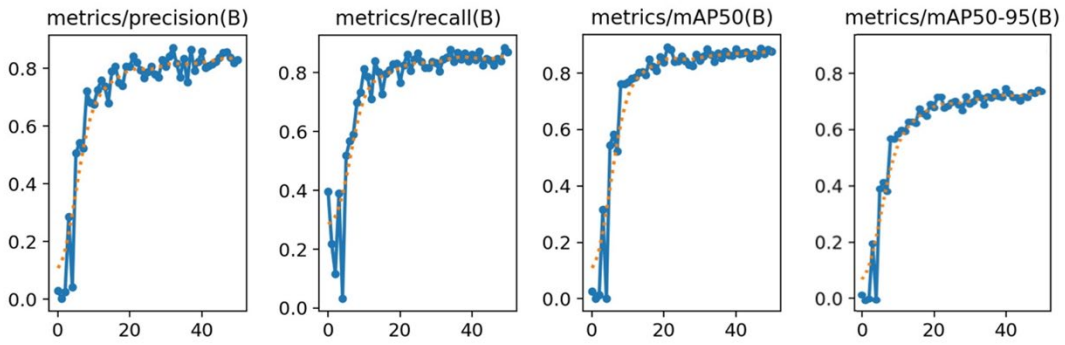

Figure 3.4. Object detection model metrics across successive training epochs

Table 3.1. Performance comparison of YOLOv8 models

	Precision	Recall	mAP50	mAP50–95
YOLOv8-s	78.8	85.2	85.5	71.5
YOLOv8-m	82.6	83.1	86.2	72.5
YOLOv8-l	81.9	85.4	87.6	72.6

Metrics used for validating tracking results are consistency, ID switching, and frame-to-frame continuity. Tracking consistency refers to the ability of the tracking algorithm to maintain continuous tracking of an object over a specified distance or period without losing its trajectory. It is quantified by counting the number of unbroken trajectories in the test dataset. We optimized the parameters of ByteTrack for our specific scenarios and achieved 98.0% consistency across test videos.

Figure 3.5. Vehicle segmentation output generated by the YOLOv8 large model

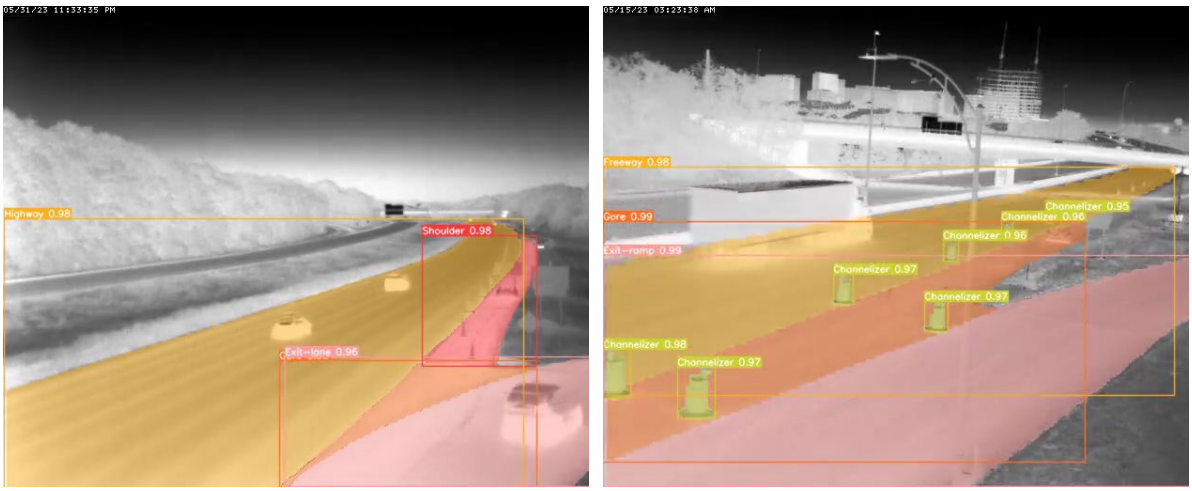

Figure 3.6. Output generated by YOLOv8 trained on the roadway segmentation dataset

Figure 3.5 and Figure 3.6 show visualization of the segmentation results; in Figure 2.1, the tracking ID assigned by the tracking module is also shown. The performance of the tracking module was particularly notable in challenging conditions, such as tracking of occluded and partially visible vehicles as shown in Figure 3.8. The results show the effectiveness of combining and fine-tuning YOLOv8 and ByteTrack for vehicle detection and tracking in thermal videos. The Python code and additional Shell scripts are available for review and download in a Github repository: https://github.com/z00bean/SmartWorkZoneControl.

3.5 Inference and Tracking on Thermal Videos

The process of analyzing thermal videos to detect and track vehicles, particularly in the challenging environments of highway work zones, involves a sophisticated pipeline that leverages the power of deep learning models alongside state-of-the-art computational resources. Utilizing NVIDIA's A100 GPUs and NVIDIA RTX 4090 graphics cards, our setup was designed for high throughput and efficiency, ensuring rapid processing of extensive video datasets without compromising accuracy or quality of the output. We leveraged both in-house server capabilities and the resources provided by the Unity cluster, a high-performance computing facility located at the Massachusetts Green High Performance Computing Center (MGHPCC).

We developed a comprehensive video processing pipeline:

1. Model Deployment: The trained YOLOv8 model and tracking module was deployed on two separate computing environments. This allowed us to process the videos from both the Medford and Danvers locations simultaneously. NVIDIA A100 and NVIDIA RTX 4090 GPUs were used.

2. Thermal Video Inference: For each thermal video, the models perform frame-by-frame inference to detect vehicles and track their trajectories. The powerful hardware enabled close to real-time processing.

3. Combining Output Postprocessing: After processing each frame, the detection and tracking results were aggregated. A script was developed to compile these results into a structured format for each video, with the combined outputs stored in a JSON file. This format was chosen for its versatility and ease of integration with further analytical tools, allowing for detailed examination of vehicle behavior and traffic patterns.

4. Video Compression: To facilitate storage and sharing of the processed videos, additional scripts were utilized to compress the output videos using ffmpeg, a leading multimedia framework. This step ensured that the insights gained from the analysis could be easily accessed and reviewed, without the need for extensive storage capacity. A typical output file in avi format of 1 hour duration could be compressed from 3.5 to 4 GB to 60 to 110 MB, a compression ratio of approximately 95%.

By seamlessly integrating vehicle detection, tracking, data aggregation, and the ability to process multiple videos concurrently, ensures that our methodology is not only powerful but also scalable and adaptable to other video-based applications.

3.6 Algorithm Development for Extracting Trajectories and Risky Merging Events

In the development of algorithms for trajectory extraction, lane usage determination, and detecting vehicle proximity to work zone control devices (i.e., traffic drums), a systematic approach was employed to harness the full potential of thermal sensor data. Following vehicle detection using the YOLOv8 model, the ByteTrack algorithm was integrated to stitch together vehicle trajectories across successive frames, ensuring robust tracking even in instances of occlusion or sudden vehicle movements. To further refine the analysis, algorithms were developed to interpret the stitched trajectories in the context of segmented lane information, allowing for the automatic determination of lane usage. Additionally, a specific focus was placed on developing a methodology to assess vehicle proximity to designated work zone control devices, leveraging the spatial data from trajectories and road segmentation. This comprehensive suite of algorithms represents a multilayered approach to understanding and improving traffic dynamics and safety around work zones.

Algorithm #1 helps in refining the tracking results by focusing on vehicles that move in the intended direction of traffic and have a significant presence across the frames, thus reducing noise and improving the accuracy of the trajectory analysis. Sample outputs are shown in Figure 3.7.

Figure 3.7. Visualization of trajectories

Algorithm #2 processes each relevant vehicle trajectory to determine whether the vehicle is using the highway or taking the exit. It leverages segmentation results to identify the vehicle's location in relation to designated areas like the highway, shoulder, exit lane, and gore. By examining the trajectory direction and the vehicle's known position within these segmented regions (line highway, exit lane, etc.) we can deduce the vehicle's path choice with a high degree of accuracy. This discernment between highway and exit lane usage is critical for understanding traffic flow patterns. The algorithm, therefore, not only categorizes each vehicle's trajectory based on its final segment of travel but also incorporates a temporal element by tracking the vehicle's progression over time. This allows for a dynamic analysis

that accounts for temporary occlusions or instances where the vehicle's path may intersect with multiple segmented regions, ensuring a comprehensive understanding of each vehicle's decision-making process and its implications on overall traffic dynamics.

Algorithm #1. Detecting relevant trajectories considering traffic direction and occlusions.

```
Input: List of segmented objects per frame, Trajectories of all tracked objects,
Direction of traffic flow
Output: List of relevant trajectories

Algorithm:
1. Initialize an empty list called relevant_trajectories
2. For each trajectory in Trajectories:
    2.1. Initialize a variable called trajectory_visibility_count to 0
    2.2. Initialize a variable called consistent_direction_count to 0
    2.3. For each frame in trajectory:
        2.3.1. If the segmented object for this trajectory in this frame is valid:
            2.3.1.1. Increment trajectory_visibility_count
            2.3.1.2. If the direction of movement for the object matches the traffic
flow direction:
                2.3.1.2.1. Increment consistent_direction_count
    2.4. Calculate visibility_ratio = trajectory_visibility_count / total number of
frames in trajectory
    2.5. Calculate direction_consistency_ratio = consistent_direction_count /
trajectory_visibility_count
    2.6. If visibility_ratio is above a predefined threshold (e.g., 0.5) and
direction_consistency_ratio is high (e.g., > 0.8):
        2.6.1. Add this trajectory to relevant_trajectories

3. For each trajectory in relevant_trajectories:
    3.1. Check for sporadic segmentation results within the trajectory:
        3.1.1. If a segmented object appears only in a single frame or sporadically
without a consistent trajectory:
            3.1.1.1. Remove the sporadic segmentation results from the trajectory

4. Return relevant_trajectories
```

(a) Danvers (b) Medford

Figure 3.8. Tracking of occluded and occluding vehicles

Algorithm #2. Detecting highway or exit lane usage and saving vehicle frames.

```
Input: List of relevant trajectories, Segmentation results for highway, shoulder, exit
lane, and gore, Direction of each trajectory
Output: List of vehicle lane usage (Highway or Exit), Saved frames for each vehicle

Algorithm:
1. Initialize an empty list called vehicle_lane_usage
2. For each trajectory in relevant trajectories:
    2.1. Initialize a variable called last_known_position to store the last frame's
position of the vehicle
    2.2. Initialize a variable called vehicle_lane to "Unknown"
    2.3. For each frame in trajectory:
        2.3.1. Determine the segmented area (highway, shoulder, exit lane, gore) where
the vehicle is located
        2.3.2. Update last_known_position with the current frame's position
        2.3.3. If the vehicle is in the exit lane or crossing the gore area:
            2.3.3.1. Set vehicle_lane to "Exit"
            2.3.3.2. Break the loop
        2.3.4. Else if the vehicle remains in the highway lane:
            2.3.4.1. Continue checking until a change is detected or trajectory ends
    2.4. If vehicle_lane remains "Unknown" by the end of trajectory:
        2.4.1. Set vehicle_lane to "Highway"
    2.5. Add the vehicle's lane usage and last_known_position to vehicle_lane_usage list
    2.6. Save the frame at last_known_position for this vehicle

3. Return vehicle_lane_usage, along with saved frames for each vehicle
```

Algorithm #3. Detecting vehicles close to the work zone.

```
Input: List of relevant trajectories, Segmentation results for road and shoulder,
Threshold distance for proximity to work zone
Output: List of vehicles close to work zone

Algorithm:
1. Initialize an empty list called vehicles_close_to_workzone
2. For each trajectory in relevant trajectories:
    2.1. For each frame in trajectory:
        2.1.1. Determine the vehicle's position on the frame
        2.1.2. Extract segmentation results for road and shoulder for the current frame
        2.1.3. Calculate the shortest distance from the vehicle's position to the
shoulder segmentation boundary
        2.1.4. If the distance is less than the threshold distance:
            2.1.4.1. Mark this frame as indicating the vehicle is close to the work zone
    2.2. If any frame in the trajectory indicates the vehicle is close to the work zone:
        2.2.1. Add this vehicle's trajectory to vehicles_close_to_workzone list

3. Return vehicles_close_to_workzone
```

Algorithm #3 iterates through each vehicle's trajectory, calculating the distance from the vehicle to the closest point on the shoulder segmentation boundary for each frame. By comparing this distance to a predefined threshold, the algorithm identifies vehicles traveling too close to work zone control devices. Such merges are referred to as last-minute or late merges in this report. In this research, our focus is to identify vehicles that merge at the last minute and get too close to the traffic drums in the lane closure taper. Vehicles that come

within a predefined *distance threshold* to the traffic drums in the taper in their trajectory are added to the list of vehicles close to the work zone, enabling targeted analysis of traffic patterns and potential safety concerns in this critical area. The *distance threshold* is a hyper parameter which must be adjusted based on location and camera position. Two sample outputs of the algorithm are given in Figure 3.9 and additional examples are provided in Appendix F.

Figure 3.9. Vehicles traveling too close to work zone lane closure taper

The charts in Figure 3.10 illustrate the relationships between freeway traffic volumes and instances of last-minute merges or late merges at the Danvers location on different days. This type of visualization could help in analyzing how traffic volume correlates with driver behavior, in this case, the tendency to merge late near the beginning of work zone taper. Besides traffic volume, factors such as taper length, presence of rumble strips, and weather could impact the occurrences of late merge. These factors are also considered in Figure 3.10. Figure 3.11 shows the late merge results for the work zone in Medford, which are averages over three days each, and offer a more aggregated view, smoothing out daily variations to highlight broader trends in merge behavior and its relationship to various impact factors.

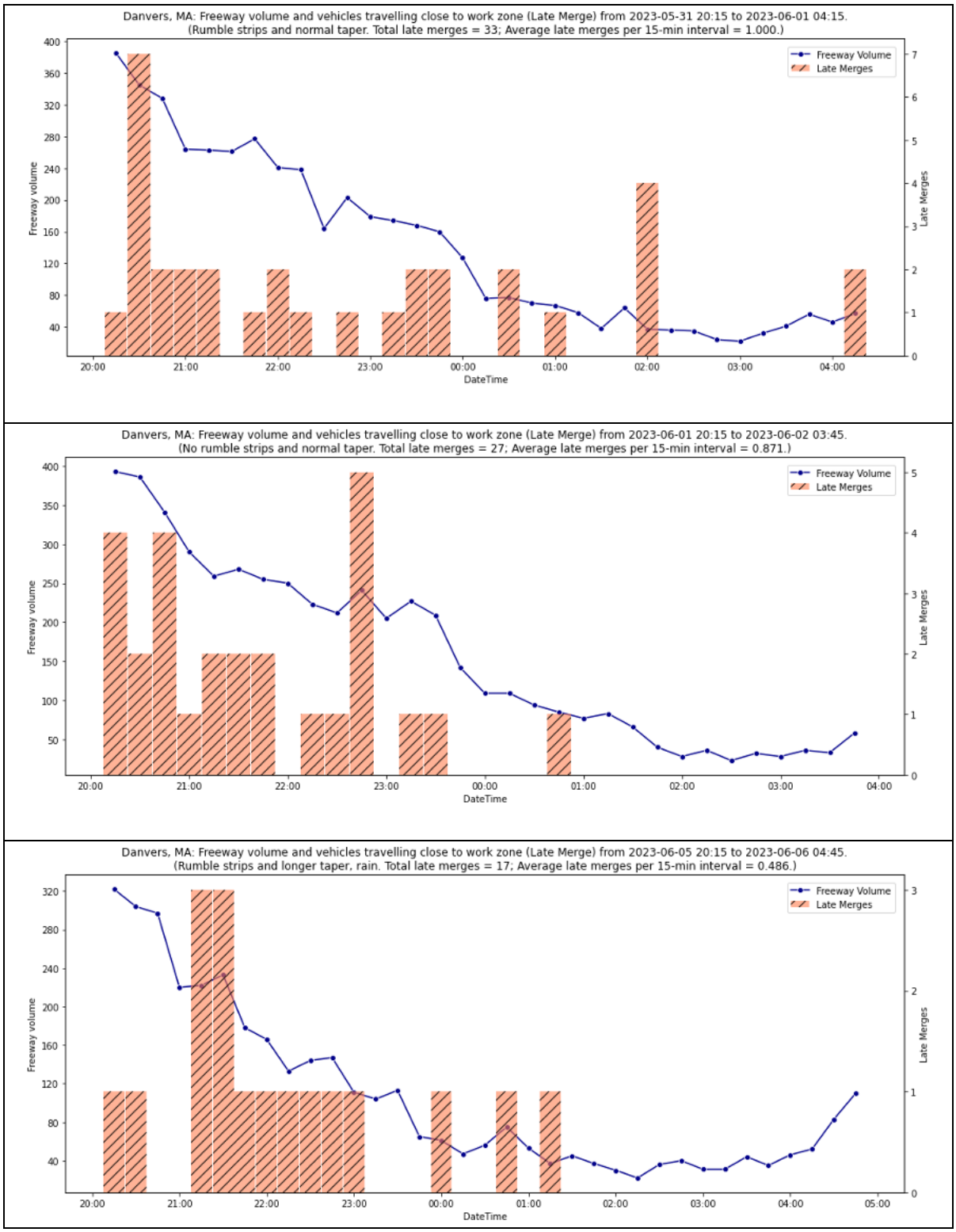

Figure 3.10. Freeway traffic volume and late merges at Danvers

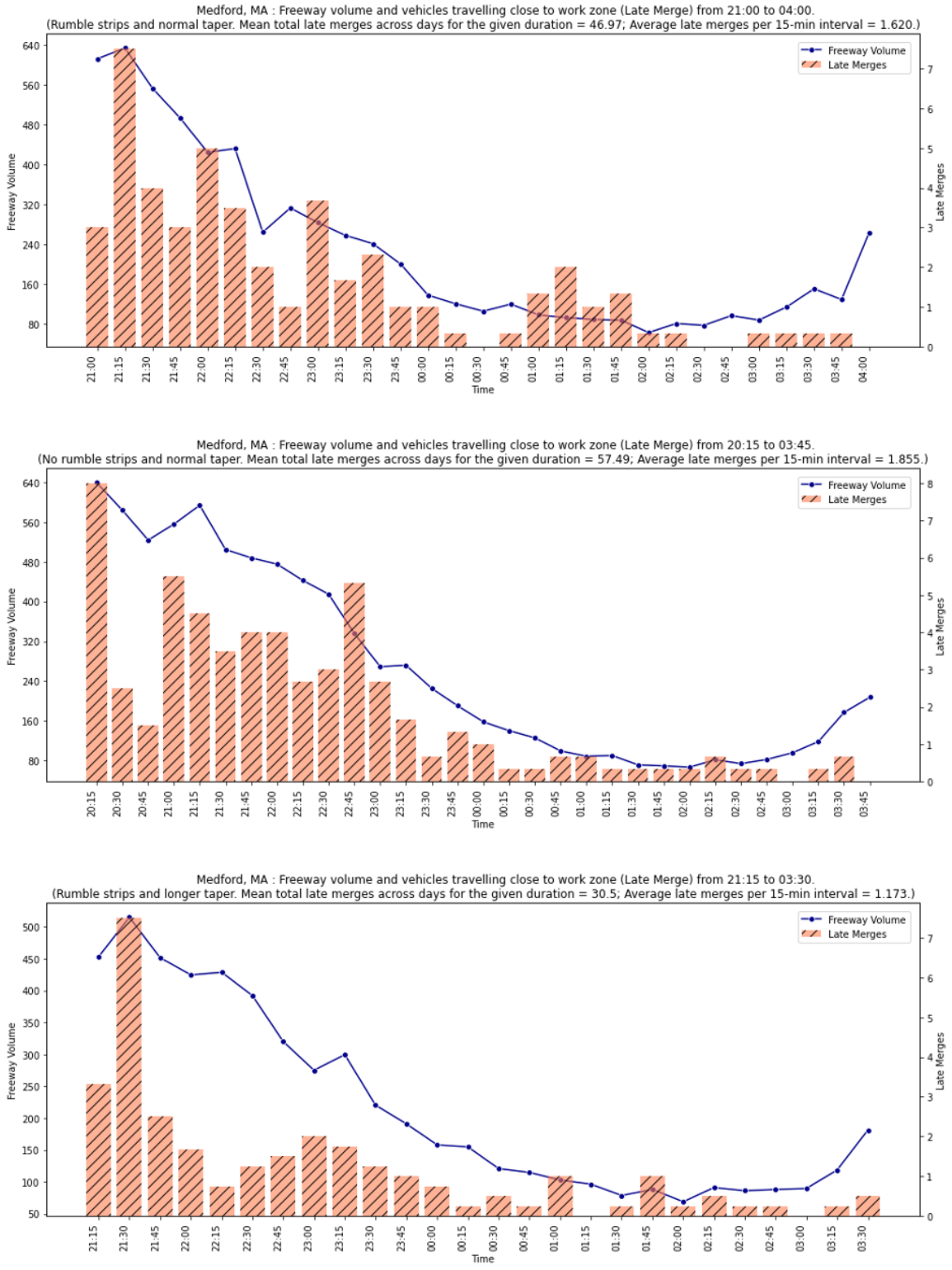

Figure 3.11. Freeway traffic volume and late merges at Medford

When interpreting these charts, it is essential to consider factors such as time of day, day of the week, and potential external influences like weather conditions, taper length, and the presence of rumble strips that could affect driver behavior. Such data visualization assists in understanding driver decisions, potentially informing the design of traffic control strategies and placement of control devices to enhance safety around work zones. Given the various factors involved, a deeper statistical analysis is necessary to quantify the correlation between such factors and the occurrences of late merges, allowing for more definitive conclusions beyond visual interpretation. The detailed statistical analysis results are provided in Section 5. Additional details of traffic volume and late merges are given in Appendix E.

3.7 Analysis of Drone Video Data

This section focuses on the utilization of both deep learning approaches and basic computer vision tracking methods for analyzing drone-captured footage, discussing their respective strengths and challenges in the context of trajectory analysis.

The application of deep learning models, such as YOLOv8, to drone video data facilitates the accurate detection and tracking of vehicles. These models excel in extracting detailed trajectory information, even in densely populated or cluttered scenes typical of work zones. They are also good at handling the variability in vehicle appearance and size seen in top-down views, enabling precise identification and continuous tracking of vehicles as they navigate through work zones.

However, a notable challenge in processing drone video data arises during nighttime conditions, where low light and glare from headlights can significantly degrade video quality. To address this problem, a guided filtering and dehazing method was implemented using Python, incorporating functions such as gamma adjustment, and edge preserving bilateral filter. These enhancements, as shown in Figure 3.12, made it possible to improve the visibility of nighttime RGB videos, ensuring consistent trajectory analysis across varying lighting conditions.

Figure 3.12. Nighttime image before and after applying enhancement

In addition to deep learning techniques for RGB videos, basic computer vision tracking methods have shown promise in analyzing thermal drone footage, especially due to the distinct features observable in top-down views. Techniques such as background subtraction, contour detection, and the use of more traditional tracking methods such as Kernelized Correlation Filter tracker, leverage the simplicity and high contrast of vehicles against the road surface. These methods are particularly effective in scenarios where deep learning models might be computationally intensive or require extensive training data. This approach, while beneficial in terms of computational efficiency and effectiveness for certain scenarios, comes with the caveat that parameter adjustments are necessary for each new location; at times, even drone movement could necessitate recalibrations, adding a layer of complexity to their application. Figure 3.13 shows two sample frames with the detected moving vehicle contours, and final detection results with bounding boxes are shown in Figure 3.16.

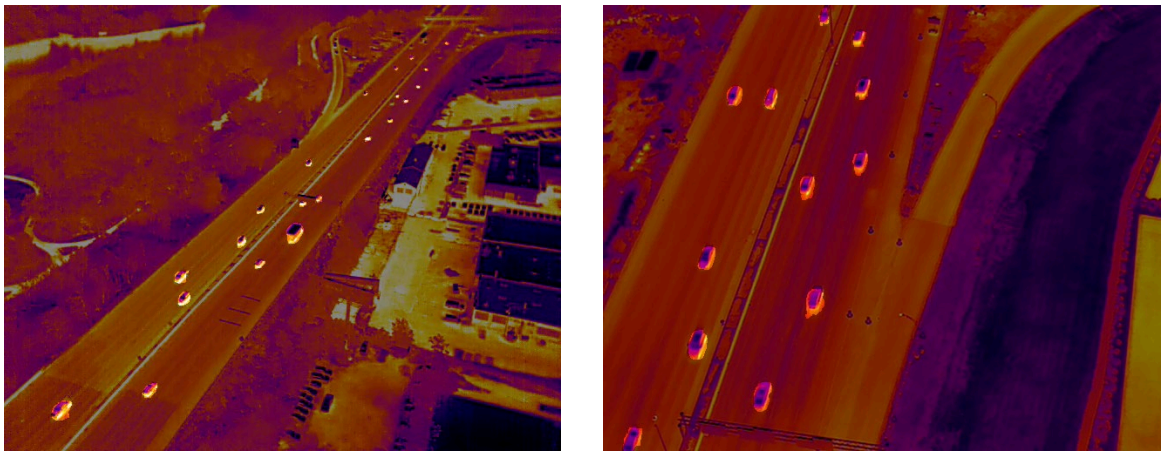

Figure 3.13. Background subtraction, contour estimation of moving objects

We created a dataset for vehicle detection consisting of 1,260 curated and annotated images. To expand the dataset, extra images were generated by duplicating frames with large vehicles and altering them with random rotations (±8 degrees), as well as minor cropping and scaling, simulating slight drone movements. Within this dataset, vehicles are classified into two categories: small and large. We implemented a new model architecture that improves upon the YOLOv8 model, to enable better detection of small objects, including the substitution of standard convolution functions with GSConv modules and an enhancement of the neck to integrate higher resolution information, specifically targeting the detection of densely packed and small OBBs.

Although YOLOv8 models effectively detect a range of objects, they can struggle with smaller objects, especially in drone-captured images that have slanted views toward the horizon, making distant vehicles appear tiny. This issue is mitigated in top-down views unless the drone is at a high altitude. In YOLOv8, outputs from the third to fifth blocks of the Path Aggregation Feature Pyramid Network (PAFPN) are typically processed, as these levels possess mature features crucial for detection tasks. To improve detection of small vehicles, the P2 layer, which has higher resolution, is added to YOLOv8's neck network, and the number of detection heads is increased to four. These changes enable the P2 feature map to

capture finer details lost in deeper layers. Figure 3.14 illustrates the modified PAFPN structure utilizing the P2 output for enhanced detection.

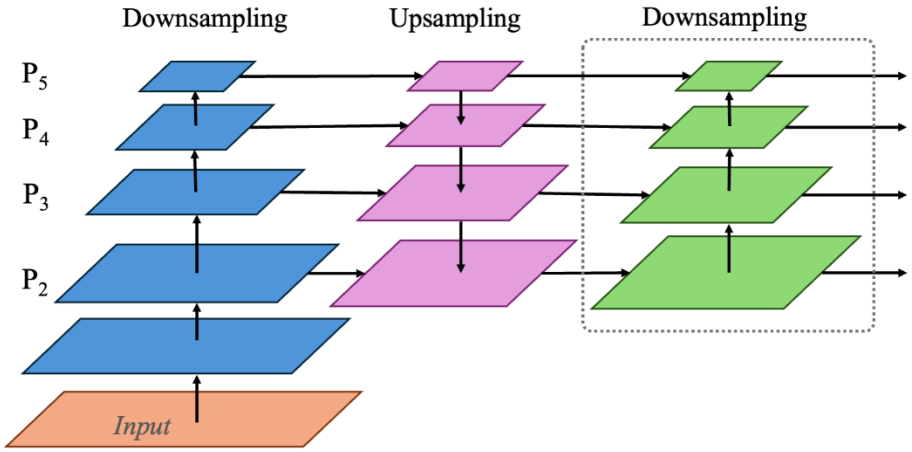

Figure 3.14. Schematic diagram of PAFPN

We also implemented a modified version of Slicing Aided Hyper Inference (SHAI) method that strategically selects image slices for fine-tuning based on their overlap with roadway segmentation results. This targeted selection ensures that our model focuses on areas of highest relevance optimizing both the efficiency and effectiveness of the detection process. Slicing aided fine-tuning (SF) involves extracting and processing these image patches or tiles and training the model using these. But unlike the traditional SF methodology, we do not select all image tiles for training the model. Also, we upscale the selected tiles to double its original size using cubic interpolation. Image tiles are only selected if they overlap with the segmentation output from the roadway segmentation model. Figure 3.15 illustrates the basic steps involved. The roadway segmentation model operates at 2 fps, which is suitable for scenarios where the drone remains mostly stationary.

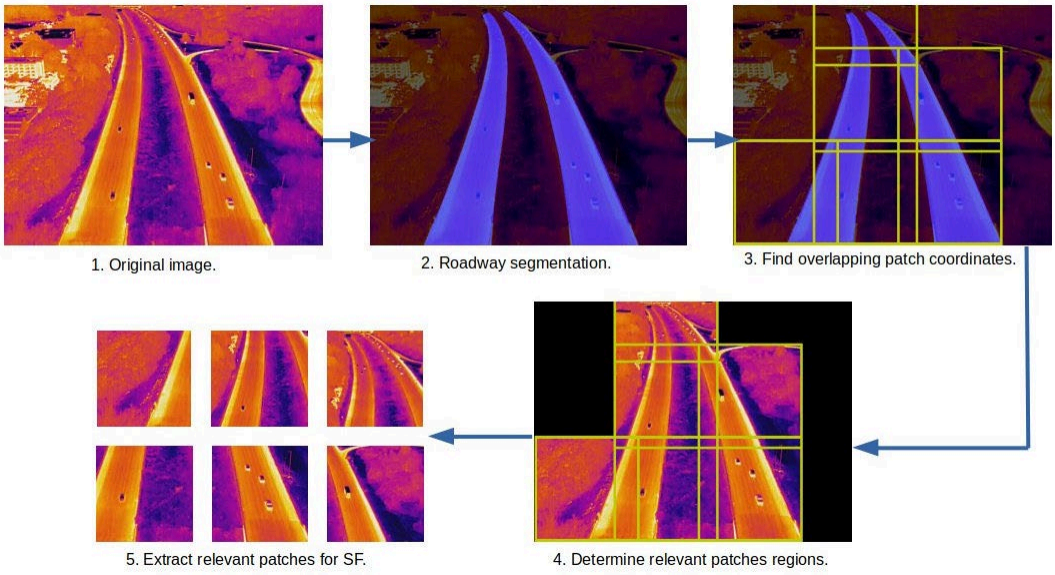

Figure 3.15. Basic steps in selective slicing using roadway segmentation information

We selected the *Medium* YOLOv8 model because it offers a balanced trade-off between performance and computational overhead. As indicated in Table 3.2. Evaluation results on Nighttime Thermal Drone datasetthis configuration achieved an mAP-50 score of 0.963 on the test set.

Table 3.2. Evaluation results on Nighttime Thermal Drone dataset

Model	Class	Precision	Recall	mAP50	mAP50–95
YOLOv8-m	All	91.4	78.5	90.0	72.3
Our model	All	**96.1**	**89.9**	**96.3**	**80.2**
Our model	*Small*	95.2	85.5	94.0	74.8
Our model	*Large*	97.0	94.2	98.6	85.1

Comparing deep learning-based methods with basic computer vision tracking, each approach has its advantages. Deep learning models offer superior accuracy and robustness in detecting and tracking vehicles but require significant computational resources and training data. On the other hand, traditional computer vision methods are less resource-intensive and can be quickly implemented but might lack the precision and adaptability of deep learning techniques, especially in complex or dynamic scenes. The unexpected movement of the drone camera can introduce inconsistencies in the video data, complicating the task of continuous object tracking. Deep learning models must be sufficiently robust or adapted to account for these variations, ensuring accurate trajectory extraction despite the instability of the aerial platform.

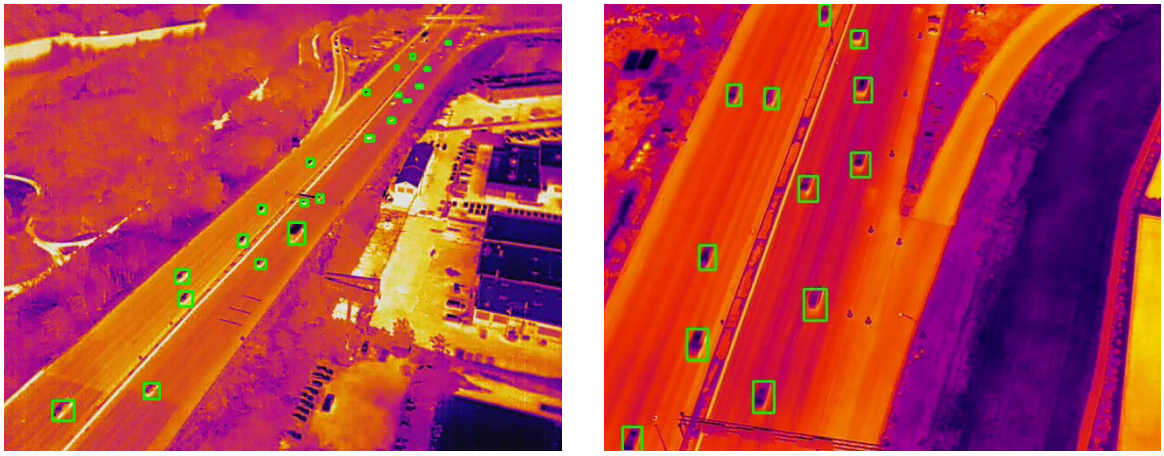

Figure 3.16. Vehicle detection and tracking using filtered-background subtraction method

In our analysis based on drone videos at the Medford location, we closely monitored 140 vehicles as they traversed over the rumble strips. Our findings revealed that only 40 of these vehicles exhibited a speed reduction greater than 15% upon encountering the rumble strips. This indicates that the presence of rumble strips, while effective for some vehicles, does not universally lead to significant speed adjustments. Furthermore, within the context of lane changes, particularly in the second lane from the left—which also leads directly to a downstream exit ramp—only 22 vehicles (or approximately 15%) engaged in immediate lane

changes within a 160-foot distance following the rumble strips. This observation underscores the complexity of interpreting vehicle behavior, as not changing lanes could also align with the intention to exit, rather than not being influenced by the rumble strips.

At the Danvers location, the analysis of trajectories for 100 vehicles revealed a consistent pattern, where a similar proportion (15%) of drivers executed immediate lane changes upon encountering rumble strips. This consistency across both locations suggests a broader trend where the presence of rumble strips influences a subset of drivers to adjust their speed or change lanes, albeit a relatively small fraction. These insights are further complicated by the operational challenges posed by abrupt movements of the drone camera, which can affect the precision of tracking vehicle movements. Nonetheless, these observations provide valuable insights into driver behavior and the partial effectiveness of rumble strips in influencing vehicular speed and lane-changing decisions in work zones.

Drone video data were manually synchronized with time stamped ground thermal video data to compare the tracking results of ground thermal and drone footage in 15-minute intervals. An example of this synchronization is given in Figure 3.17, and additional examples are given in Figure 8.43 of Appendix D.

Figure 3.17. Thermal video and drone video at Medford on 05/15/2023, 22:17

Table 3.3. Ground thermal and drone video footage results for Medford

Date	Hour	15-min	Total Volume	Late Merges	Total Volume (Drone)	Late Merge (Drone)
5/8/2023	23	0	294	4	267	3
5/8/2023	23	30	239	1	218	1
5/9/2023	21	30	641	5	598	5
5/9/2023	22	0	420	7	352	5
5/9/2023	22	30	389	0	331	0
5/9/2023	23	0	308	4	261	4
5/15/23	22	30	450	2	396	2
5/15/23	23	0	268	3	237	3

Table 3.3 and Table 3.4 compare the total traffic volume and vehicles traveling close to the work zone, as determined from the analysis of ground thermal and drone video footage. The presence of shadows and dark areas within the video frame occasionally results in the omission of certain vehicle trajectories, particularly those of darker colored vehicles. This analysis is based on complete 15-minute segments for which entire drone videos are available.

Table 3.4. Ground thermal and drone video footage results for Danvers

Date	Hour	15-min	Total Volume	Late Merges	Total Volume (Drone)	Late Merge (Drone)
5/31/2023	20	45	340	2	332	2
5/31/2023	21	15	268	2	264	2
5/31/2023	21	45	283	1	271	1
6/1/2023	20	30	407	2	394	2
6/1/2023	21	0	298	1	286	1
6/1/2023	21	30	272	1	270	2

In the case of the Danvers site, thermal drone footage was utilized due to the limitations of RGB drone videos under low-light conditions. Examples comparing RGB and thermal drone in varying light conditions are provided in Figure 8.42 in Appendix D. This comparison underscores the limitations of RGB drone footage in providing usable data, particularly in low-light environments.

In the analysis of drone-captured video data, several limitations were observed despite preprocessing efforts to enhance the RGB footage. Challenges included persistent dark areas and occlusions, such as gantries and shadows cast by gantries, which particularly affected the detection of vehicles. This limitation led to occasional underestimation of vehicle volumes, with a noted marginal error in total volume calculations attributable to timing discrepancies. However, these conditions did not significantly hinder the identification of late merges, as the illumination from work zone lighting mitigated the impact of occlusions. Despite the challenges presented by drone video analysis, it is important to acknowledge that drone footage remains a valuable asset for vehicle trajectory analysis, particularly when adequate lighting is available. The unobstructed aerial perspective provided by drones, especially under daylight conditions, significantly enhances the quality and accuracy of the data collected, making it an indispensable tool for comprehensive traffic study and assessment.

The integration of drone video data into trajectory analysis represents a promising frontier in traffic monitoring and work zone safety evaluation. While deep learning approaches offer comprehensive insights and high accuracy, basic computer vision tracking methods provide a more accessible alternative for certain applications. The choice between these methods depends on the specific requirements of the analysis, including the need for precision, computational efficiency, and adaptability to varying conditions.

This page left blank intentionally.

4.0 Radar Data Analysis

The radar data collection effort is described in Section 2, which includes details on the data collection time periods and locations. This section presents how the collected radar data was further processed to remove noise. Based on this cleaned dataset, average vehicle speed profiles were generated. These profiles demonstrate how drivers, on average, adjust their speeds under various traffic control settings when approaching a highway work zone. The processed speed data is then utilized in the regression models in Section 5 to analyze the impacts of different traffic control strategies.

4.1 Data Processing and Cleaning

The direct output of the radar sensors was in binary format, which was converted to generate vehicle ID, time stamp, x and y coordinates, vehicle speed, vehicle length, and so forth. The converted radar data was noisy due to the impacts of environmental factors and had to be further cleaned to remove fragmented trajectories and ghost targets. The cleaning process involved several steps to ensure data accuracy and integrity.

- First, the radar unit assigns cyclic IDs between 0 and 255 to targets. This approach is fine for a short time period when there are fewer than 256 targets. However, it creates duplicate IDs over time. Therefore, a script was written to update target IDs. This is an important but relatively straightforward process since duplicate IDs are typically separated by clear time gaps.

- To remove ghost targets, trajectories were filtered based on their distances to the radar sensor and trajectory lengths. Trajectories that were too far from/close to the sensor (i.e., outside the highway boundary) were excluded.

- Some of the short trajectories were caused by vehicle occlusions, as the radar was mounted on the roadside. We considered the longest continuous trajectory as the baseline and used a threshold value of 80% of this longest trajectory length for data cleaning. This process excluded all trajectories shorter than the threshold.

- Furthermore, some trajectories had gaps in the middle that were probably due to occlusions. These gaps were typically 2–3 seconds long but did not happen often. Since we had plenty of data samples, we decided to remove these trajectories. After the data cleaning, we compared the traffic counts derived from the thermal videos (treated as the ground truth) and the remaining radar samples. We found that approximately 77% of the vehicle trajectories were captured by the radar.

4.2 Lane-Speed Segmentation

Understanding vehicle speed distribution by lane in a work zone is helpful. Given the resolution of the thermal cameras and their mounting positions, obtaining such speed data from radar is more practical. However, the mounting positions of the radar sensors make it difficult to directly differentiate vehicle trajectories and speeds by lane. Therefore, the following algorithm was developed.

When deriving vehicle speed distributions, the raw radar data was separated by both time and space. A time window of t=1 hour was considered. This time window should not be too long or short. A very long time window cannot capture temporal variations in the data, whereas a very short window may result in insufficient data points. The radar sensors sampled each vehicle's speed at multiple locations along a road segment. In this study, these speed data points were separated based on their locations using 30-ft long segments. Similar to the time window length, segments that are too long may result in a loss of data granularity. Conversely, segments that are too short could lead to the generation of distribution patterns that appear very noisy. By separating the raw speed data based on time and space, the resultant distributions show the average speed profile of how vehicles approach a work zone.

Algorithm #4 Lane-speed segmentation algorithm.

```
1: Initialize variables such as Timewindow list, Distance list and lists to store data,
left lane ID: l_ID and right lane ID: r_ID
2: Set window_count = 1
3: For{each time window in Timewindow}
4:      Extract data within the current time window
5:      For{each segment along the Distance}
6:         Padding all the trajectories to have the same length of records
7:          Determine the mean positions of each records and select two out (END0 and
END1) for the segment
8:          Classify vehicles into left and right lanes based on their positions
relative to the lane center (line across END0 and END1)
9:          Store the IDs of vehicles in the left and right lanes (l_ID, r_ID)
10:     EndFor
11:     Initialize lists to store statistics for left and right lanes: l_mean_speed,
l_sample r_mean_speed$, r_sample
12:     For{each segments along the Distance}
13:        Query and select the IDs shared by the current and next segment
14:        Calculate statistics (mean speed and sample size) for the left and right
lanes based on the selected ID
15:        Append the calculated statistics to respective lists
16:     EndFor
17:     Update the window count
18: EndFor
```

Based on the preceding results, we further separated the radar speed data by the left two lanes and the right two lanes utilizing a data-driven process. Within a 30-ft segment, each valid speed data point is represented by a set of x, y, and speed measures. Based on the x and y values, these data points were clustered into two groups, representing the left two lanes and the right two lanes. This study also attempted to cluster the speed data into four groups, each representing a single lane. However, this turned out to be challenging given the quality of the

vehicle lateral position data. For future data collection, mounting radar sensors directly above the traffic on a fixed structure would help to generate more accurate vehicle lateral position measurements, making it possible to separate vehicles by lane.

Some vehicles changed lanes within a 30-ft segment. In this case, we excluded their corresponding trajectories in that particular segment during the speed distribution calculation. Algorithm #4 summarizes the radar data cleaning and processing steps.

4.3 Speed Distribution Analysis

Figure 4.1 shows some sample speed distribution analysis results for the Medford site. The first and third columns are for the M2-Upstream radar (i.e., radar at Location M2 facing upstream), while the second and forth columns are for the M2-Downstream radar. By positioning radar data in this way, the speed profiles in the same row from the first and the second columns can be concatenated to show how drivers adjust speeds as they approach a work zone. Similarly, subfigures in the same row from the third and the fourth columns can be viewed in one group. The horizontal axis indicates the distances between vehicles and the radar unit. The two radar units were located right next to each other at the Medford site. Therefore, vehicles first approached the radar facing upstream and drove away from the radar facing downstream as the horizontal axis values suggest. The vertical axis is for speed.

Rumble strips and a normal taper were deployed in Medford on May 9, 2023. The data in Figure 4.1 clearly suggest that the left two lanes had higher average speeds than the right two lanes. There was a blind zone between the coverage areas of the two radar units. It is interesting to observe some speed fluctuations within this blind zone. The trends (e.g., increasing, decreasing) in these fluctuations are not always consistent. This is likely caused by lane-changing activities in the blind zone, for example, fast vehicles changing from a left lane into a right lane, and slow vehicles in a right lane accelerating and moving into a left lane. Another possible reason is that vehicles traveled toward the M2-Upstream radar but drove away from the M2-Downstream radar. Compared to receding targets, approaching targets can be better detected. Figure 4.1 also indicates vehicles clearly decreased speed gradually and slightly as they traveled downstream toward the work zone lane closure taper. Additional speed distributions for the Medford site can be found in Figure 8.1 through Figure 8.5 in Appendix A.

As shown in Figure 8.6 through Figure 8.8 in Appendix A, the Danvers site is slightly different from the Medford site. The second radar (D2-Downstream) covers an area downstream of the beginning of the lane closure taper. Some vehicles covered by the first radar (D1-Downstream) may have exited the highway and not been captured by the second radar (D2-Downstream). At the Danvers site, both radar units were facing receding vehicles. The average speed of vehicles in the left two lanes remained relatively constant from the D1-Downstream radar to the D2-Downstream radar, while the average speed of vehicles in the right lanes increased. This was most likely due to slow vehicles exiting the highway just before the coverage area of the D2-Downstream radar. We compared the data from two dates (05/31/2023 and 06/01/2023), where the only main difference was the presence or absence of

rumble strips. However, we did not observe any obvious changes in vehicle speeds, suggesting that rumble strips did not significantly slow vehicles down at this site. Also, the vehicle speeds in both the left and right lanes remained largely unchanged between the upstream and downstream segments.

The work zones in Medford and Danvers were set up only during the night, from about 8:30 p.m. to 5 a.m., while the work zone in Campton was in place all day for nearly two weeks. Another major difference is that the Campton site lane closure taper was about 2,000 ft downstream of an on ramp and was not affected by any exit ramp. At the Campton site (see Figure 8.9 through Figure 8.15 in Appendix A), vehicles in both lanes clearly reduced speed as they approached the beginning of the lane closure taper. During congested periods, speed decreased to as low as 40 mph. The right lane typically exhibited slower speeds than the left lane, possibly due to the interference of vehicles cutting in. The approaching speed between 10 and 11 p.m. was typically around 60 mph, consistently lower than those during other periods, except for very congested ones.

Evaluating and comparing the effectiveness of various traffic control strategies based on descriptive analysis results is challenging, because it is difficult to control all other factors and filter out the impact of a single variable. Therefore, statistical analysis was conducted to model the data from all three sites, and the results are provided in the next section.

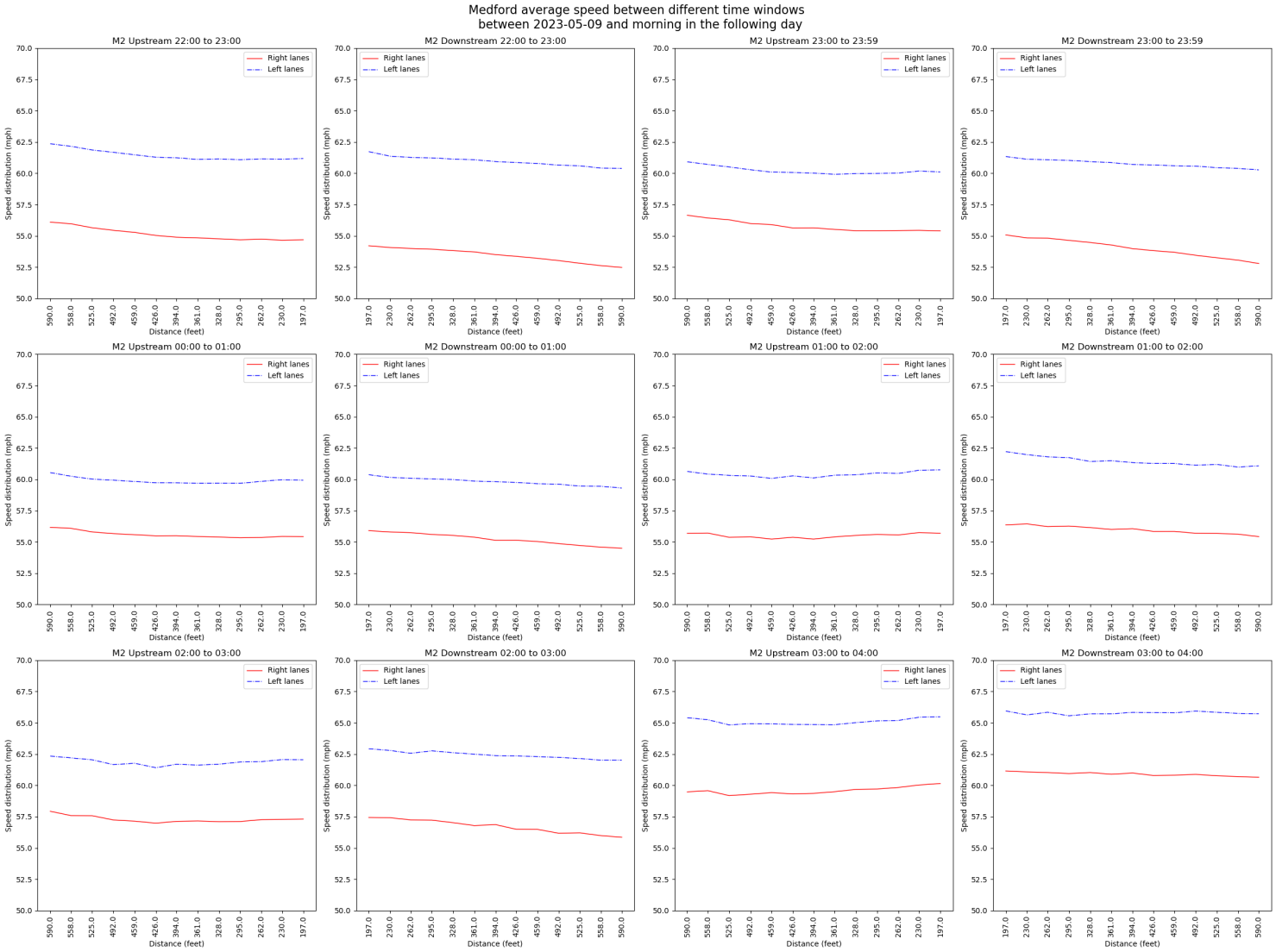

Figure 4.1. Medford speed profile: late May 9, 2023, and early May 10, 2023

This page left blank intentionally.

5.0 Regression Analysis

Section 4 provided a descriptive analysis of speeds at different work zones. However, vehicle speed and merge behaviors are potentially affected by several factors, such as congestion, FSLS, PCMS, and rumble strips. It is difficult to rely solely on descriptive statistics to quantify the impacts of a single factor, because the values of other factors also change. Therefore, this section employs regression analysis to investigate the impacts of individual factors on vehicle speeds and last-minute merges.

5.1 Variable Definition

This section describes the variables considered in the regression analysis. For the Medford and Danvers sites, the following variables are considered:

- Total_FREEWAY: Freeway traffic volume measured in number of vehicles for every 15 minutes.
- Total_EXIT: Exit ramp traffic volume measured in vehicles for every 15 minutes.
- Long: This variable is 1 when a longer lane closure taper was used (0 otherwise).
- Normal: This variable is 1 when a normal lane closure taper was used (0 otherwise).
- Rumble: This variable is 1 when transverse rumble strips were installed (0 otherwise).
- mean_abs_speed: Mean average speed at the middle of the covered road segment measured in miles per hour. This is averaged across all vehicles observed in every 15 minutes.
- Num_LM_merge: The number of last-minute merges observed at the beginning of lane closure taper. This is counted for every 15 minutes.

Two sets of regression models have been developed. The first set uses *mean_abs_speed* as the dependent variable, and the second one considers the *Num_LM_merge* as the dependent variable. Table 5.1 lists the independent variables utilized in different regression models.

Note that in the last-minute merge models, variable *Long* is not included. This is because such models only utilize data from work zone scenarios. Therefore, between *Long* and *Normal*, only one variable is needed, since *Long* = 1 is equivalent to *Normal* = 0. For the speed models, we also include data points for some non-work zone scenarios. Therefore, both *Long* and *Normal* are considered. When both variables equal 0, the corresponding data point is for a non-work zone scenario.

Table 5.1. Independent variables utilized in the Medford and Danvers regression models

Speed Model	Last-Minute Merge Model	Independent Variable
✓	✓	Total_FREEWAY
✓	✓	Total_EXIT
✓	—	Long
✓	✓	Normal
✓	✓	Rumble
—	✓	mean_abs_speed

For the Campton data, we developed two similar sets of regression models for speed and risky merges. The following independent variables were considered:

- VOLUME: Defined in the same way as Total_FREEWAY for the Medford and Danvers sites.
- UP: This variable is for the status of the flashing speed limit sign (FSLS). UP = 0 if the FSLS is folded down. Otherwise, UP = 1.
- ON: ON = 0 if the flashing beacons on the FSLS are off. Otherwise, ON = 1. Note that when UP = 0, ON will also be 0.
- ME: This variable is for the status of the portable changeable message sign (PCMS), which displays two sets of messages. ME = 0 if the PCMS displays "POSSIBLE SLOW OR STOPPED" and "TRAFFIC AHEAD BE AWARE." ME = 1 if the PCMS displays "LEFT LANE CLOSED" and "MM 86.4 MERGE EARLY."
- mean_abs_speed: Defined in the same way as for the Medford and Danvers sites.
- Daylight: The value Daylight = 1 indicates the duration between sunrise and sunset on each day.

For the Campton speed model, only the first four variables listed are included as independent variables. For the Campton risky merge model, all five variables are considered as independent variables. The risky merges for the Campton site are defined in Figure 5.1. Because of the camera mounting position, it is possible to observe the area prior to the lane closure taper. This area is divided into green, yellow, and red zones. Depending on how vehicles approach the work zone, their trajectories are classified into safe, somewhat risky, risky, and extremely risky. In the Campton regression analysis, the total number of risky and extremely risky events in 15-minute intervals is used as the dependent variable.

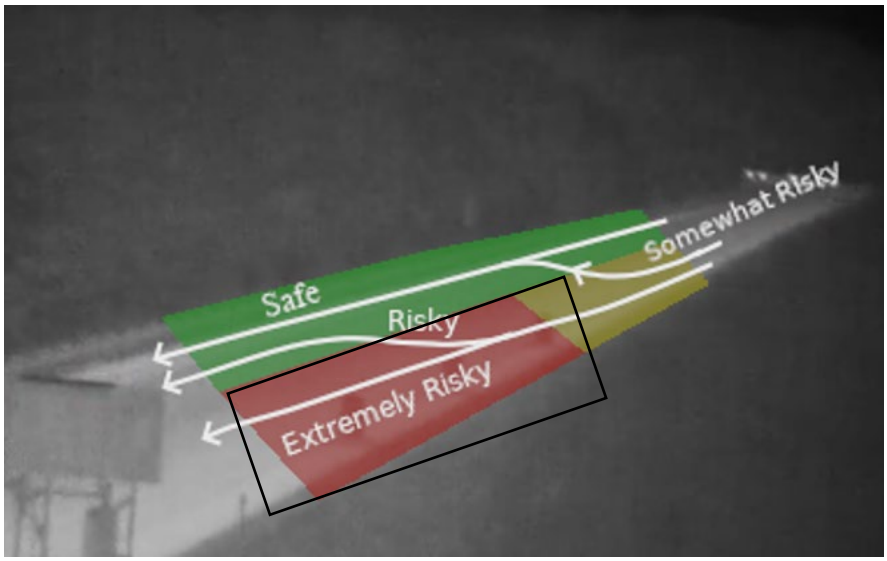

Figure 5.1. Vehicle tracking and detection of risky last-minute merges

Among the variables, freeway and exit ramp traffic volumes were derived using thermal videos and AI techniques. Speeds were derived based on radar data. Last-minute merges and risky merges were counted using AI models. Specifically, we segmented both vehicles and travel lanes. In this way, the impacts of occasional changes in the camera field of view (due to vibration) on vehicle tracking can be mitigated. By assessing the overlap between vehicle segmentation masks and the segmented risky region (e.g., red zone inside the rectangle in Figure 5.1), we were able to detect risky last-minute merges and record the corresponding frame numbers and time stamps. The speed, traffic volume, and last-minute/risky merge data were aggregated using 15-minute intervals so that each hour resulted in four data points.

5.2 Multicollinearity and Variable Selection

In multiple linear regression, it is important to carefully choose independent variables to mitigate multicollinearity, which occurs when two or more independent variables are highly correlated with each other. Significant multicollinearity can lead to inaccurate estimates of the individual effects of each independent variable or predictor.

Two categories of methods can be used to address the multicollinearity issue. The first category involves using regularization techniques such as Ridge Regression and Lasso Regression to penalize the inclusion of highly correlated predictors. The second category attempts to identify and remove highly correlated predictors, utilizing methods such as variance inflation factor (VIF) analysis. In our last-minute/risky merge analysis for the Medford and Danvers sites, the VIF method was used, which revealed a high level of correlation between predictors “Normal” and “Long.” This is not surprising since we considered last-minute merges when there was a work zone, and a work zone either had a normal taper or a longer taper. In the speed regression analysis, normal traffic scenarios

without a work zone were also included. In this case, the VIF analysis did not show any significant multicollinearity issues.

Furthermore, the predictors have varying ranges of values; for instance, traffic volume may range from tens to hundreds, while rumble strip data is binary. To facilitate variable importance comparison, we standardized those noncategorical predictors.

5.3 Regression Results

The regression analysis generates extensive results that are presented in Figure 5.2 through Figure 5.8. The results for the Medford and Danvers sites are further summarized in Table 5.2, since the two sites share the same work zone control strategies. Table 5.3 summarizes the results for the Campton site. Throughout the remainder of this subsection, only variables that are statistically significant at the 0.05 level will be discussed.

The same work zone control strategies were deployed at Medford and Danvers, which were transverse rumble strips and different lane closure taper lengths. In Table 5.2, statistically insignificant variables are shown in italic font. The results suggest that Normal Taper, Longer Taper, and Rumble Strips all contribute to decreasing speeds. However, the results are inconsistent and should be interpreted with caution. The relationship between "Normal/Longer Taper" and "reduced speeds" might be correlational rather than causal. Since we also incorporate data from non-work-zone scenarios in speed regression analysis, the reduction in speeds may be attributed to the presence of a work zone, which correlates with either a "Normal" or a "Longer" taper. Additionally, Rumble Strips are associated with significant speed reductions only at the Medford M3 location but not at other locations. This inconsistency might be attributed to the disturbance caused by exiting vehicles. Overall, the speed regression results at the Medford and Danvers sites suggest that

- No statistically significant and consistent evidence show that Rumble Strips can reduce vehicle approaching speed; and
- Although both Normal and Longer tapers are associated with speed reductions in most cases, such relationships are inconsistent. They most likely are due to correlation rather than causation and should be interpreted with caution. There is no consistent evidence showing that a longer taper is more beneficial in reducing vehicle approaching speed.

At the two Medford locations (i.e., M2 and M3), freeway volume is positively associated with speed, while exit volume is negatively associated with speed. Both variables are statistically significant at the 0.05 confidence level. This result seems reasonable and demonstrates the impact of exiting traffic on vehicle speed. As vehicles exit the freeway, they gradually decelerate, which affects the average speed. At the two Danvers locations (i.e., D1 and D2), only the Total_EXIT variable at D2 is statistically significant at the 0.05 level and is positively associated with speed. This seemingly contradictory result is due to the location of D2, which is downstream of the exit ramp. (Note that M3 at Medford is upstream of the exit ramp.) Therefore, more exiting traffic does not negatively affect the average freeway speed.

Table 5.2. Medford and Danvers regression results

Dependent Variable	Location	Independent Variable	Coefficient	p-value
Speed	Medford M2	Total_FREEWAY	6.17	0.00
	Medford M2	Total_EXIT	−9.90	0.00
	Medford M2	Long	−1.55	0.02
	Medford M2	Normal	−2.15	0.00
	Medford M2	*Rumble*	*−0.54*	*0.25*
	Medford M3	Total_FREEWAY	17.54	0.00
	Medford M3	Total_EXIT	−22.23	0.00
	Medford M3	*Long*	*0.30*	*0.67*
	Medford M3	Normal	−1.57	0.00
	Medford M3	Rumble	−2.28	0.00
Last-Minute Merge	Medford Lane Closure Taper	*Total_FREEWAY*	*−0.01*	*0.97*
	Medford Lane Closure Taper	Total_EXIT	7.54	0.00
	Medford Lane Closure Taper	*mean_abs_speed*	*−1.19*	*0.23*
	Medford Lane Closure Taper	*Normal*	*−0.71*	*0.07*
	Medford Lane Closure Taper	*Rumble*	*−0.52*	*0.20*
Speed	Danvers D1	*Total_FREEWAY*	*1.75*	*0.13*
	Danvers D1	*Total_EXIT*	*1.89*	*0.39*
	Danvers D1	Long	−4.07	0.00
	Danvers D1	Normal	−3.51	0.00
	Danvers D1	*Rumble*	*0.44*	*0.46*
	Danvers D2	*Total_FREEWAY*	*−0.78*	*0.51*
	Danvers D2	Total_EXIT	4.79	0.03
	Danvers D2	Long	−5.08	0.00
	Danvers D2	Normal	−3.77	0.00
	Danvers D2	*Rumble*	*0.67*	*0.26*
Last-Minute Merge	Danvers Lane Closure Taper	Total_FREEWAY	1.78	0.01
	Danvers Lane Closure Taper	*Total_EXIT*	*1.13*	*0.20*
	Danvers Lane Closure Taper	*mean_abs_speed*	*0.74*	*0.14*
	Danvers Lane Closure Taper	*Normal*	*−0.02*	*0.92*
	Danvers Lane Closure Taper	*Rumble*	*0.24*	*0.36*

For the Medford site, Total_EXIT traffic is positively associated with last-minute merges, and all other independent variables are statistically insignificant. This is probably because some through vehicles followed exiting vehicles and failed to merge early. For the Danvers site, only the Total_FREEWAY variable is statistically significant and is positively associated with last-minute merges. This result is also understandable because drivers tend to merge late in congested traffic.

The Campton site regression results in Table 5.3 are more intuitive and easier to interpret than those for the Medford and Danvers sites. For the speed modeling results, only one

variable, “ON,” is statistically significant at the 0.05 level. This suggests that a FSLS is more effective than PCMS and static speed limit signs in reducing vehicle speed. This finding aligns with common understanding. Compared to PCMS, FSLS appears to be a more direct and effective way of communicating warning messages to drivers. Drivers do not need to read long messages to comprehend what is happening ahead of them.

The results of the risky merge regression analysis also indicate that both FSLS and PCMS are effective in encouraging early merging. However, FSLS appears to be twice as effective as PCMS. Traffic volume shows a strong positive correlation with risky merges. This is reasonable. In fact, late merge (not risky merge) is often encouraged when the traffic is congested [*14*], although it may inevitably lead to risky merging scenarios as defined in this study. The true risk of a merge should be assessed by accounting for vehicle speeds and time headways.

Additionally, the adjusted R^2 value (Figure 5.8) for the Campton site risky merge model is 0.768, which is much higher than those for the Medford and Danvers sites. This suggests that the Campton site risky merges can be properly explained by three factors: FSLS, PCMS, and traffic volume. At Danvers and Medford, the last-minute merges probably also depend on other factors not observed during our study. Another possibility is that the relationship between last-minute merges and the independent variables is nonlinear.

The adjusted R^2 value (Figure 5.9) for the Campton site speed model is 0.101, which is lower than those for the Danvers and Medford sites. This is likely due to the exclusion of significant factors, such as the presence of construction workers, in the Campton site model. Unlike the Campton site, both the Medford and Danvers sites experienced construction activities throughout the entire work zone.

Last but not least, the Campton dataset covers both daytime and nighttime, which is different from the Danvers and Medford work zones. To quantify the impacts of the time of day on work zone speed and late merges, we developed additional models for the Campton site and presented the results in Table 5.4, Figure 5.10, and Figure 5.11. Because the data was collected in the summer of 2023, daylight spanned from 5:30 a.m. to 8:15 p.m. We considered nighttime as the baseline. After incorporating the daytime factor, the R^2 values for the merge and speed regression models increased to 0.782 and 0.166, respectively (Figure 5.10 and Figure 5.11). This indicates that including the daylight factor is necessary and can improve the models’ goodness of fit. Based on the new models, both displaying “merge early” message (ME=1) and higher traffic volumes can reduce vehicle approaching speeds. Higher speeds will increase the chance of risky merges. In addition, drivers tend to drive slower and merge later at nighttime than in daytime work zones.

Table 5.3. Campton results without considering the time of day

Dependent variable	Independent variable	Coefficient	p-value
Speed	*Volume*	*−0.83*	*0.22*
	UP	*0.13*	*0.84*
	ON	−2.48	0.00
	ME	*−0.76*	*0.18*
Risky Merge	Volume	31.97	0.00
	mean_abs_speed	*1.42*	*0.43*
	UP	*1.08*	*0.13*
	ON	−4.52	0.00
	ME	−2.01	0.00

Table 5.4. Campton results considering the time of day

Dependent variable	Independent variable	Coefficient	p-value
Speed	Volume	−5.59	0.00
	UP	*0.47*	*0.43*
	ON	−3.22	0.00
	ME	−1.09	0.05
	Daylight	2.81	0.00
Risky Merge	Volume	37.07	0.00
	mean_abs_speed	3.88	0.03
	UP	*0.71*	*0.31*
	ON	−3.57	0.00
	ME	−1.61	0.01
	Daylight	−2.98	0.00

```
==============================================================================
Dep. Variable:         mean_abs_speed   R-squared:                       0.287
Model:                            OLS   Adj. R-squared:                  0.271
Method:                 Least Squares   F-statistic:                     17.55
Date:                Mon, 18 Mar 2024   Prob (F-statistic):           1.35e-14
Time:                        23:16:05   Log-Likelihood:                -500.45
No. Observations:                 224   AIC:                             1013.
Df Residuals:                     218   BIC:                             1033.
Df Model:                           5
Covariance Type:            nonrobust
==============================================================================
                 coef    std err          t      P>|t|      [0.025      0.975]
------------------------------------------------------------------------------
const         62.6205      0.382    164.053      0.000      61.868      63.373
Total_FREEWAY  6.1744      1.872      3.298      0.001       2.484       9.864
Total_EXIT    -9.9012      1.943     -5.097      0.000     -13.730      -6.072
Long          -1.5465      0.656     -2.357      0.019      -2.840      -0.253
Normal        -2.1494      0.462     -4.650      0.000      -3.060      -1.238
Rumble        -0.5382      0.465     -1.157      0.249      -1.455       0.379
==============================================================================
Omnibus:                       15.775   Durbin-Watson:                   0.802
Prob(Omnibus):                  0.000   Jarque-Bera (JB):               17.026
Skew:                           0.655   Prob(JB):                     0.000201
Kurtosis:                       3.332   Cond. No.                         23.5
==============================================================================
```

Figure 5.2. Medford M2 upstream speed regression results

```
==============================================================================
Dep. Variable:         mean_abs_speed   R-squared:                       0.395
Model:                            OLS   Adj. R-squared:                  0.379
Method:                 Least Squares   F-statistic:                     24.95
Date:                Mon, 18 Mar 2024   Prob (F-statistic):           2.58e-19
Time:                        23:40:06   Log-Likelihood:                -437.67
No. Observations:                 197   AIC:                             887.3
Df Residuals:                     191   BIC:                             907.0
Df Model:                           5
Covariance Type:            nonrobust
==============================================================================
                 coef    std err          t      P>|t|      [0.025      0.975]
------------------------------------------------------------------------------
const         62.9441      0.467    134.723      0.000      62.023      63.866
Total_FREEWAY 17.5414      3.045      5.761      0.000      11.536      23.547
Total_EXIT   -22.2271      3.035     -7.324      0.000     -28.213     -16.241
Long           0.3032      0.710      0.427      0.670      -1.096       1.703
Normal        -1.5700      0.517     -3.036      0.003      -2.590      -0.550
Rumble        -2.2811      0.464     -4.913      0.000      -3.197      -1.365
==============================================================================
Omnibus:                       18.528   Durbin-Watson:                   1.049
Prob(Omnibus):                  0.000   Jarque-Bera (JB):               40.830
Skew:                           0.406   Prob(JB):                     1.36e-09
Kurtosis:                       5.077   Cond. No.                         35.1
==============================================================================
```

Figure 5.3. Medford M2 downstream speed regression results

```
==============================================================================
Dep. Variable:                  Merge   R-squared:                       0.436
Model:                            OLS   Adj. R-squared:                  0.415
Method:                 Least Squares   F-statistic:                     21.31
Date:                Mon, 18 Mar 2024   Prob (F-statistic):           9.31e-16
Time:                        23:42:21   Log-Likelihood:                -281.56
No. Observations:                 144   AIC:                             575.1
Df Residuals:                     138   BIC:                             592.9
Df Model:                           5
Covariance Type:            nonrobust
==============================================================================
                 coef    std err          t      P>|t|      [0.025      0.975]
------------------------------------------------------------------------------
const          1.4264      0.759      1.878      0.062      -0.075       2.928
Total_FREEWAY -0.0836      2.139     -0.039      0.969      -4.314       4.147
Total_EXIT     7.5361      2.322      3.246      0.001       2.945      12.127
mean_abs_speed -1.1920     0.994     -1.199      0.233      -3.158       0.774
Normal         -0.7112     0.391     -1.820      0.071      -1.484       0.061
Rumble         -0.5225     0.409     -1.277      0.204      -1.332       0.287
==============================================================================
Omnibus:                       95.655   Durbin-Watson:                   1.583
Prob(Omnibus):                  0.000   Jarque-Bera (JB):              845.643
Skew:                           2.224   Prob(JB):                     2.35e-184
Kurtosis:                      14.007   Cond. No.                         32.7
==============================================================================
```

Figure 5.4. Medford last-minute merge regression results

```
==============================================================================
Dep. Variable:         mean_abs_speed   R-squared:                       0.290
Model:                            OLS   Adj. R-squared:                  0.278
Method:                 Least Squares   F-statistic:                     23.30
Date:                Tue, 19 Mar 2024   Prob (F-statistic):           1.29e-19
Time:                        14:16:09   Log-Likelihood:                -710.61
No. Observations:                 291   AIC:                             1433.
Df Residuals:                     285   BIC:                             1455.
Df Model:                           5
Covariance Type:            nonrobust
==============================================================================
                 coef    std err          t      P>|t|      [0.025      0.975]
------------------------------------------------------------------------------
const         66.6470      0.312    213.621      0.000      66.033      67.261
Total_FREEWAY  1.7525      1.158      1.513      0.131      -0.527       4.032
Total_EXIT     1.8912      2.218      0.853      0.394      -2.474       6.256
Long          -4.0751      0.721     -5.651      0.000      -5.495      -2.656
Normal        -3.5109      0.474     -7.412      0.000      -4.443      -2.579
Rumble         0.4377      0.597      0.733      0.464      -0.738       1.613
==============================================================================
Omnibus:                       21.022   Durbin-Watson:                   0.687
Prob(Omnibus):                  0.000   Jarque-Bera (JB):               39.832
Skew:                           0.400   Prob(JB):                     2.24e-09
Kurtosis:                       4.626   Cond. No.                         18.0
==============================================================================
```

Figure 5.5. Danvers D1 downstream speed regression results

```
==============================================================================
Dep. Variable:         mean_abs_speed   R-squared:                       0.334
Model:                            OLS   Adj. R-squared:                  0.323
Method:                 Least Squares   F-statistic:                     28.80
Date:                Tue, 19 Mar 2024   Prob (F-statistic):           1.18e-23
Time:                        14:24:19   Log-Likelihood:                -719.29
No. Observations:                 293   AIC:                             1451.
Df Residuals:                     287   BIC:                             1473.
Df Model:                           5
Covariance Type:            nonrobust
==============================================================================
                 coef    std err          t      P>|t|      [0.025      0.975]
------------------------------------------------------------------------------
const         68.0606      0.315    215.999      0.000      67.440      68.681
Total_FREEWAY -0.7756      1.172     -0.662      0.509      -3.083       1.531
Total_EXIT     4.7889      2.233      2.144      0.033       0.393       9.185
Long          -5.0755      0.723     -7.025      0.000      -6.498      -3.653
Normal        -3.7730      0.479     -7.870      0.000      -4.717      -2.829
Rumble         0.6678      0.595      1.123      0.263      -0.503       1.839
==============================================================================
Omnibus:                       35.620   Durbin-Watson:                   0.610
Prob(Omnibus):                  0.000   Jarque-Bera (JB):               54.403
Skew:                           0.753   Prob(JB):                     1.54e-12
Kurtosis:                       4.479   Cond. No.                         18.0
==============================================================================
```

Figure 5.6. Danvers D2 downstream speed regression results

```
==============================================================================
Dep. Variable:                  Merge   R-squared:                       0.309
Model:                            OLS   Adj. R-squared:                  0.282
Method:                 Least Squares   F-statistic:                     11.54
Date:                Tue, 19 Mar 2024   Prob (F-statistic):           3.19e-09
Time:                        14:32:10   Log-Likelihood:                -199.87
No. Observations:                 135   AIC:                             411.7
Df Residuals:                     129   BIC:                             429.2
Df Model:                           5
Covariance Type:            nonrobust
==============================================================================
                 coef    std err          t      P>|t|      [0.025      0.975]
------------------------------------------------------------------------------
const         -0.3672      0.360     -1.020      0.309      -1.079       0.345
Total_FREEWAY  1.7792      0.668      2.665      0.009       0.458       3.100
Total_EXIT     1.1266      0.866      1.301      0.196      -0.587       2.841
mean_abs_speed 0.7418      0.502      1.479      0.142      -0.251       1.734
Normal        -0.0246      0.230     -0.107      0.915      -0.479       0.430
Rumble         0.2411      0.265      0.911      0.364      -0.282       0.764
==============================================================================
Omnibus:                       58.668   Durbin-Watson:                   2.053
Prob(Omnibus):                  0.000   Jarque-Bera (JB):              207.627
Skew:                           1.596   Prob(JB):                     8.21e-46
Kurtosis:                       8.169   Cond. No.                         16.4
==============================================================================
```

Figure 5.7. Danvers last-minute merge regression results

```
==============================================================================
Dep. Variable:                      y   R-squared:                       0.770
Model:                            OLS   Adj. R-squared:                  0.768
Method:                 Least Squares   F-statistic:                     348.5
Date:                Mon, 18 Mar 2024   Prob (F-statistic):          1.99e-163
Time:                        22:40:07   Log-Likelihood:                -1424.9
No. Observations:                 526   AIC:                             2862.
Df Residuals:                     520   BIC:                             2887.
Df Model:                           5
Covariance Type:            nonrobust
==============================================================================
                 coef    std err          t      P>|t|      [0.025      0.975]
------------------------------------------------------------------------------
const         -2.1603      1.396     -1.547      0.122      -4.903       0.582
VOLUME        31.9679      0.779     41.029      0.000      30.437      33.499
UP             1.0821      0.714      1.516      0.130      -0.321       2.485
ON            -4.5271      0.538     -8.418      0.000      -5.584      -3.471
ME            -2.0094      0.653     -3.076      0.002      -3.293      -0.726
mean_abs_speed  1.4238     1.802      0.790      0.430      -2.115       4.963
==============================================================================
Omnibus:                       94.384   Durbin-Watson:                   1.312
Prob(Omnibus):                  0.000   Jarque-Bera (JB):              433.746
Skew:                           0.708   Prob(JB):                     6.51e-95
Kurtosis:                       7.217   Cond. No.                         21.8
==============================================================================
```

Figure 5.8. Campton last-minute merge regression results without considering time of day

```
==============================================================================
Dep. Variable:         mean_abs_speed   R-squared:                       0.108
Model:                            OLS   Adj. R-squared:                  0.101
Method:                 Least Squares   F-statistic:                     15.76
Date:                Mon, 18 Mar 2024   Prob (F-statistic):           3.46e-12
Time:                        23:01:54   Log-Likelihood:                 529.51
No. Observations:                 526   AIC:                            -1049.
Df Residuals:                     521   BIC:                            -1028.
Df Model:                           4
Covariance Type:            nonrobust
==============================================================================
                 coef    std err          t      P>|t|      [0.025      0.975]
------------------------------------------------------------------------------
const          0.7562      0.007    101.939      0.000       0.742       0.771
VOLUME        -0.0233      0.019     -1.232      0.218      -0.060       0.014
UP             0.0035      0.017      0.203      0.839      -0.031       0.038
ON            -0.0694      0.013     -5.459      0.000      -0.094      -0.044
ME            -0.0213      0.016     -1.342      0.180      -0.052       0.010
==============================================================================
Omnibus:                      272.483   Durbin-Watson:                   1.622
Prob(Omnibus):                  0.000   Jarque-Bera (JB):             3178.829
Skew:                          -1.985   Prob(JB):                         0.00
Kurtosis:                      14.370   Cond. No.                         8.49
==============================================================================
```

Figure 5.9. Campton speed regression results without considering time of day

OLS Regression Results

Dep. Variable:	y	R-squared:	0.782
Model:	OLS	Adj. R-squared:	0.779
Method:	Least Squares	F-statistic:	310.3
Date:	Wed, 17 Apr 2024	Prob (F-statistic):	4.41e-168
Time:	17:00:07	Log-Likelihood:	-1411.0
No. Observations:	526	AIC:	2836.
Df Residuals:	519	BIC:	2866.
Df Model:	6		
Covariance Type:	nonrobust		

	coef	std err	t	P>|t|	[0.025	0.975]
const	-3.6360	1.389	-2.618	0.009	-6.365	-0.907
VOLUME	37.0667	1.224	30.273	0.000	34.661	39.472
mean_abs_speed	3.8766	1.816	2.135	0.033	0.309	7.444
UP	0.7054	0.700	1.008	0.314	-0.669	2.080
ON	-3.5697	0.554	-6.439	0.000	-4.659	-2.481
ME	-1.6050	0.641	-2.503	0.013	-2.865	-0.345
Daylight	-2.9823	0.562	-5.309	0.000	-4.086	-1.879

Omnibus:	75.278	Durbin-Watson:	1.386
Prob(Omnibus):	0.000	Jarque-Bera (JB):	324.648
Skew:	0.554	Prob(JB):	3.19e-71
Kurtosis:	6.686	Cond. No.	24.6

Figure 5.10. Campton last-minute merge regression results considering time of day

OLS Regression Results

Dep. Variable:	mean_abs_speed	R-squared:	0.166
Model:	OLS	Adj. R-squared:	0.158
Method:	Least Squares	F-statistic:	20.65
Date:	Wed, 17 Apr 2024	Prob (F-statistic):	7.72e-19
Time:	16:54:01	Log-Likelihood:	-1333.9
No. Observations:	526	AIC:	2680.
Df Residuals:	520	BIC:	2705.
Df Model:	5		
Covariance Type:	nonrobust		

	coef	std err	t	P>|t|	[0.025	0.975]
const	63.4667	0.263	240.931	0.000	62.949	63.984
VOLUME	-5.5864	1.028	-5.436	0.000	-7.605	-3.567
UP	0.4729	0.603	0.784	0.434	-0.712	1.658
ON	-3.2233	0.457	-7.053	0.000	-4.121	-2.325
ME	-1.0925	0.551	-1.982	0.048	-2.176	-0.009
Daylight	2.8117	0.469	5.998	0.000	1.891	3.733

Omnibus:	262.980	Durbin-Watson:	1.769
Prob(Omnibus):	0.000	Jarque-Bera (JB):	3357.990
Skew:	-1.860	Prob(JB):	0.00
Kurtosis:	14.806	Cond. No.	12.3

Figure 5.11. Campton speed regression results considering time of day

6.0 Conclusions and Discussion

Given their substantial impacts on traffic operations and safety, highway work zones are attracting increasing attention. This study focuses on utilizing vehicle segment speed profiles and trajectory data collected in the field to evaluate four work zone control strategies:

- Transverse rumble strips.
- Normal versus longer lane closure taper lengths.
- Flashing speed limit sign.
- Portable changeable message sign.

Ultrahigh-definition radar and thermal camera sensors were utilized to collect data from two work zones in Massachusetts. In addition, radar and thermal video data collected from a work zone in New Hampshire was kindly made available for this study by the New England Transportation Consortium. Compared to previous studies that relied on speed data measured at limited locations, this research utilizes (1) vehicle speed profiles along a road segment, and (2) vehicle trajectories at the beginning of a work zone lane closure taper. Such detailed data makes it possible to closely examine how drivers react to different work zone control strategies.

This study is the first application of ultrahigh-definition radars to track vehicles along a road segment. It demonstrates the feasibility of using radars to generate vehicle trajectories, classify them, and separate their trajectories by lanes. The radar data collection process has provided valuable lessons that can guide future research and data collection endeavors.

This project has also developed YOLOv8-based deep learning models to process the collected thermal video data and extract vehicle trajectories. The exploration of deep-learning-based trajectory data extraction and processing within the scope of this project has generated important insights into vehicle merging behavior at nighttime work zone lane closure tapers. This study demonstrates, for the first time, the potential of thermal cameras and deep learning in studying nighttime work zone safety and traffic operations.

Based on the derived speed and last-minute merge data, both descriptive and statistical analyses have been conducted. Key findings from our research are the following:

- The developed deep learning models accurately detect and track vehicles from thermal videos during both daytime and nighttime. They can categorize vehicles into small, medium, and large classes, enabling a nuanced examination of how different vehicle types interact with work zone layouts.
- The deep learning models also segment critical roadway features, allowing for the detection of vehicles' proximity to work zone lane closure tapers. This provides important insights into potential safety hazards and operational inefficiencies.

- This research found no consistent and statistically significant evidence demonstrating that transverse rumble strips effectively reduce vehicle speeds as they approach a work zone or encourage early merging. Similarly, there is no clear evidence indicating that a longer lane closure taper length is either more or less effective than the normal taper length in achieving these outcomes.
- Both the flashing speed limit sign (FSLS) and portable changeable message sign (PCMS) are helpful in encouraging early merging. However, FSLS appears to be twice as effective as PCMS.
- Both FSLS and PCMS appear to be statistically effective in reducing vehicle approaching speed when the daytime factor is considered. However, FSLS is three times more effective than PCMS.
- Providing a taper length longer than what is specified in the MassDOT Work Zone Safety Manual [*3*] does not appear to be necessary.

The two work zones in Massachusetts both had exit ramps near the lane closure taper, which made it challenging to distinguish the effects of exiting vehicles from the impacts of taper length and transverse rumble strips. For future research, it would be beneficial to explore work zones unaffected by on and off ramps. Also, increasing the sample size and collecting data from more work zones would be helpful. Additionally, mounting radar and camera sensors directly above the traffic could provide clearer data.

7.0 References

1 National Work Zone Safety Information Clearinghouse. Work Zone Traffic Crash Trends and Statistics. Available online at https://workzonesafety.org/work-zone-data/work-zone-traffic-crash-trends-and-statistics/, accessed on March 17, 2024.

2 FHWA, Making Work Zones Work Better. Available online at https://ops.fhwa.dot.gov/aboutus/one_pagers/wz.htm, accessed on March 17, 2024.

3 Massachusetts DOT. Work Zone Safety: Temporary Traffic Control – Typical Details and Massachusetts Guidelines for MassDOT, Municipalities, Utilities, and Contractors.

4 Xie, Y., Liu, R., Bhuyan, Z., Chen, D., Ge, T., Shirazi, M., Vergara, E., & Aviles-Ordonez, J. (2023). Current Status of Transportation Data Analytics and Pilot Case Studies Using Artificial Intelligence (AI). New England Transportation Consortium Project Report NETC124.

5 Jocher, G., Chaurasia, A., & Qiu, J. (2023). Ultralytics YOLO (Version 8.0.0) [Computer software]. https://github.com/ultralytics/ultralytics.

6 Zhang, Y., Sun, P., Jiang, Y., Yu, D., Yuan, Z., Luo, P., Liu, W., & Wang, X. (2021). ByteTrack: Multi-Object Tracking by Associating Every Detection Box. European Conference on Computer Vision.

7 Wu, Z., Fuller, N.W., Theriault, D.H., & Betke, M. (2014). A Thermal Infrared Video Benchmark for Visual Analysis. 2014 IEEE Conference on Computer Vision and Pattern Recognition Workshops, 201-208.

8 Muhammad Ali Farooq, Waseem Shariff, Faisal Khan, Peter Corcoran, Cosmin Rotariu. "C3I Thermal Automotive Dataset." doi: 10.21227/jf21-rt22.

9 Davis, J.W., & Keck, M.A. (2005). A Two-Stage Template Approach to Person Detection in Thermal Imagery. 2005 Seventh IEEE Workshops on Applications of Computer Vision (WACV/MOTION'05) - Volume 1, 1, 364-369.

10 National Mittal, U., & Chawla, P. (2022). Vehicle detection and traffic density estimation using ensemble of deep learning models. Multimedia Tools and Applications, 82, 10397-10419.

11 Kang, Q., Zhao, H., Yang, D., Ahmed, H.S., & Ma, J. (2020). Lightweight convolutional neural network for vehicle recognition in thermal infrared images. Infrared Physics & Technology.

12 Bhuyan, Z., Chen, Q., Xie, Y., Cao, Y., & Liu, B. (2023). Modeling the Risk of Truck Rollover Crashes on Highway Ramps Using Drone Video Data and Mask-RCNN. IEEE 26th International Conference on Intelligent Transportation Systems (ITSC), 4052-4058.

13 Rafique, A.A., Al-Rasheed, A., Ksibi, A., Ayadi, M., Jalal, A., Alnowaiser, K., Meshref, H., Shorfuzzaman, M., Gochoo, M., & Park, J. (2023). Smart Traffic Monitoring Through Pyramid Pooling Vehicle Detection and Filter-Based Tracking on Aerial Images. IEEE Access, 11, 2993-3007.

14 Algomaiah, M., & Li, Z. (2021). Exploring work zone late merge strategies with and without enabling connected vehicles technologies. Transportation research interdisciplinary perspectives, 9, 100316.

8.0 Appendices

Appendix A. Speed Distributions

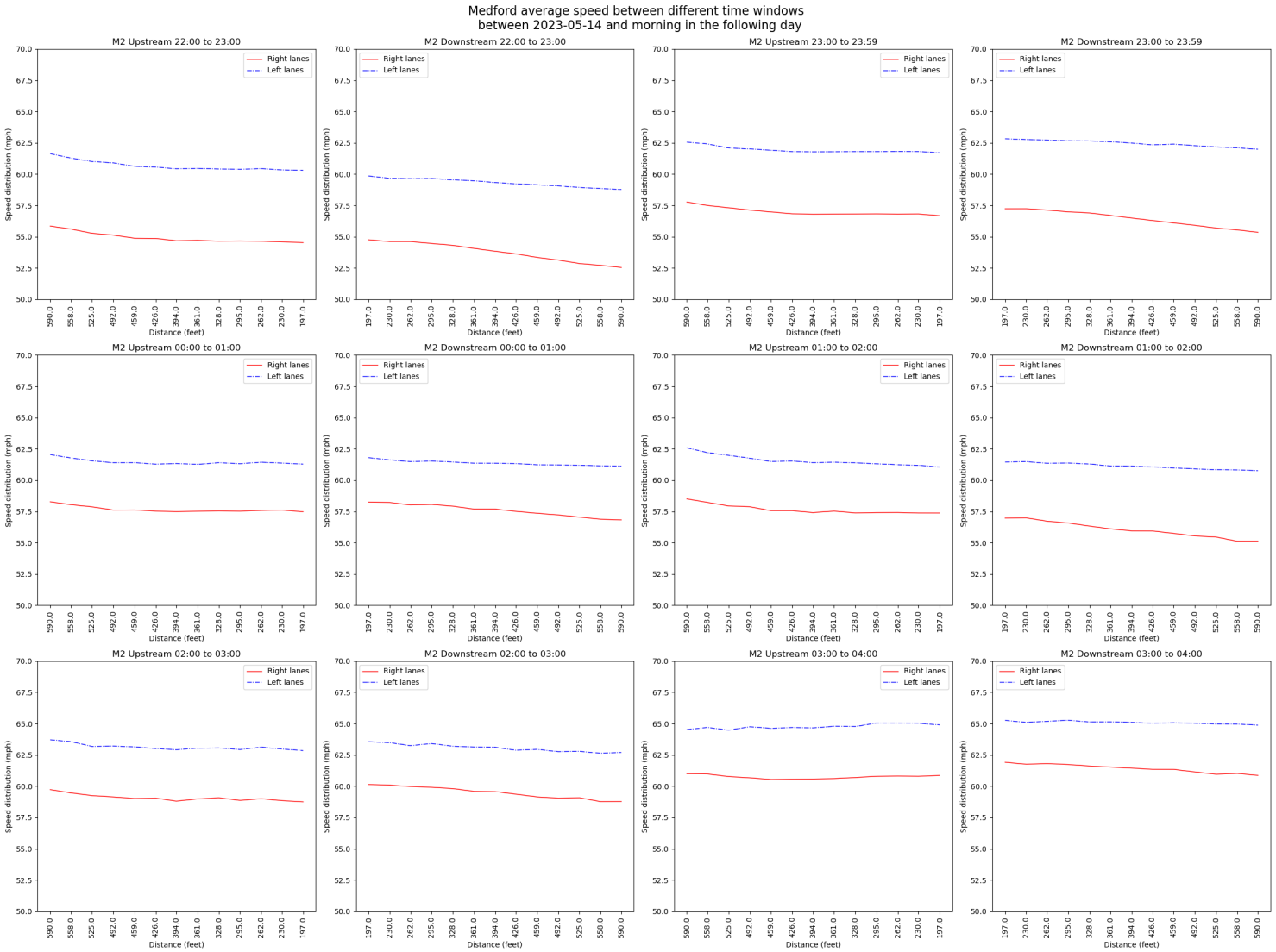

Figure 8.1. Medford speed profile on late 5-14-2023 and early 5-15-2023

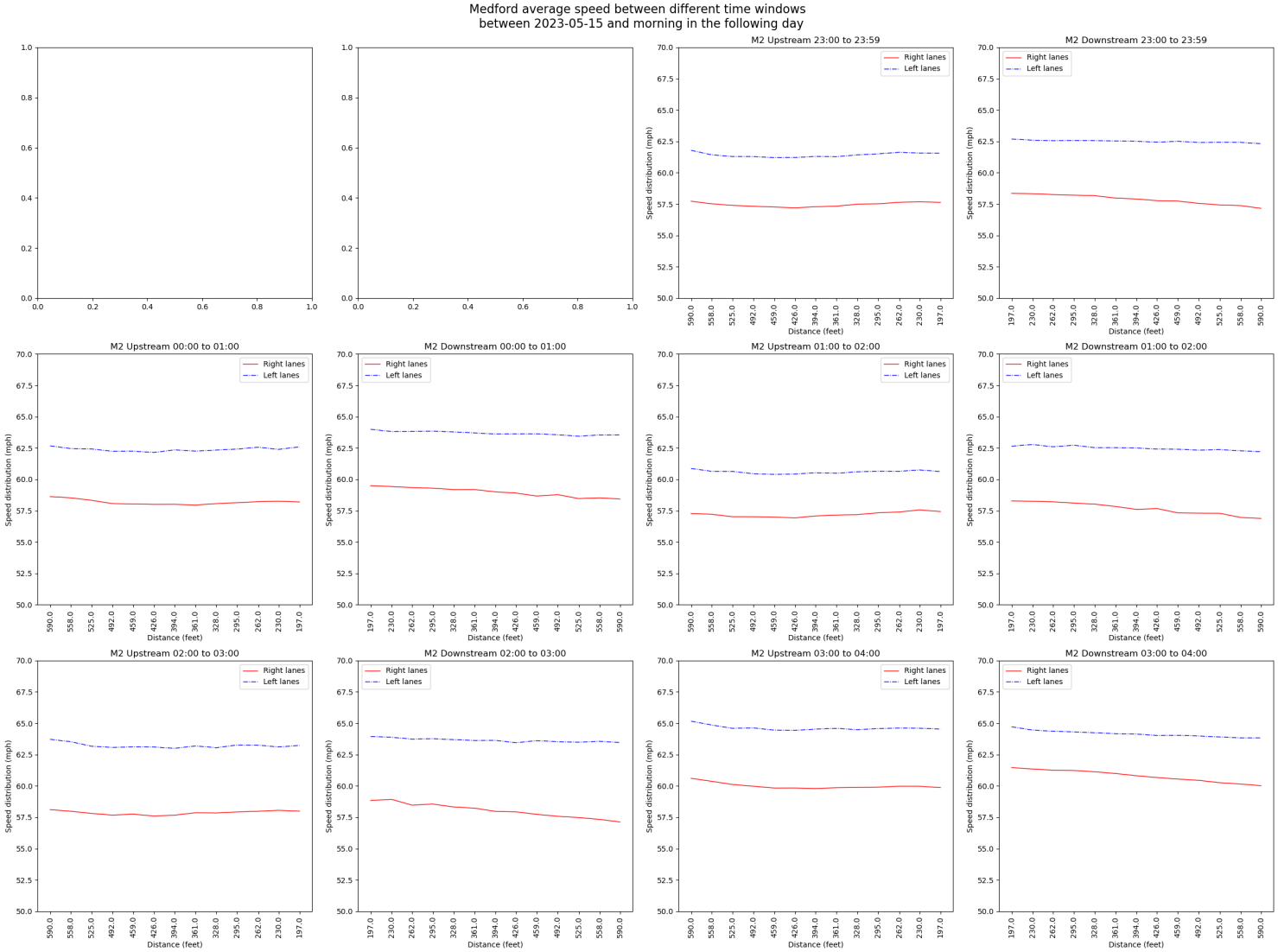

Figure 8.2. Medford speed profile on late 5-15-2023 and early 5-16-2023

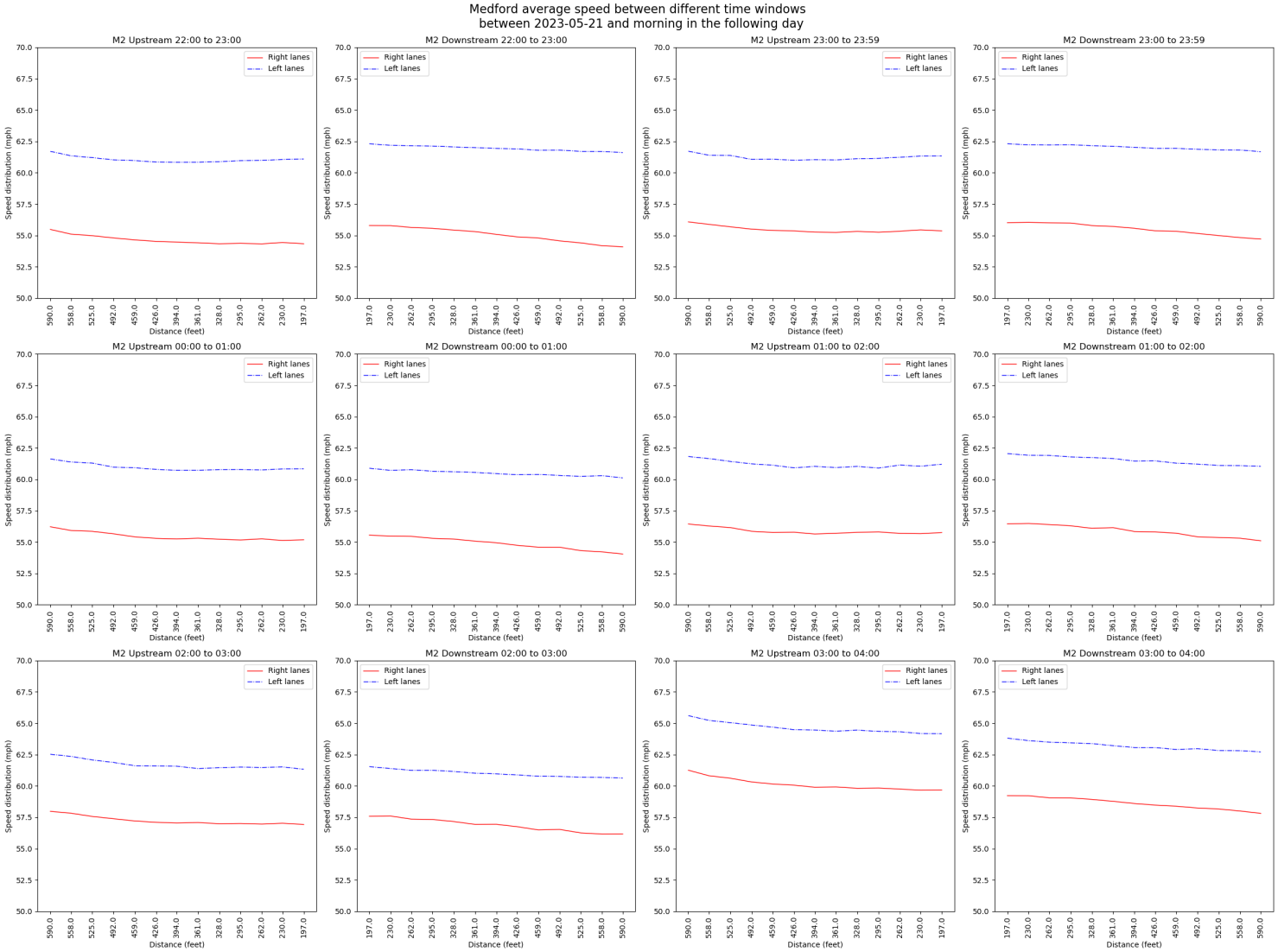

Figure 8.3. Medford speed profile on late 5-21-2023 and early 5-22-2023

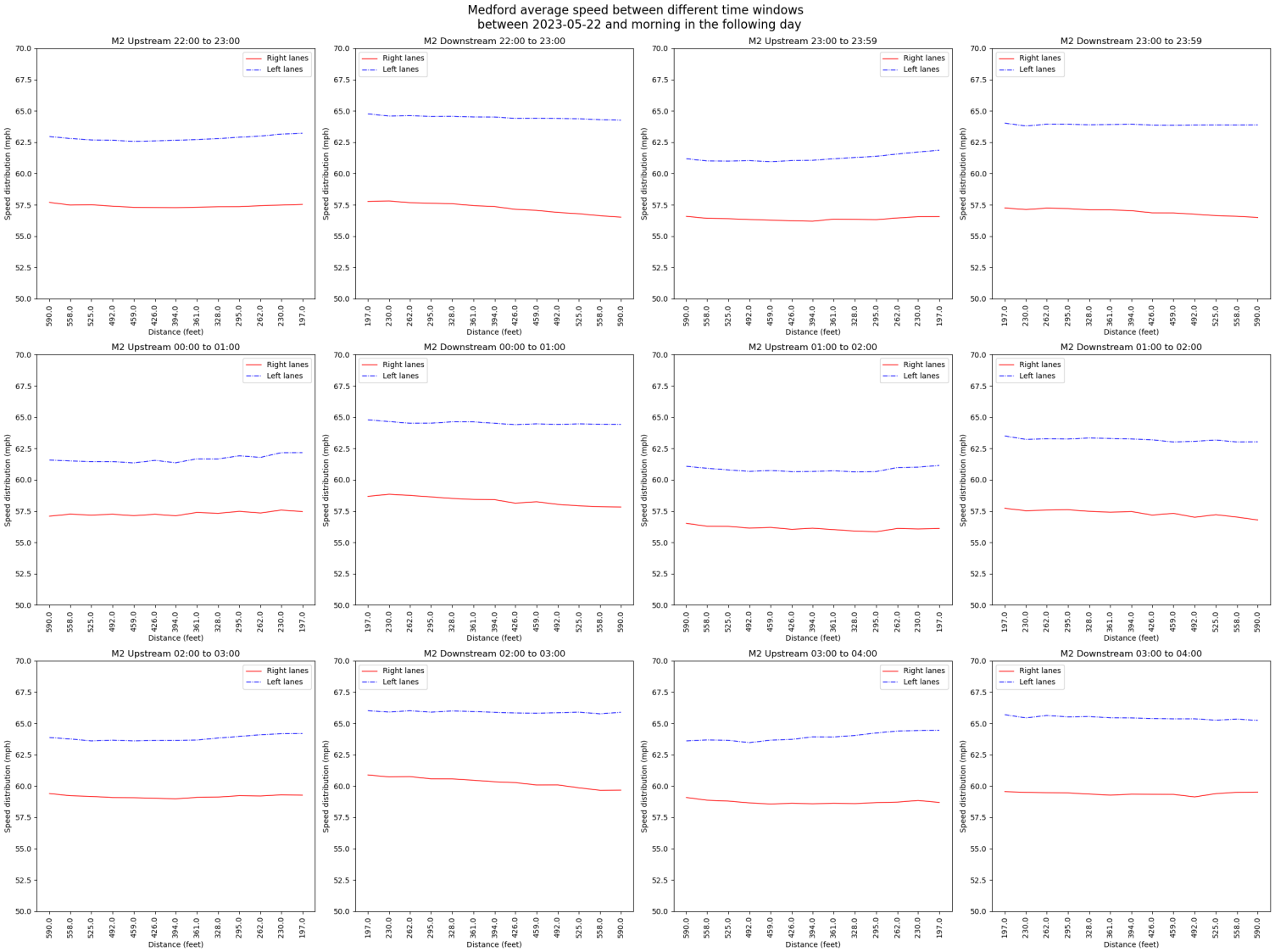

Figure 8.4. Medford speed profile on late 5-22-2023 and early 5-23-2023

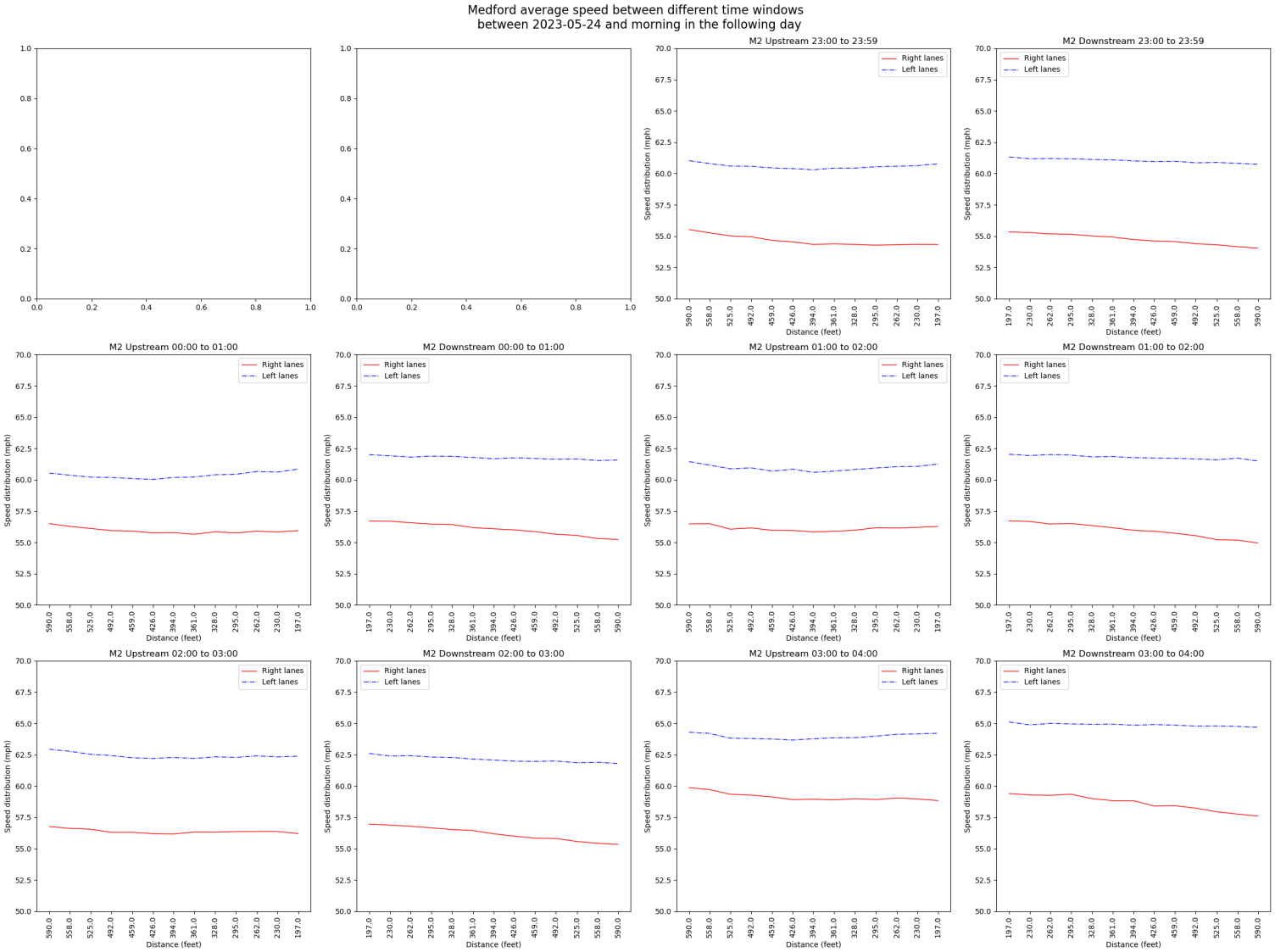

Figure 8.5. Medford speed profile on late 5-24-2023 and early 5-25-2023

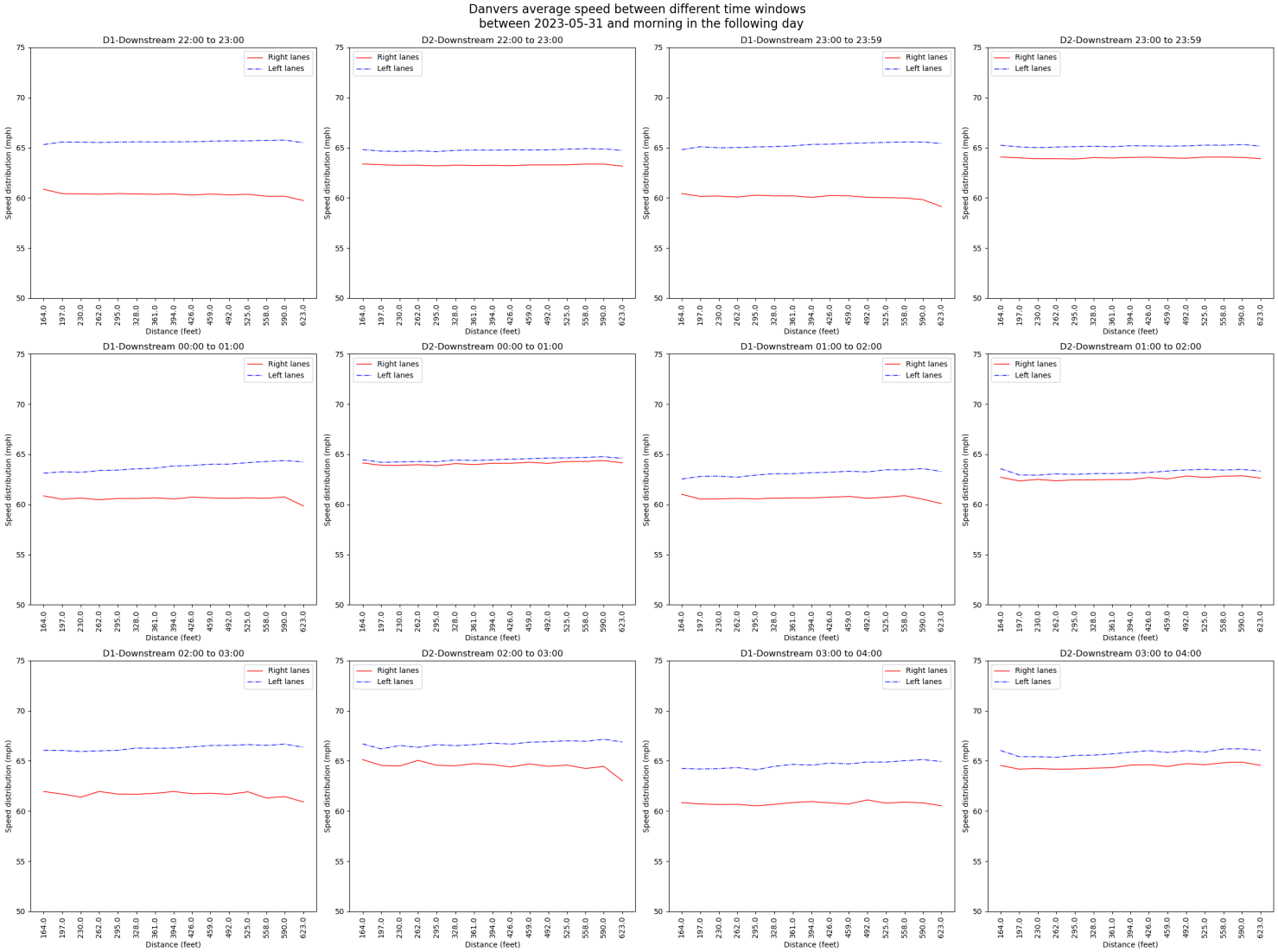

Figure 8.6. Danvers speed profile on late 5-31-2023 and early 6-01-2023

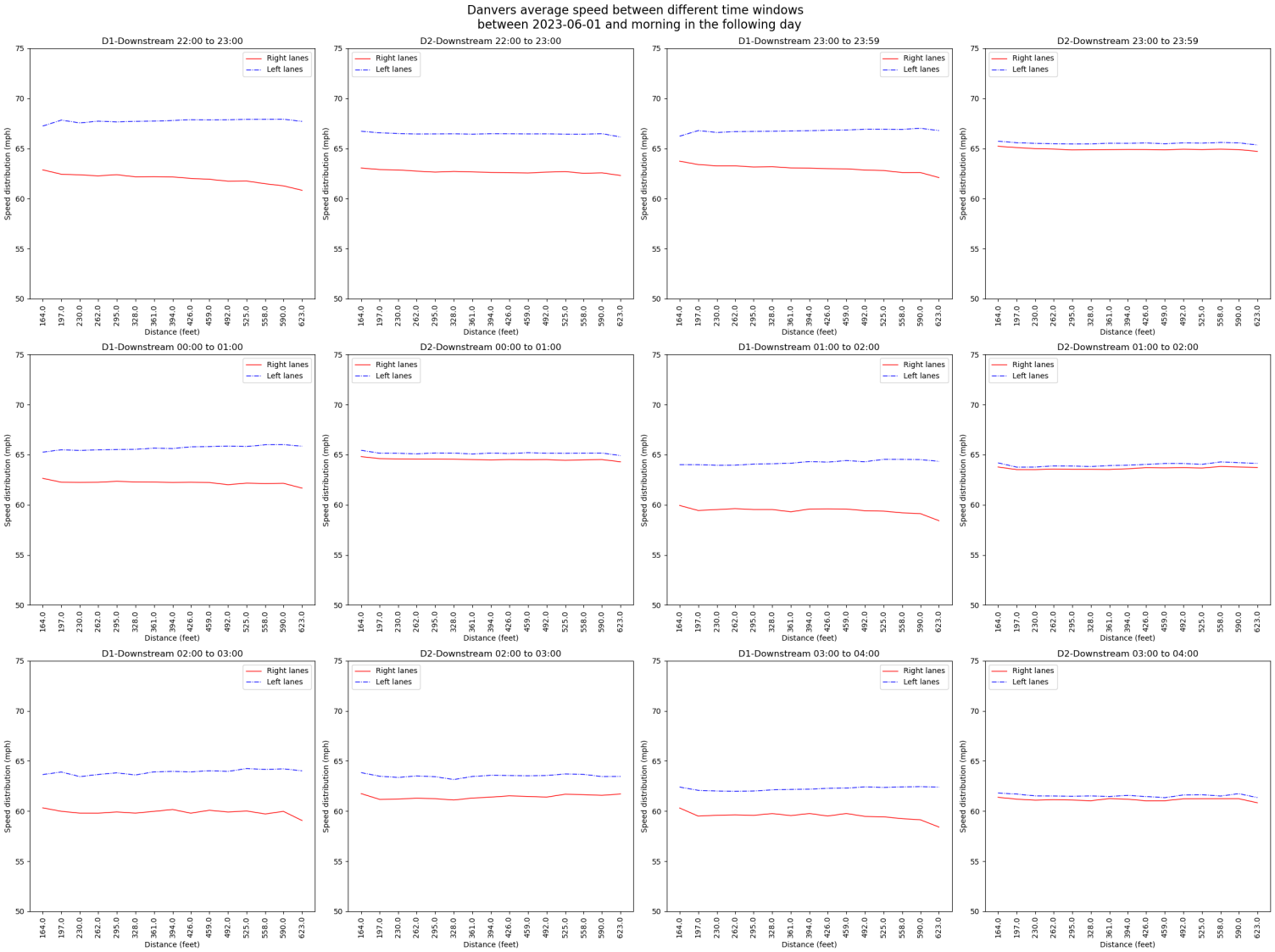

Figure 8.7. Danvers speed profile on late 6-01-2023 and early 6-02-2023

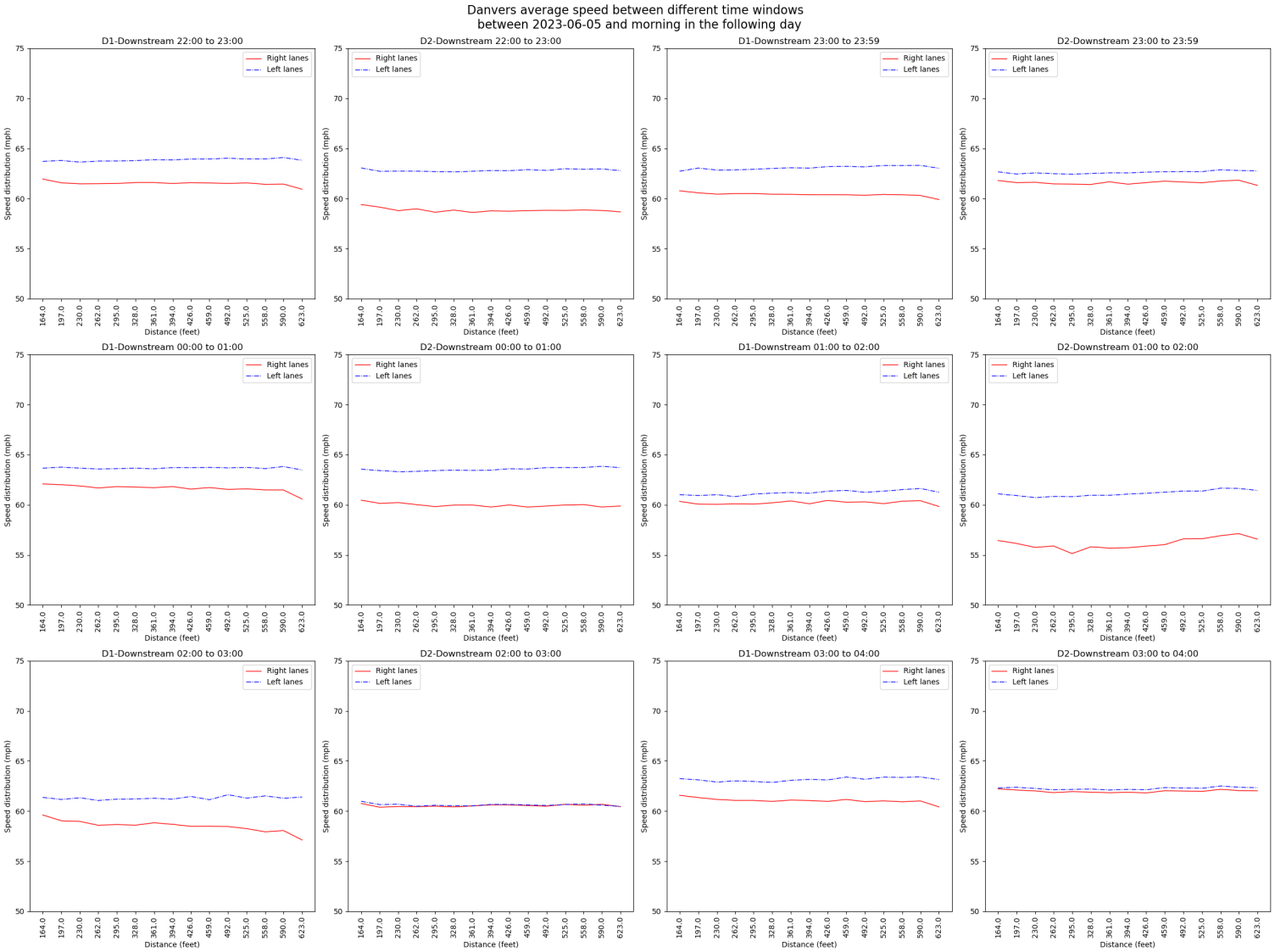

Figure 8.8. Danvers speed profile on late 6-05-2023 and early 6-06-2023

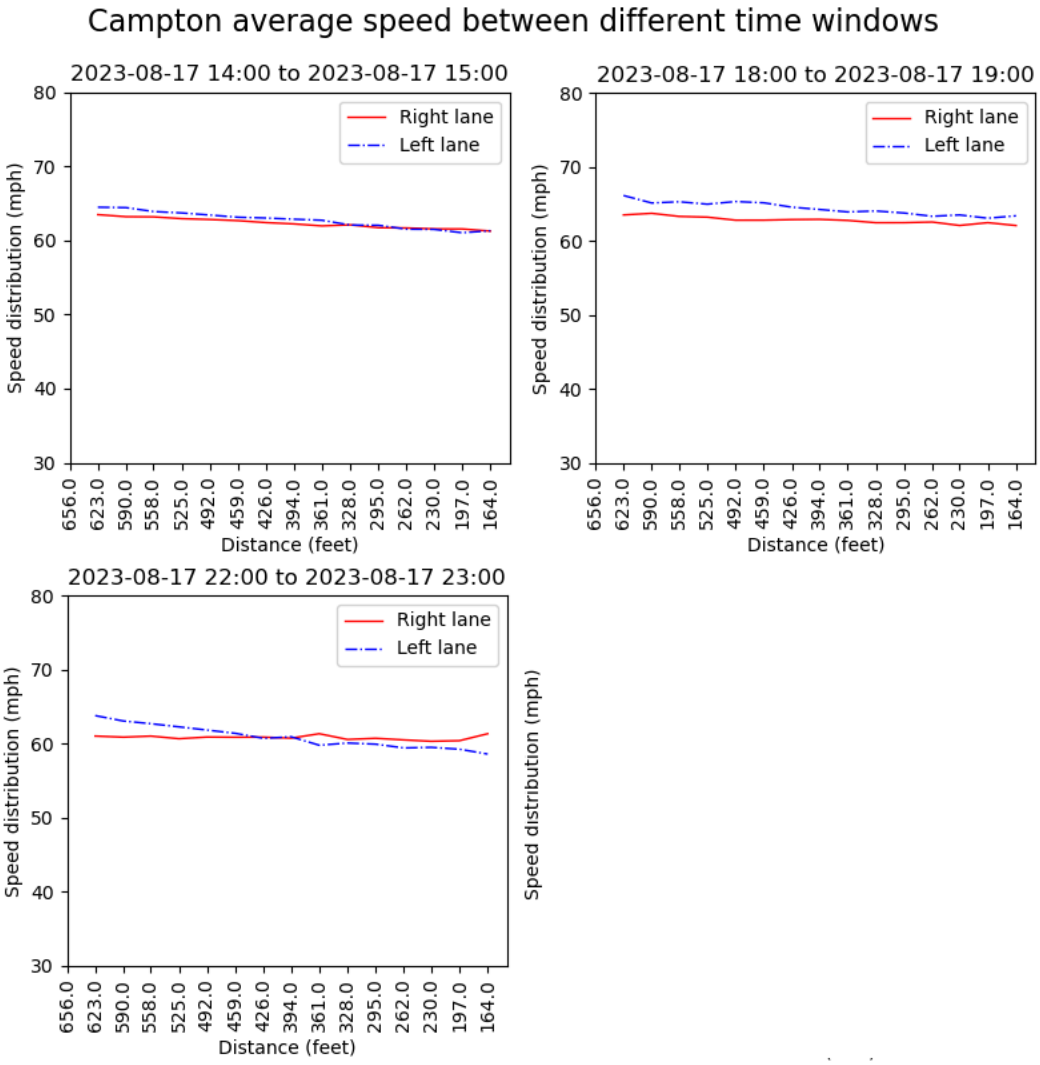

Figure 8.9. Campton speed profile on 8-17-2023

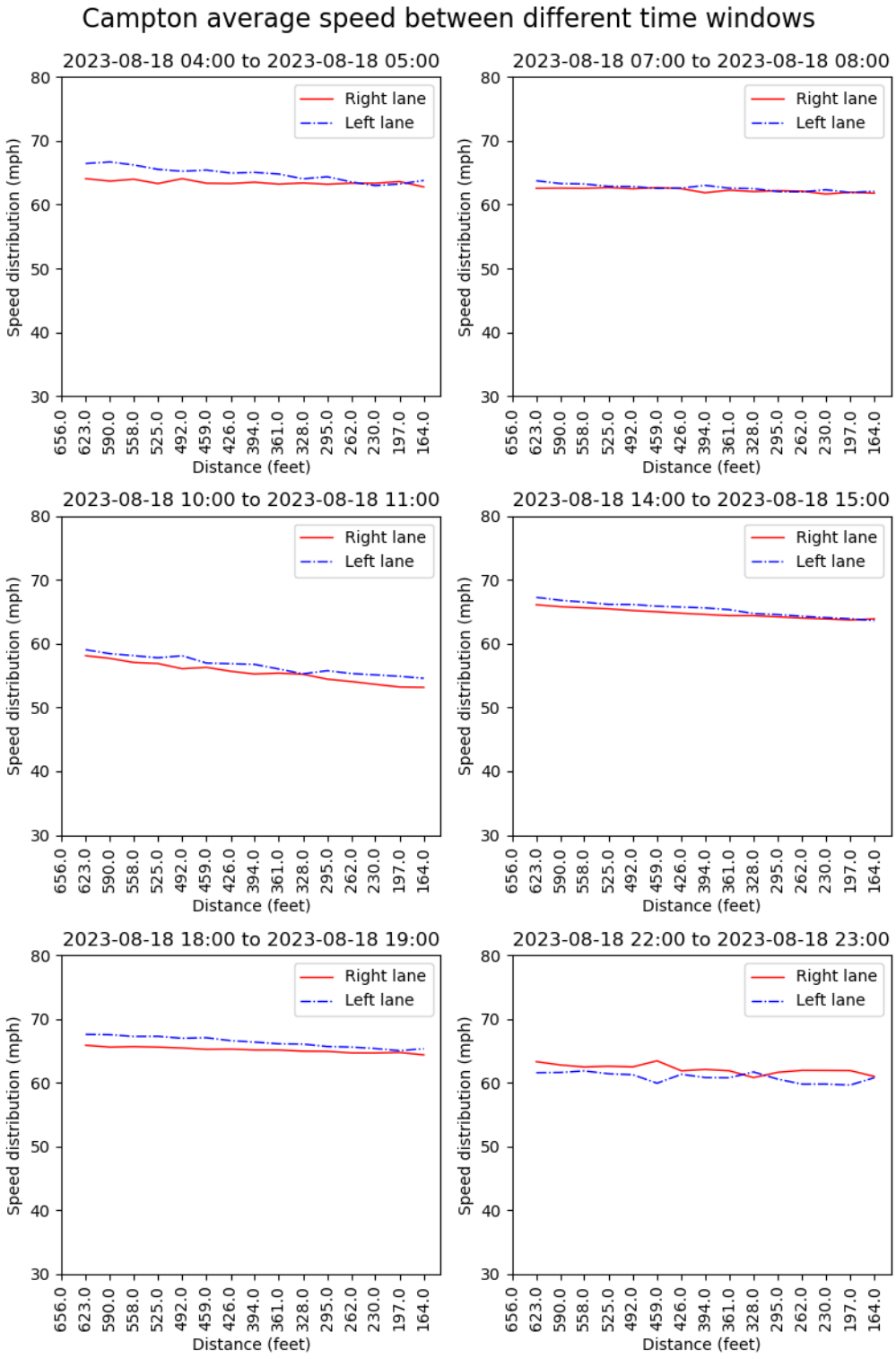

Figure 8.10. Campton speed profile on 8-18-2023

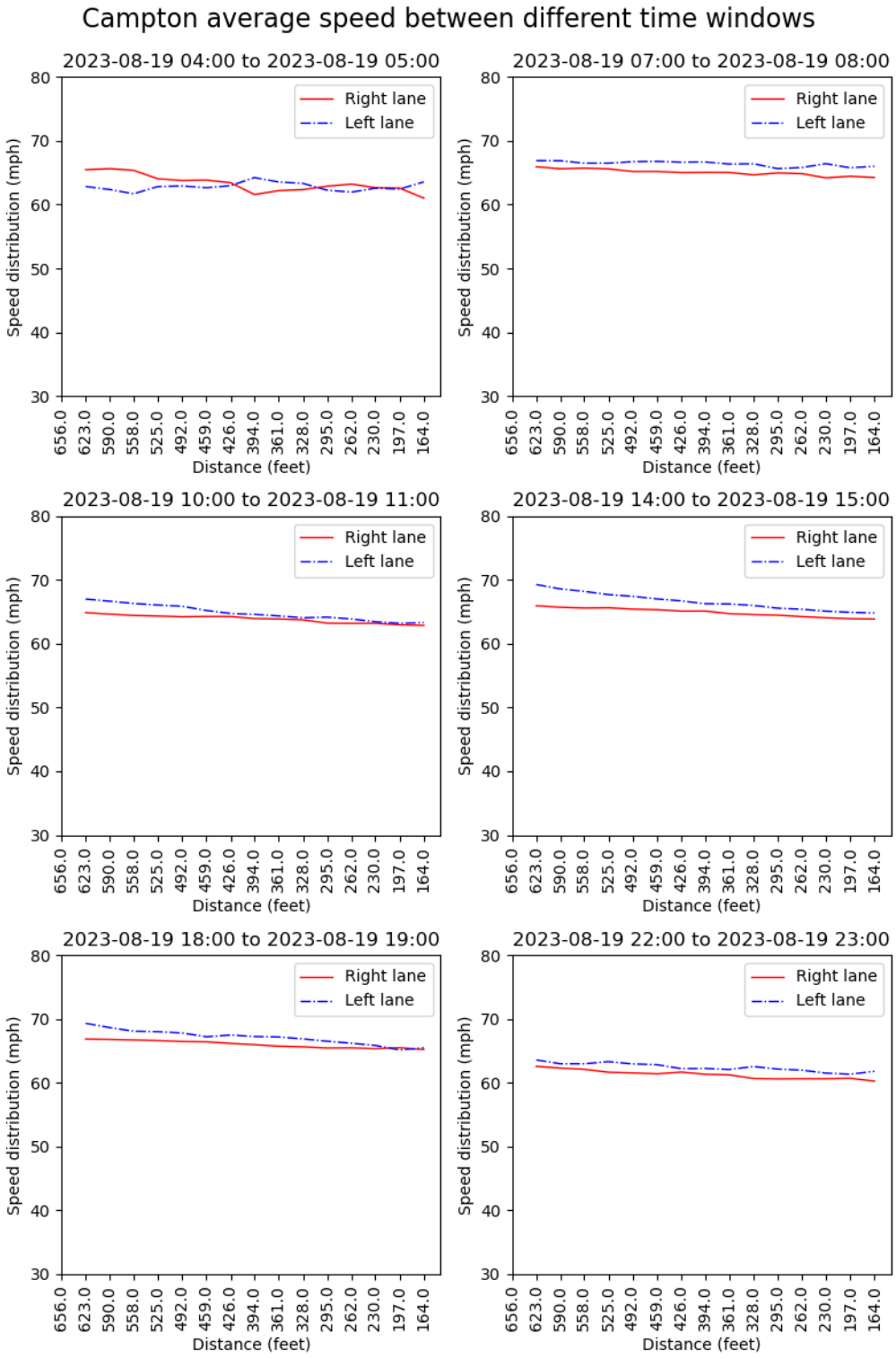

Figure 8.11. Campton speed profile on 8-19-2023

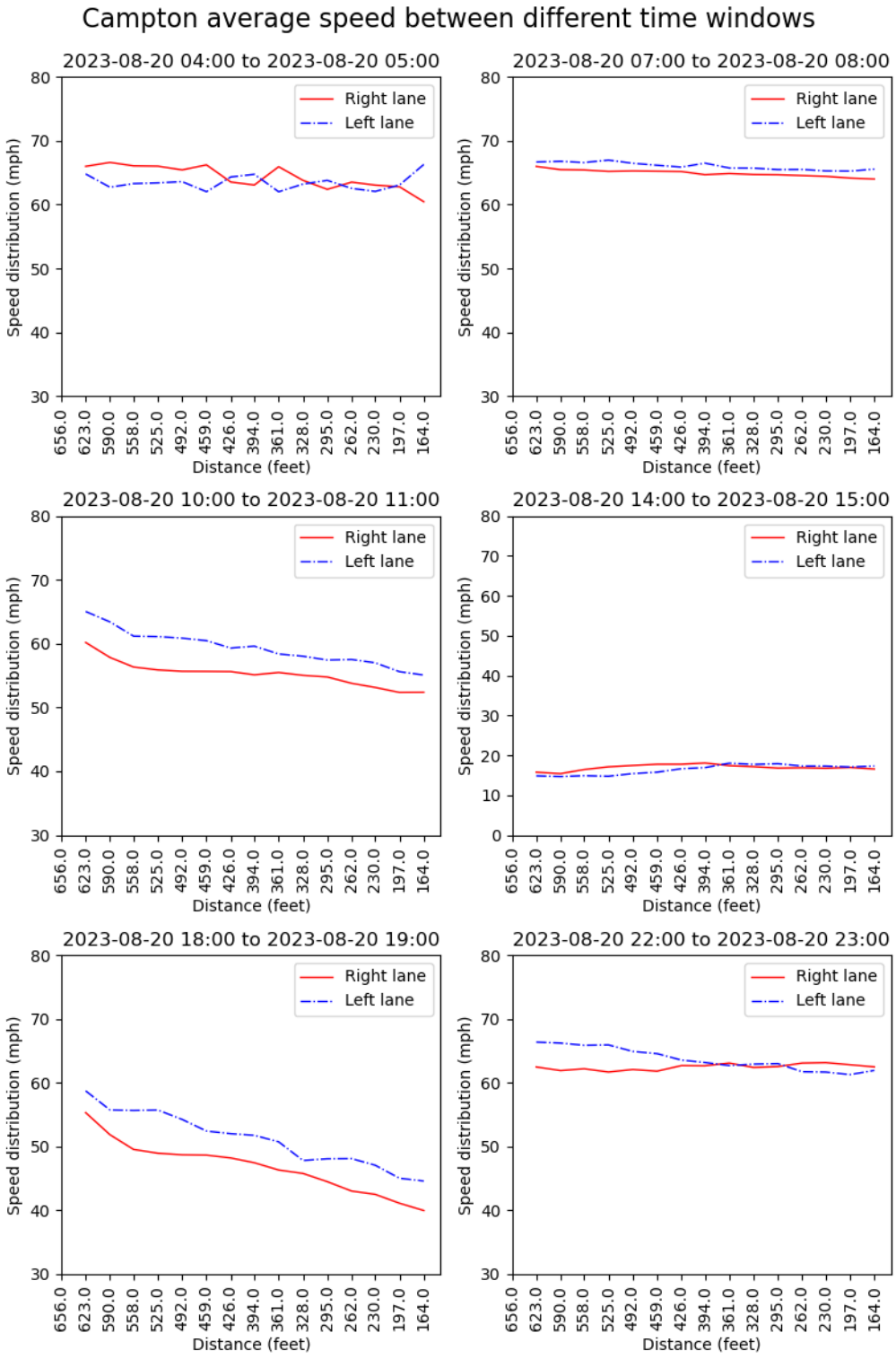

Figure 8.12. Campton speed profile on 8-20-2023

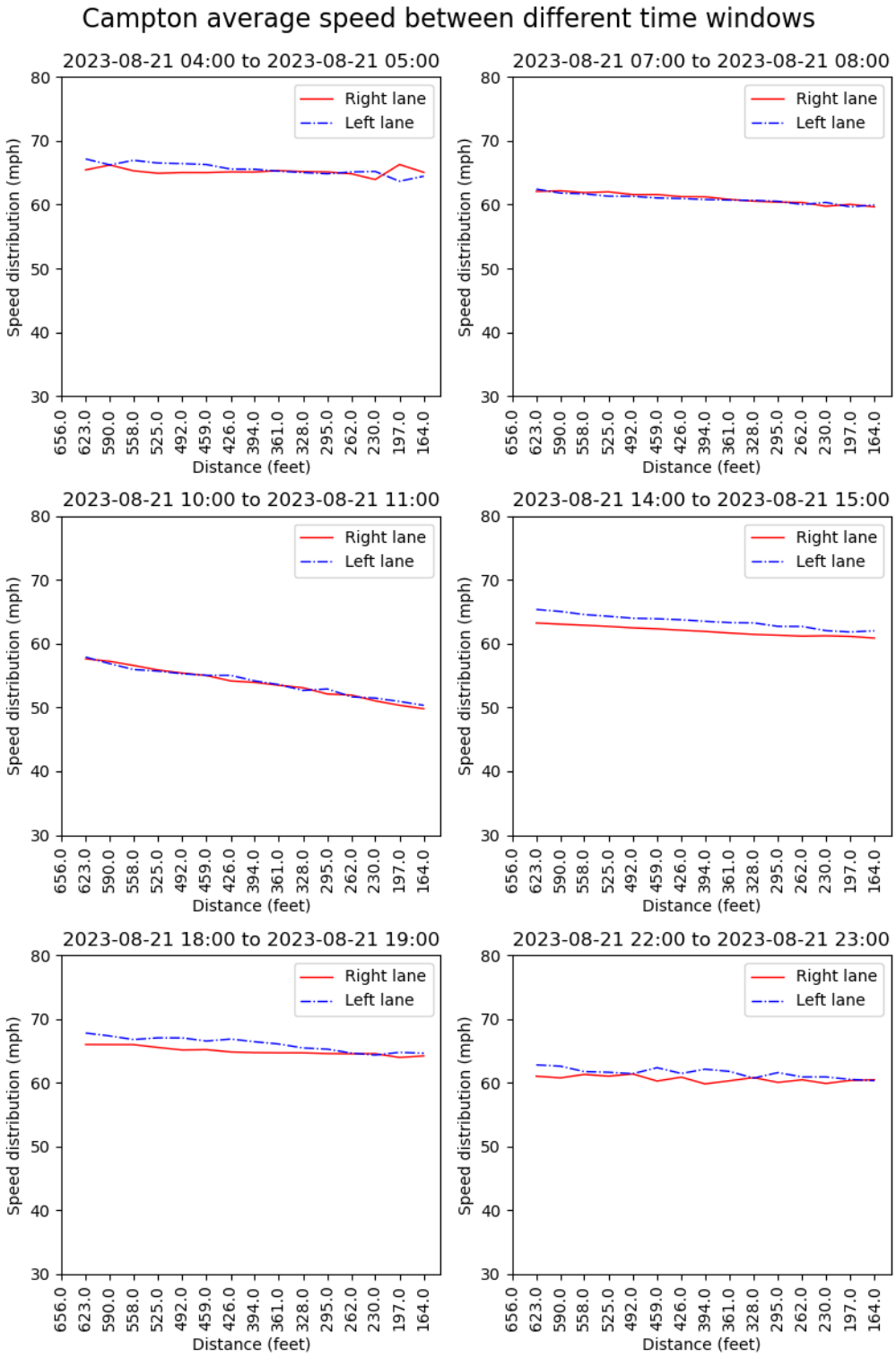

Figure 8.13. Campton speed profile on 8-21-2023

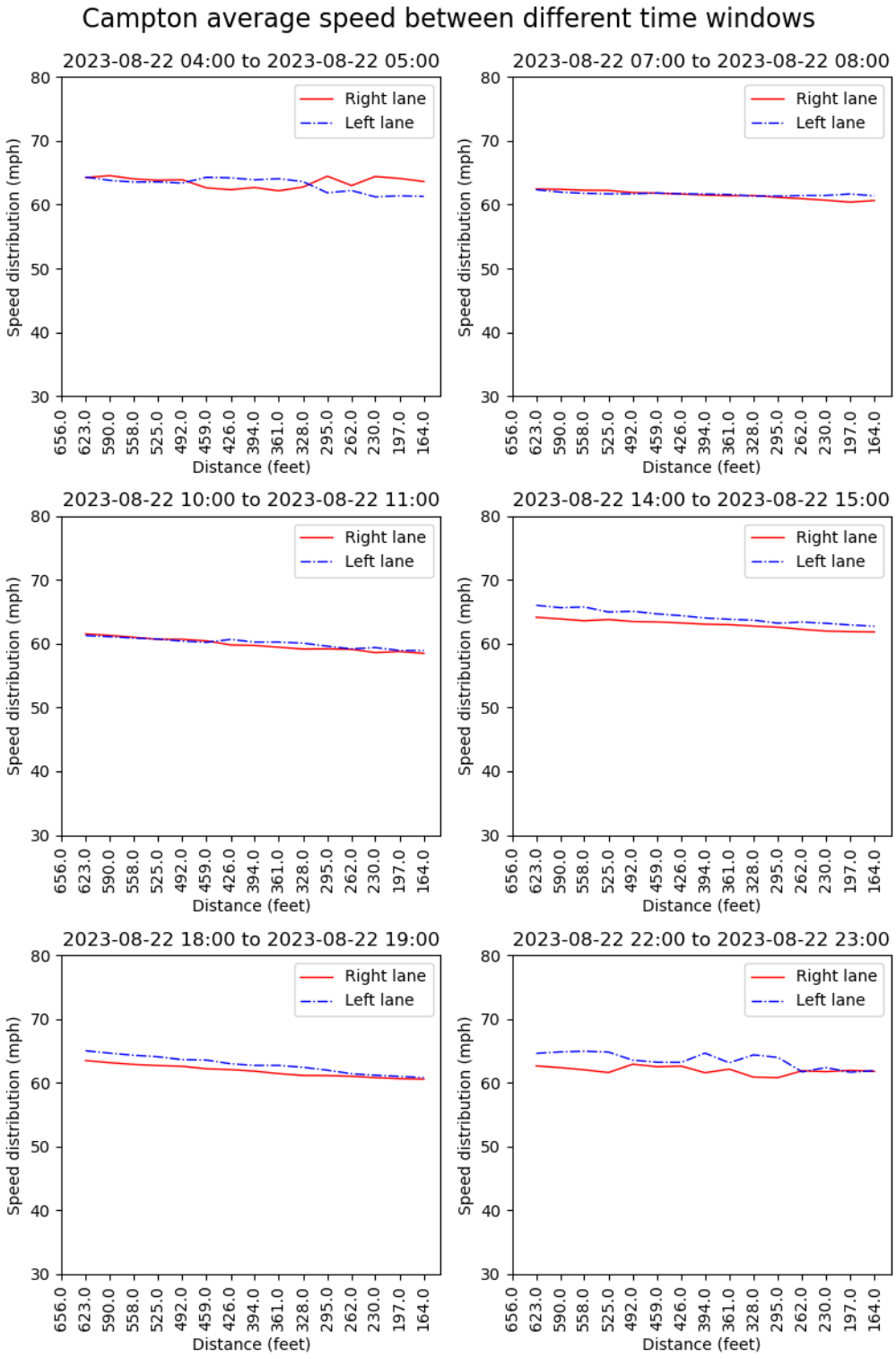

Figure 8.14. Campton speed profile on 8-22-2023

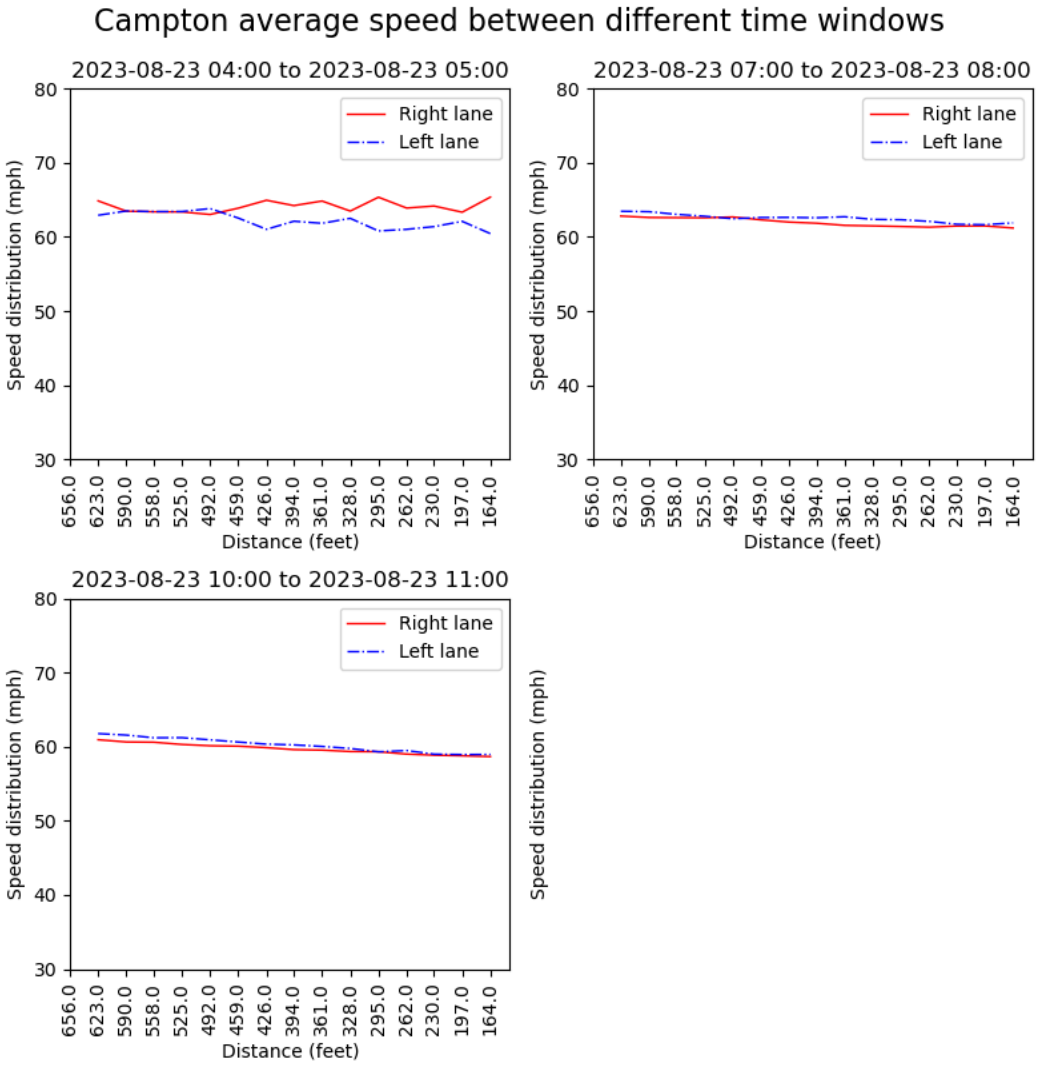

Figure 8.15. Campton speed profile on 8-23-2023

Appendix B. Traffic Volume Data

Figure 8.16 through Figure 8.28 show the freeway mainline and exit ramp traffic volumes at the Medford and Danvers sites.

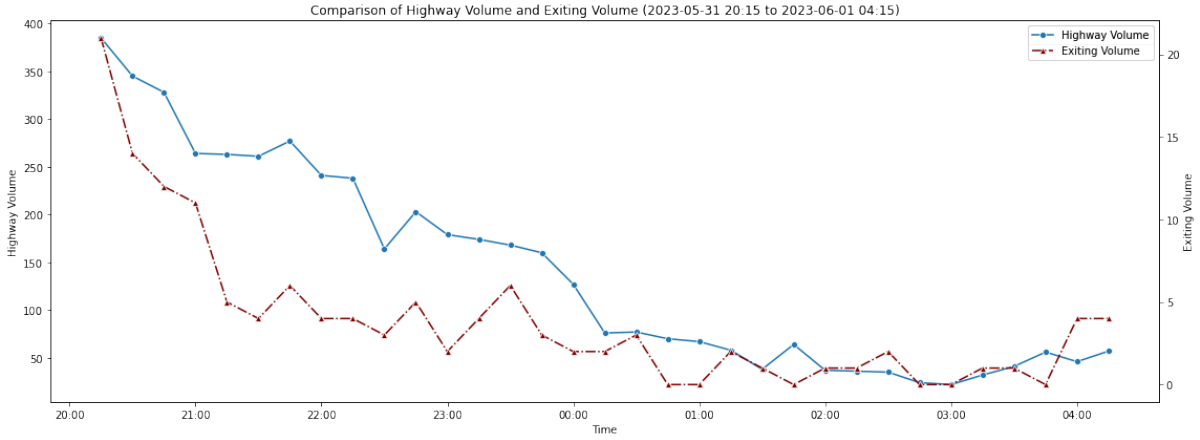

Figure 8.16. Danvers: 5-31-2023 (Rumble strips + normal taper)

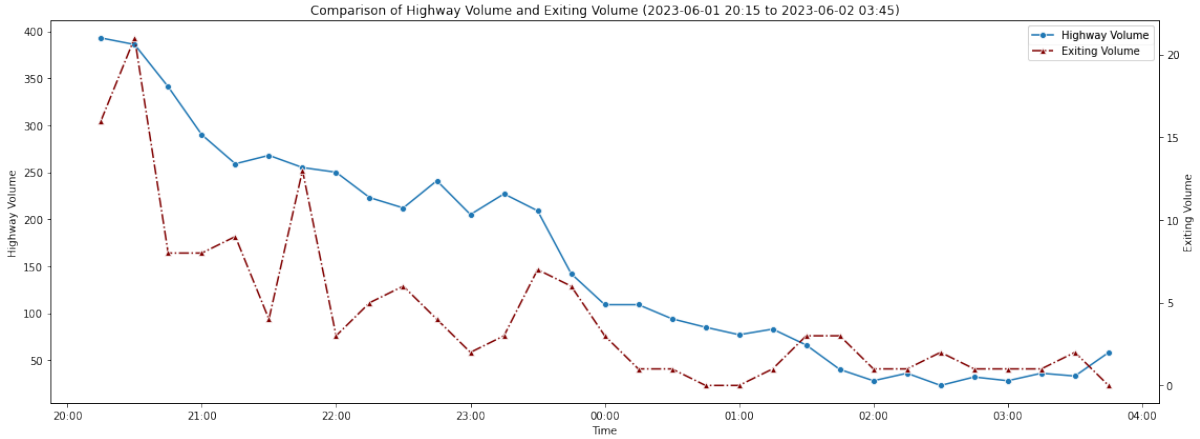

Figure 8.17. Danvers: 6-01-2023 (No rumble strips + normal taper)

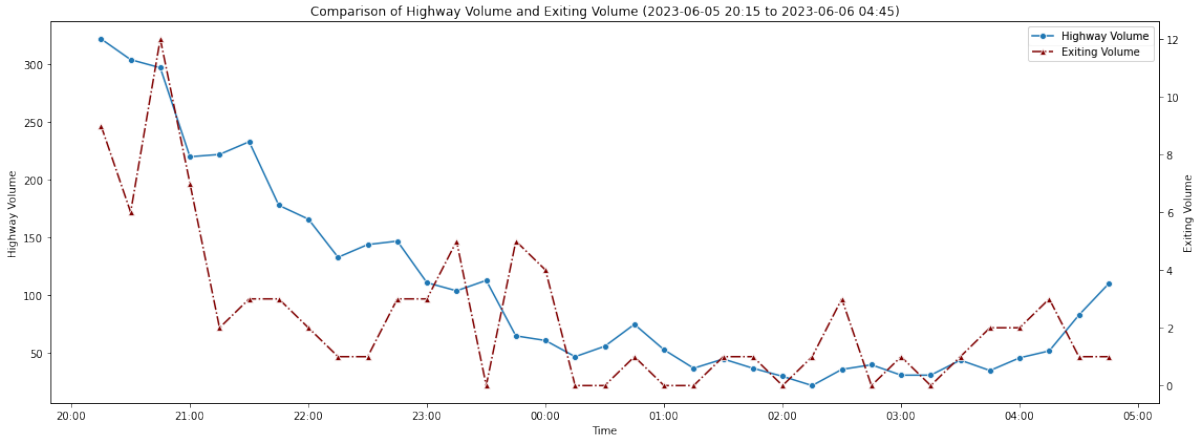

Figure 8.18. Danvers: 6-05-2023 (Rumble strip + longer taper)

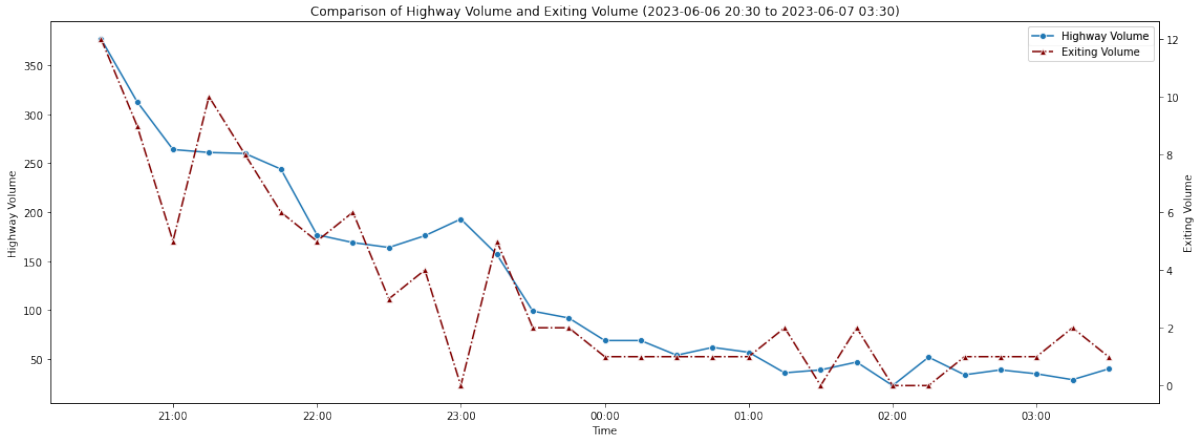

Figure 8.19. Danvers: 6-06-2023 (Rumble strip + longer taper)

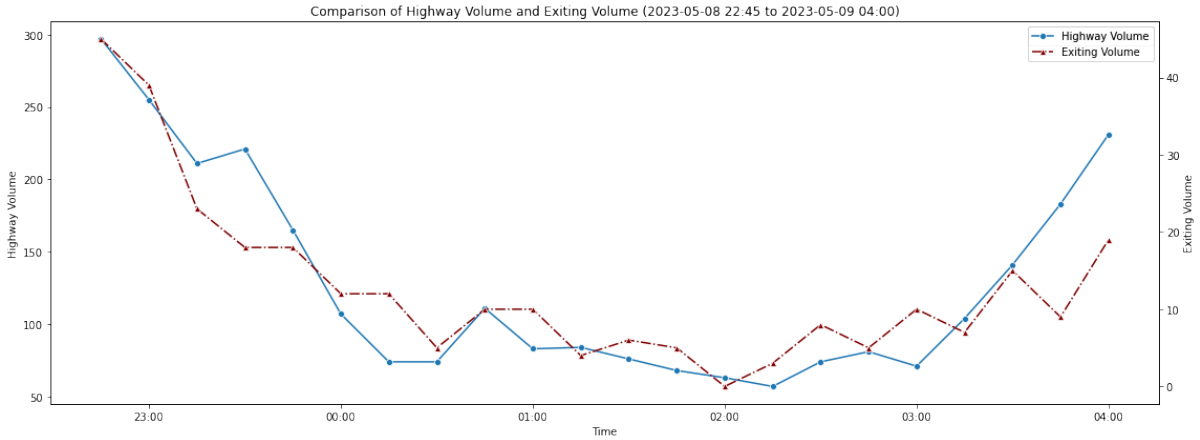

Figure 8.20. Medford: 5-08-2023 (Rumble strips + normal taper - Day 1)

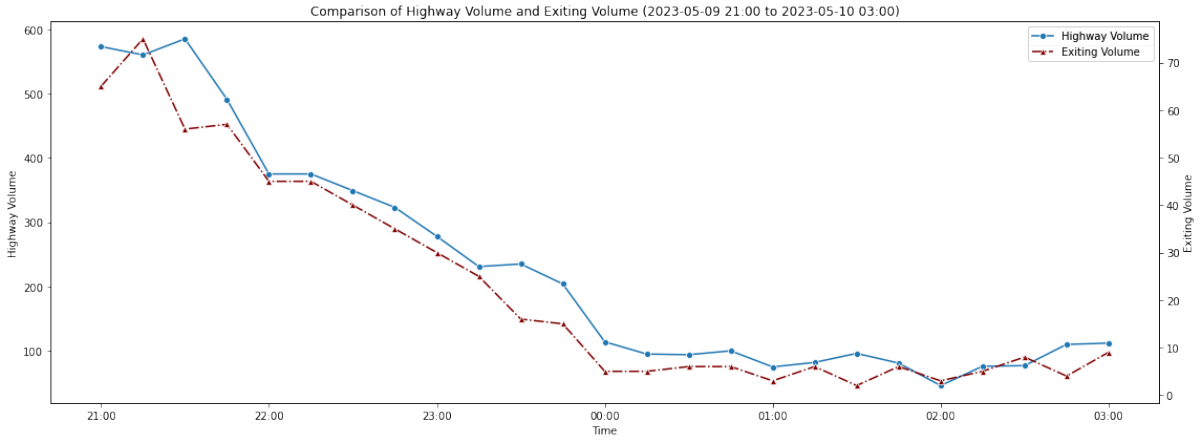

Figure 8.21. Medford: 5-09-2023 (Rumble strips + normal taper - Day 2)

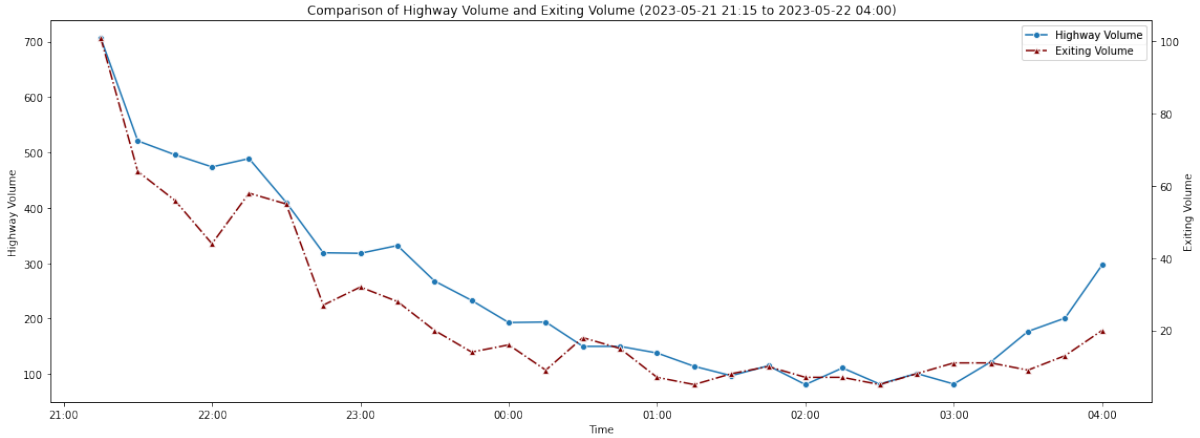

Figure 8.22. Medford: 5-21-2023 (Rumble strips + normal taper - Day 3)

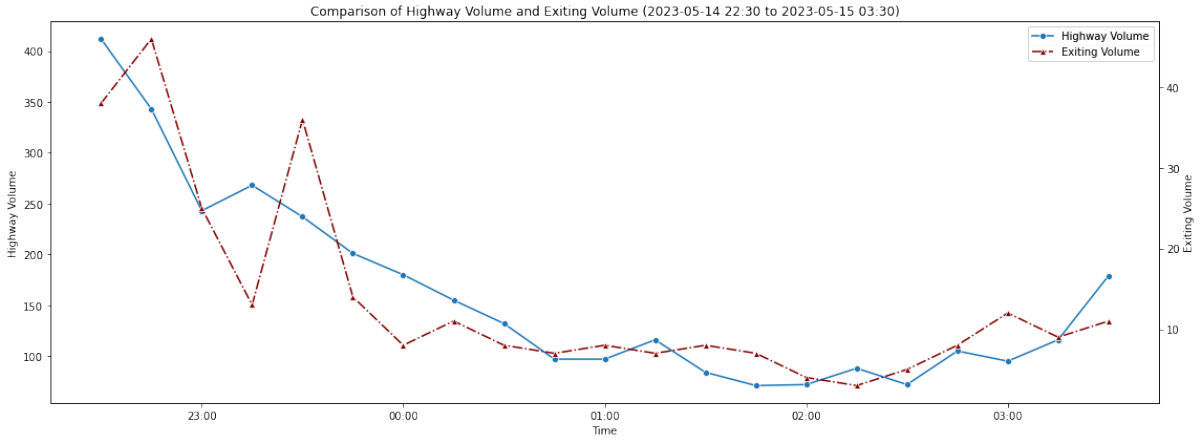

Figure 8.23. Medford: 5-08-2023 (No rumble strips + normal taper - Day 1)

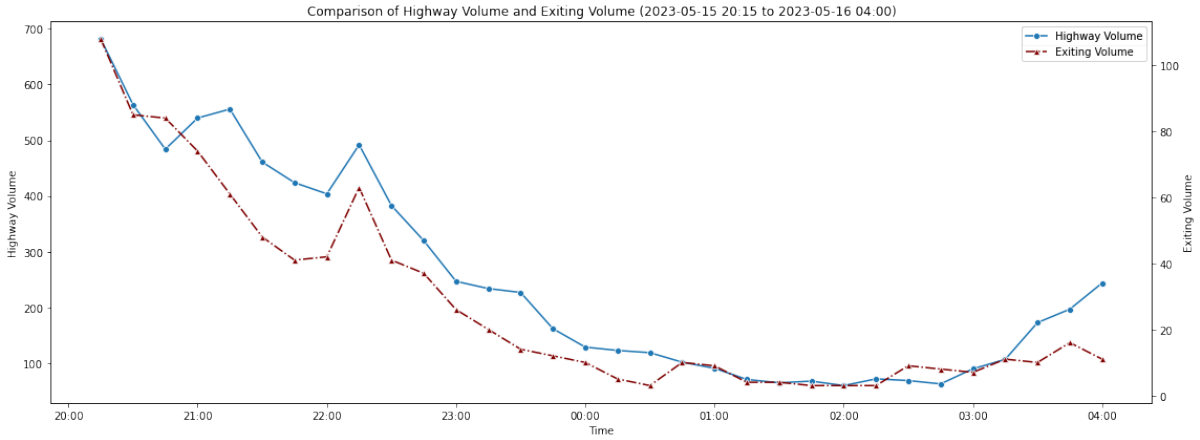

Figure 8.24. Medford: 5-15-2023 (No rumble strips + normal taper - Day 2)

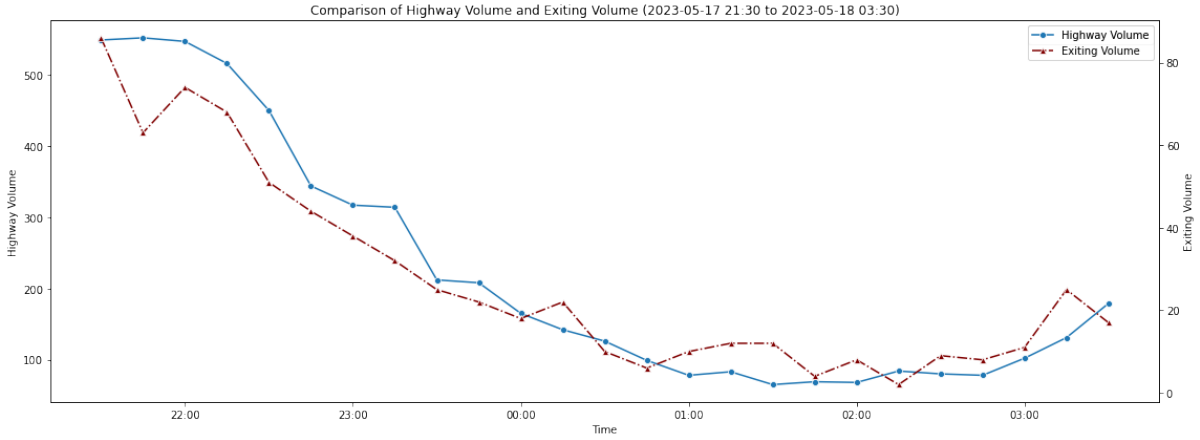

Figure 8.25. Medford: 5-17-2023 (No rumble strips + normal taper - Day 3)

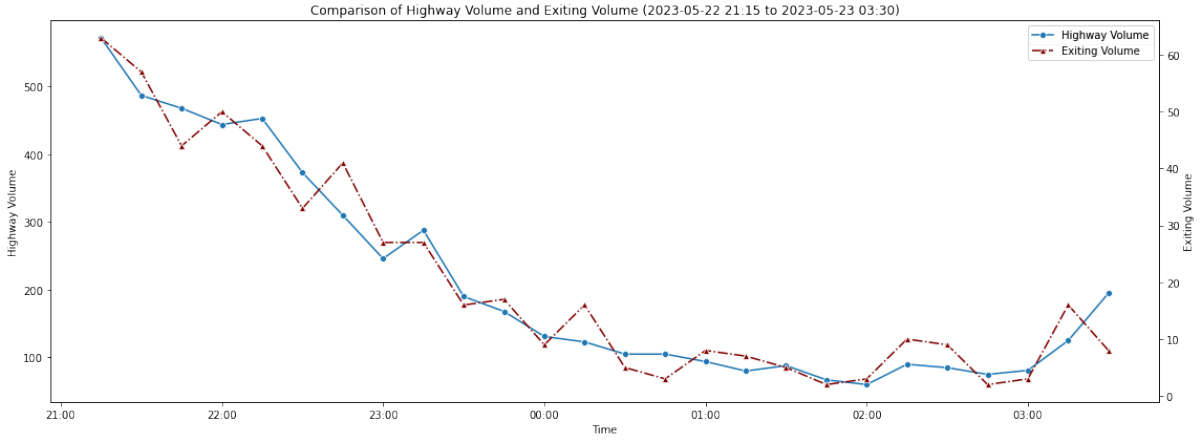

Figure 8.26. Medford: 5-22-2023 (Rumble strips + longer taper - Day 1)

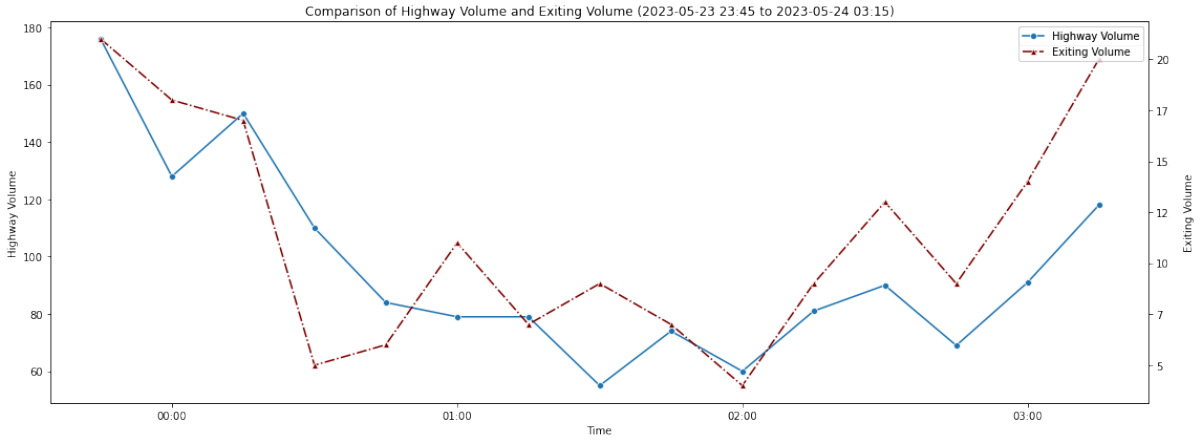

Figure 8.27. Medford: 5-23-2023 (Rumble strips + longer taper - Day 2)

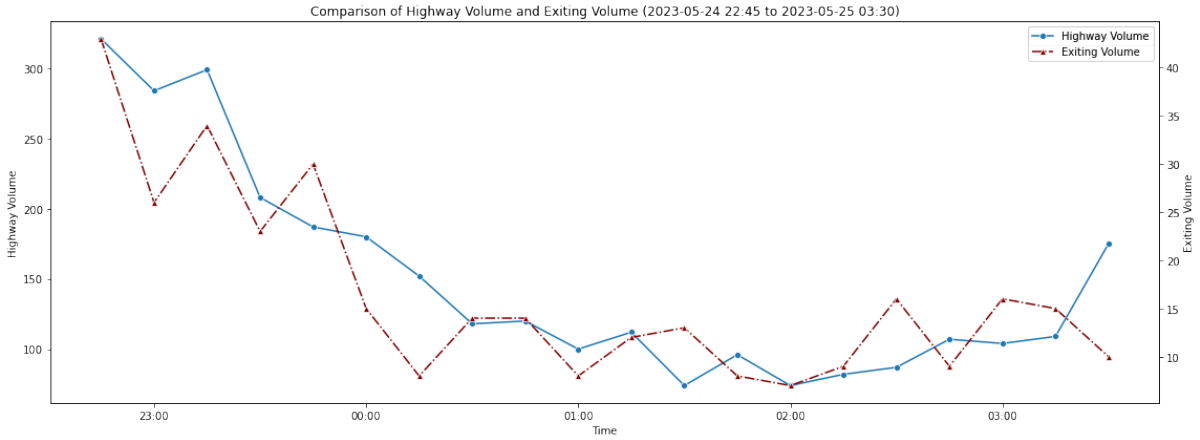

Figure 8.28. Medford: 5-24-2023 (Rumble strips + longer taper - Day 3)

Appendix C. Late Merge Data

The values shown in Figure 8.29 through Figure 8.41 represent aggregated vehicle volumes calculated over 15-minute intervals. For instance, a time stamp of 4:15 a.m. on the *x*-axis refers to the period from 4:15 to 4:30 a.m. Consequently, if the work zone concludes at 4:30 a.m., the final data points (both bars, which represent the late merges, and points, which represent the freeway volume) correspond to the 4:15 on the *x*-axis.

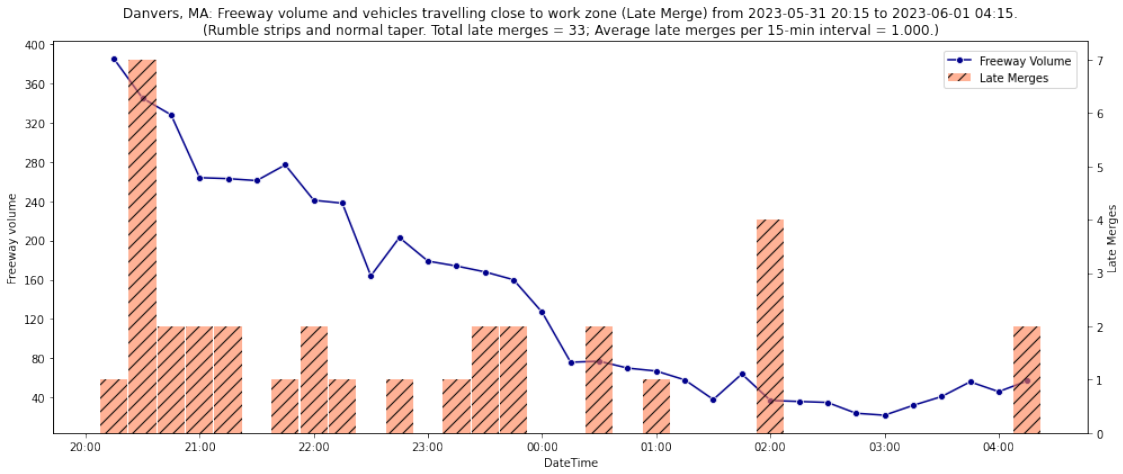

Figure 8.29. Danvers: 05-31-2023 (Rumble strips + normal taper)

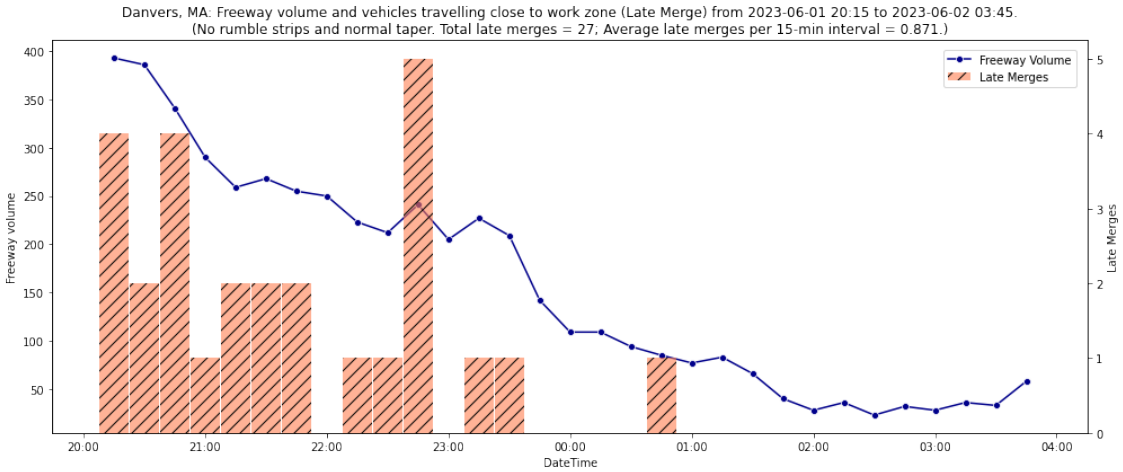

Figure 8.30. Danvers: 06-01-2023 (No rumble strips + normal taper)

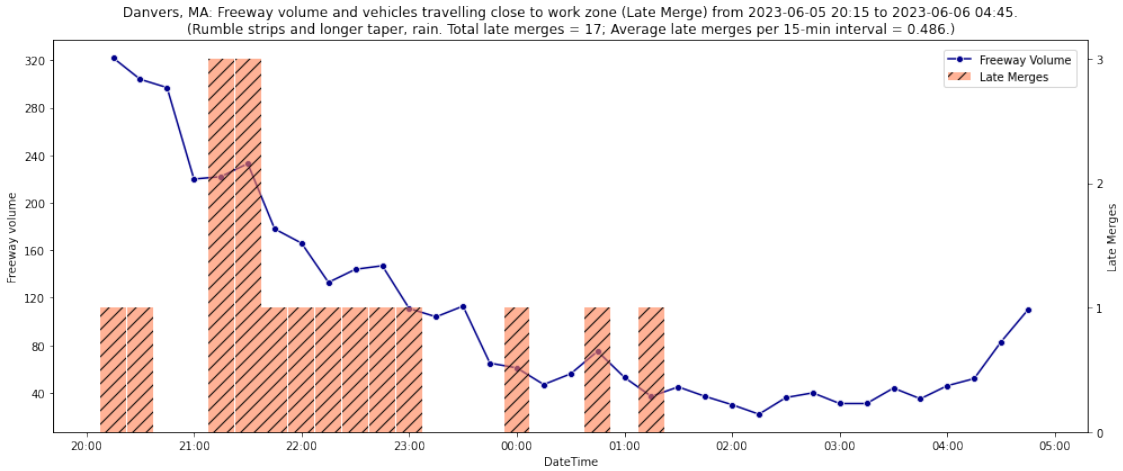

Figure 8.31. Danvers: 06-05-2023 (Rumble strip + longer taper)

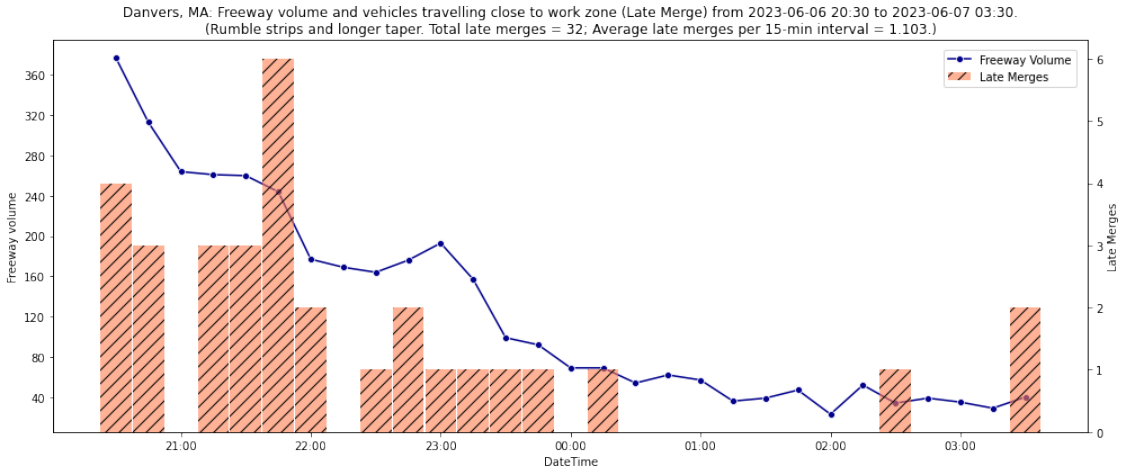

Figure 8.32. Danvers: 06-06-2023 (Rumble strip + longer taper)

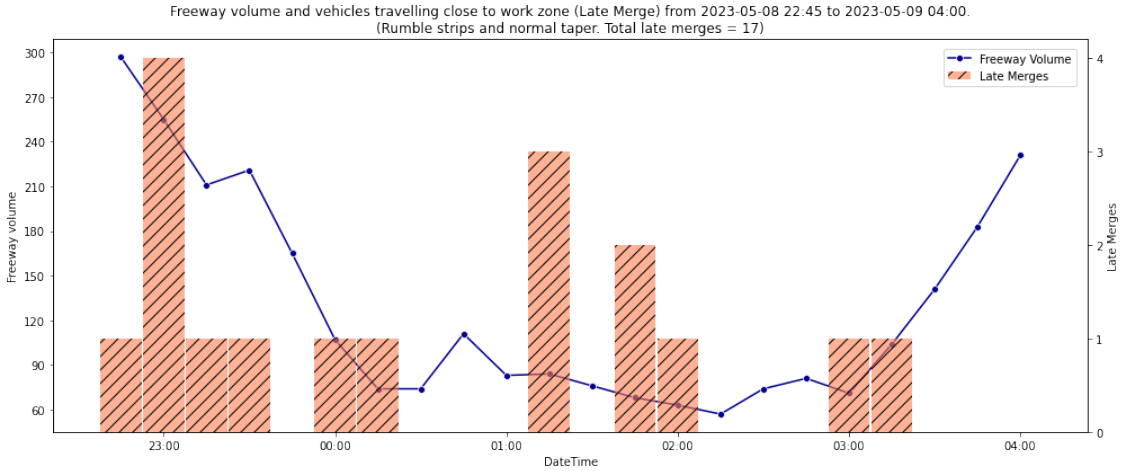

Figure 8.33. Medford: 05-08-2023 (Rumble strips + normal taper – Day 1)

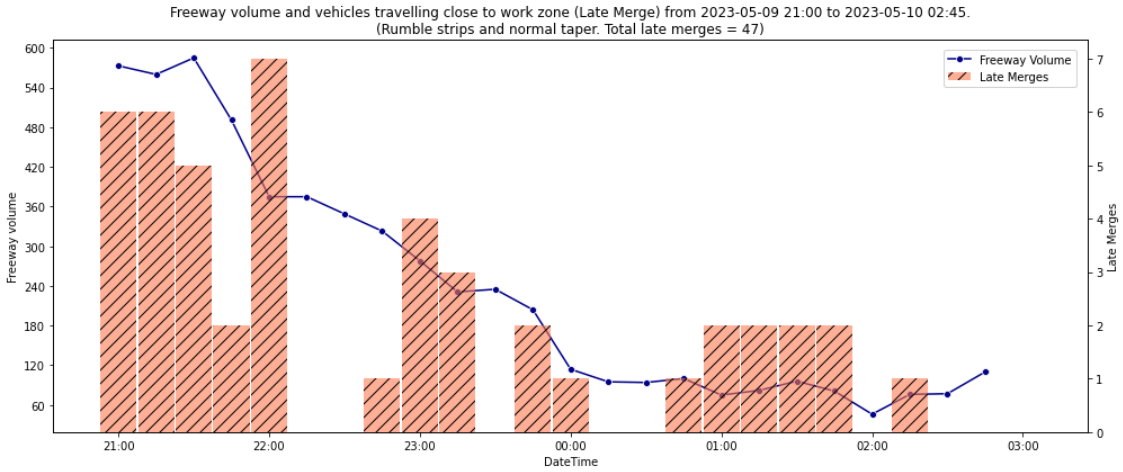

Figure 8.34. Medford: 05-09-2023 (Rumble strips + normal taper – Day 2)

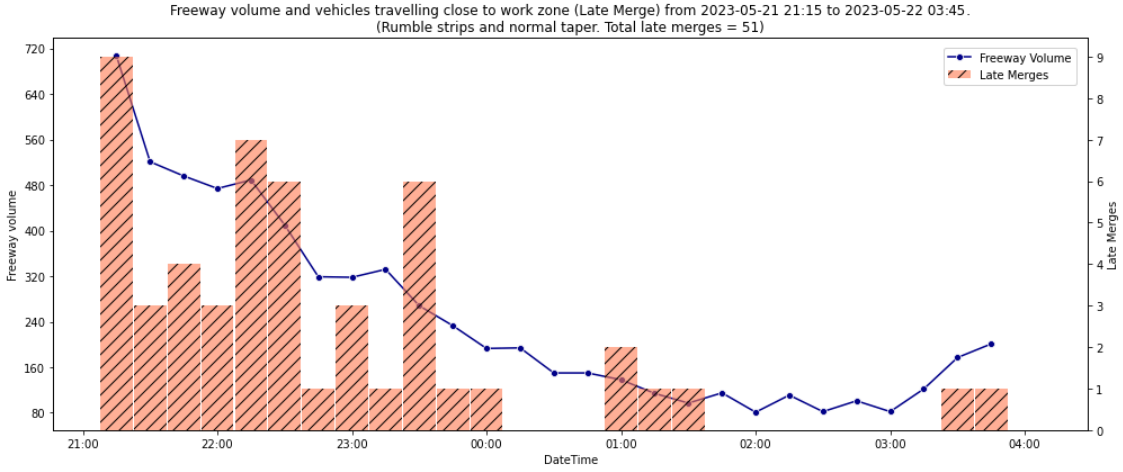

Figure 8.35. Medford: 05-21-2023 (Rumble strips + normal taper – Day 3)

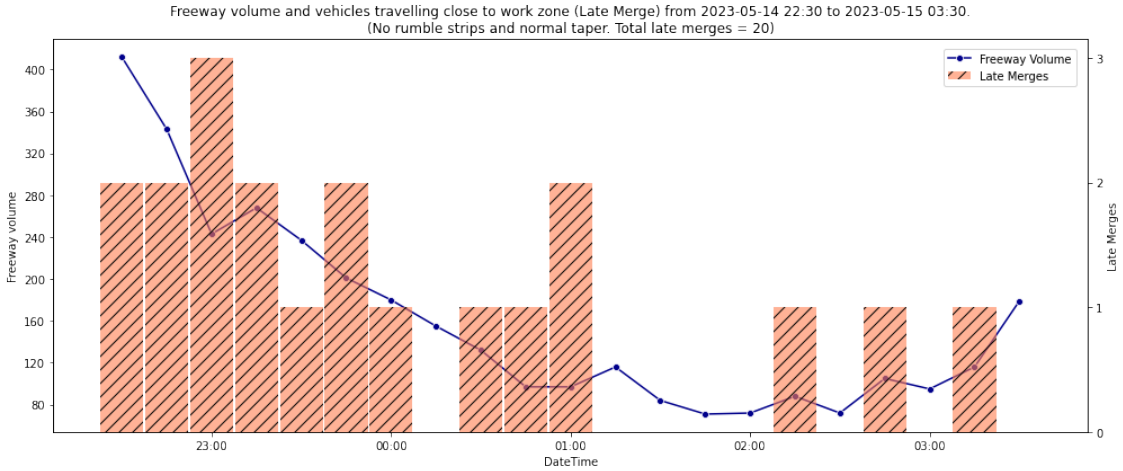

Figure 8.36. Medford: 05-14-2023 (No rumble strips + normal taper – Day 1)

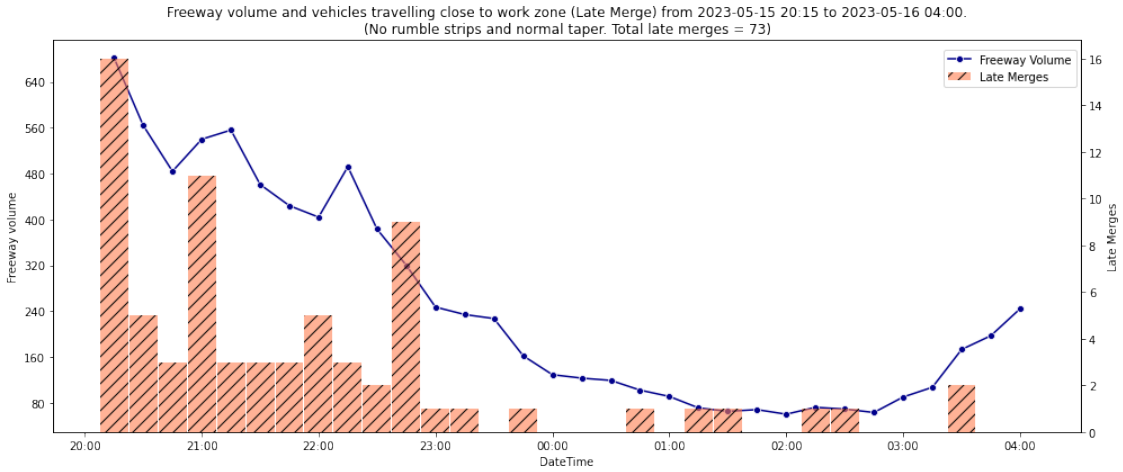

Figure 8.37. Medford: 05-15-2023 (No rumble strips + normal taper – Day 2)

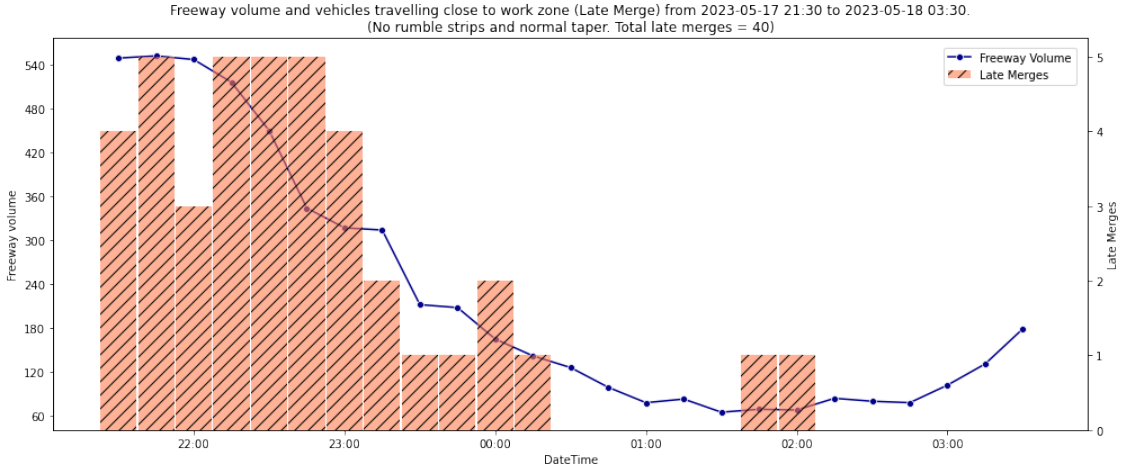

Figure 8.38. Medford: 05-17-2023 (No rumble strips + normal taper – Day 3)

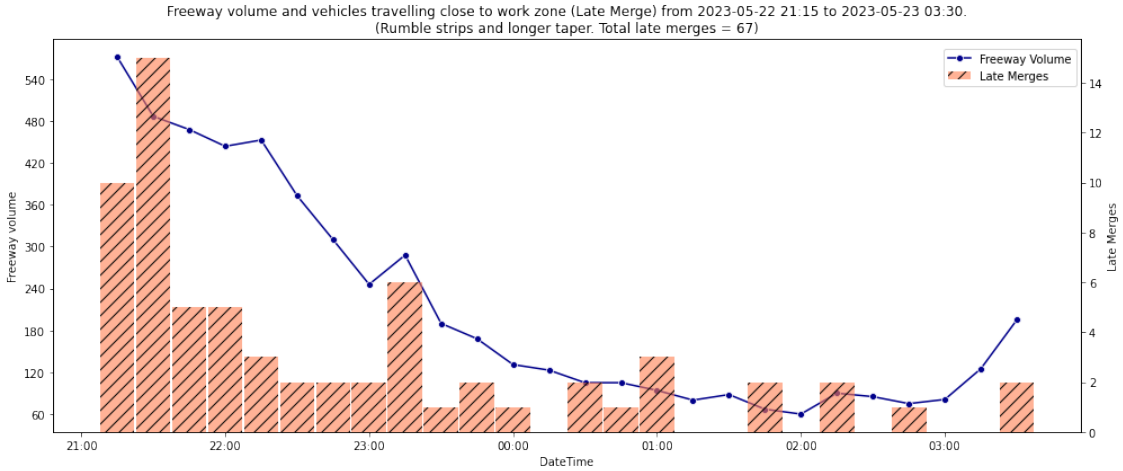

Figure 8.39. Medford: 05-22-2023 (Rumble strips + longer taper – Day 1)

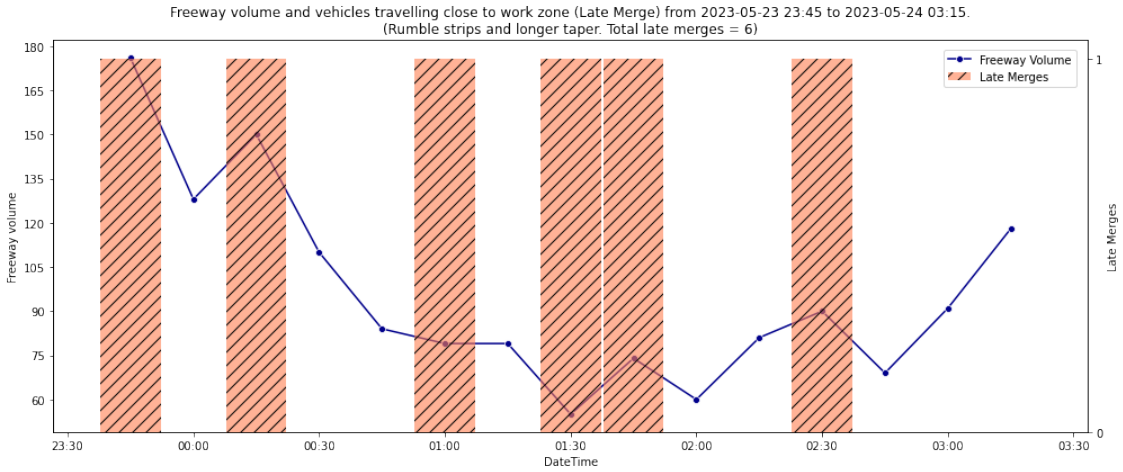

Figure 8.40. Medford: 05-23-2023 (Rumble strips + longer taper – Day 2)

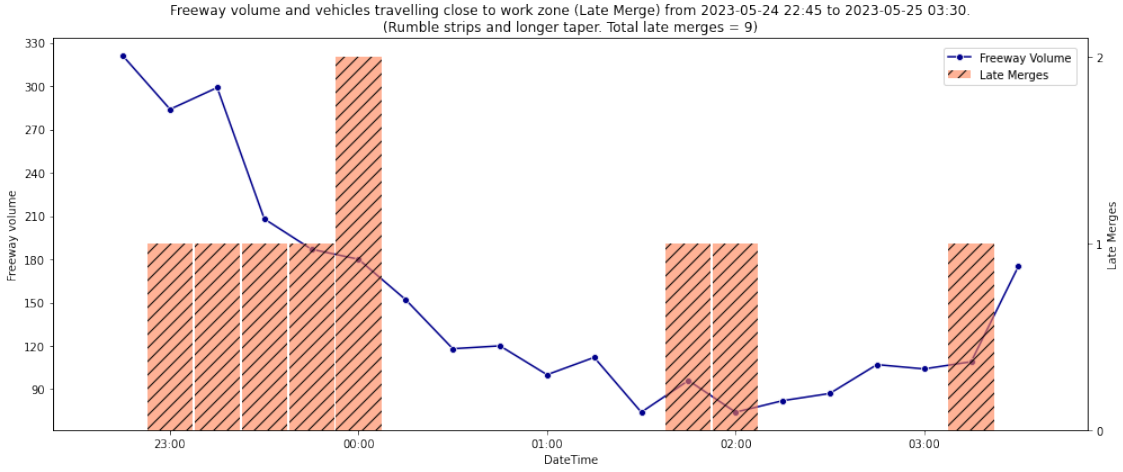

Figure 8.41. Medford: 05-24-2023 (Rumble strips + longer taper – Day 3)

Appendix D. Drone Video Data

Table 8.1. Drone data collection at Medford

Date	Location	Start Time	Duration (min)	Type	Number of Clips	Size (GB)
05/08/2023	North	21:20	11	RGB	3	5.3
	North	21:49	19	RGB	3	8.6
	North	22:16	20	RGB	3	9.0
	North	22:46	15	RGB	2	6.8
	North	23:09	19	RGB	3	9.0
	Central	21:26	9	RGB	1	4.1
	South	21:35	12	RGB	2	5.8
	South	21:53	25	RGB	3	11.2
	South	22:22	24	RGB	3	10.8
	South	22:50	23	RGB	3	10.8
	South	23:18	23	RGB	3	10.3
05/09/2023	North	21:06	20	RGB	3	9.0
	North	21:35	24	RGB	3	10.9
	North	10:07	12	RGB	3	5.4
	North	10:28	21	RGB	3	9.5
	North	10:58	21	RGB	3	9.9
	South	21:02	22	RGB	3	9.9
	South	21:28	25	RGB	3	11.2
	South	21:57	25	RGB	3	11.2
	South	22:29	25	RGB	3	11.2
	South	22:58	24	RGB	3	10.8
05/15/2023	North	21:20	10	RGB + Thermal	1+1	1.4
	North	21:47	13	RGB + Thermal	1+1	1.8
	North	22:14	19	RGB + Thermal	1+1	2.6
	North	22:43	20	RGB + Thermal	1+1	2.7
	North	23:09	19	RGB + Thermal	1+1	2.6
	South	21:21	20	RGB	3	9.0
	South	21:57	26	RGB	3	11.9
	South	22:28	26	RGB	3	11.7
	South	23:00	27	RGB	3	12.1
05/23/2023	North	21:23	18	RGB + Thermal	1 + 1	2.5
	North	21:50	22	RGB + Thermal	1 + 1	2.9
	North	22:19	18	RGB + Thermal	1 + 1	2.5
	North	22:43	17	RGB + Thermal	1 + 1	2.3
	North	23:11	15	RGB + Thermal	1 + 1	2.1
	South	21:25	21	RGB + Thermal	2 + 2	5.9
	South	21:56	26	RGB + Thermal	2 + 2	7.3
	South	22:28	27	RGB + Thermal	2 + 2	7.5
	South	22:59	26	RGB + Thermal	2 + 2	7.3

Table 8.2. Drone data collection at Danvers

Date	Location	Start Time	Duration (min)	Type	Number of Clips	Size (GB)
05/31/2023	North	20:29	25	RGB + Thermal	2 + 2	7.1
	North	20:59	26	RGB + Thermal	2 + 2	7.4
	North	21:30	26	RGB + Thermal	2 + 2	7.2
	North	21:58	25	RGB + Thermal	2 + 2	7.0
	South	20:23	19	RGB + Thermal	1 + 1	2.6
	South	20:47	16	RGB + Thermal	1 + 1	2.2
	South	21:12	16	RGB + Thermal	1 + 1	2.3
	South	21:40	18	RGB + Thermal	1 + 1	2.4
	South	22:02	16	RGB + Thermal	1 + 1	2.2
06/01/2023	North	20:25	25	Thermal	1	1.2
	North	20:54	26	Thermal	1	1.2
	North	21:26	26	Thermal	1	1.2
	North	21:56	26	Thermal	1	1.2
	South	20:19	18	RGB + Thermal	1 + 1	2.5
	South	20:44	18	RGB + Thermal	1 + 1	2.5
	South	21:07	16	RGB + Thermal	1 + 1	2.2
	South	21:33	17	RGB + Thermal	1 + 1	2.4
	South	21:58	18	RGB + Thermal	1 + 1	2.4
06/062023	North	19:03	19	Thermal	1	0.89
	North	20:30	21	Thermal	1	0.97
	North	21:06	18	RGB + Thermal	2 + 2	5.0
	North	21:32	23	RGB + Thermal	2 + 2	6.6
	South	20:24	12	RGB + Thermal	1 + 1	1.7
	South	20:44	17	RGB + Thermal	1 + 1	2.4
	South	21:06	62	RGB + Thermal	4 + 4	8.5

Figure 8.42. RGB versus thermal drone footage under varying light conditions in Danvers

Figure 8.43. RGB drone versus thermal ground frames at Medford

Appendix E. Detailed Traffic Volume and Last-Minute Merge Data

Table 8.3 through Table 8.6 provide detailed traffic volume and last-minute merge data for Danvers and Medford. In these tables, the columns labeled “F,” “E,” and “LM” represent “Freeway Traffic Volume,” “Exit Ramp Traffic Volume,” and “Number of Late Merges,” respectively.

Iin the subsequent tables the recorded start and end times of the work zone are rounded to the beginning or end of the hour; for instance, if the work zone commences at 22:30, the entry will be listed under the 22:00 hour column. This does not imply the work zone started precisely at 22:00. For accurate timings, please consult the work zone schedule for Danvers detailed in Table 2.3.

Table 8.3. Danvers

Date	Hour 0			Hour 1			Hour 2			Hour 3			Hour 4			Hour 20			Hour 21			Hour 22			Hour 23		
	F	E	LM	F	E	LM	F	E	LM	F	E	LM	F	E	LM	F	E	LM	F	E	LM	F	E	LM	F	E	LM
5/31/23	–	–	–	–	–	–	–	–	–	–	–	–	–	–	–	1058	47	10	1065	26	5	846	16	4	681	15	5
6/1/23	350	7	2	227	3	1	132	4	4	151	2	0	103	8	2	1120	45	10	1072	34	7	926	18	7	783	18	2
6/2/23	397	5	1	266	7	0	119	5	0	155	4	0	–	–	–	–	–	–	–	–	–	–	–	–	–	–	–
6/5/23	–	–	–	–	–	–	–	–	–	–	–	–	–	–	–	923	27	2	853	15	7	590	7	4	393	13	1
6/6/23	239	5	2	172	2	1	128	4	0	141	4	0	291	7	0	690	21	7	1029	29	12	686	18	5	541	9	4
6/7/23	254	4	1	179	5	0	148	2	1	104	4	2	–	–	–	–	–	–	–	–	–	–	–	–	–	–	–

The work zone schedule for Medford is detailed in Table 2.2.

Table 8.4. Medford with rumble strips + normal taper

Date	Hour 0			Hour 1			Hour 2			Hour 3			Hour 4			Hour 21			Hour 22			Hour 23		
	F	E	LM	F	E	LM	F	E	LM	F	E	LM	F	E	LM	F	E	LM	F	E	LM	F	E	LM
5/8/23	–	–	–	–	–	–	–	–	–	–	–	–	–	–	–	–	–	–	297	45	1	852	98	6
5/9/23	366	39	2	311	25	5	275	16	1	499	41	2	231	19	0	2209	253	19	1422	165	8	948	86	9
5/10/23	403	22	2	334	17	8	309	20	1	–	–	–	–	–	–	–	–	–	–	–	–	–	–	–
5/21/23	–	–	–	–	–	–	–	–	–	–	–	–	–	–	–	1724	221	16	1692	184	17	1151	94	11
5/22/23	687	58	1	464	30	4	375	27	0	582	44	2	–	–	–	–	–	–	–	–	–	–	–	–

Table 8.5. Medford with no rumble strips + normal taper

Date	Hour 0			Hour 1			Hour 2			Hour 3			Hour 4			Hour 20			Hour 21			Hour 22			Hour 23		
	F	E	LM	F	E	LM	F	E	LM	F	E	LM	F	E	LM	F	E	LM	F	E	LM	F	E	LM	F	E	LM
5/14/23	–	–	–	–	–	–	–	–	–	–	–	–	–	–	–	–	–	–	–	–	–	755	84	4	949	88	8
5/15/23	564	34	3	368	30	2	337	20	2	390	32	1	–	–	–	1730	277	24	1981	224	20	1599	183	19	870	72	3
5/16/23	473	28	1	295	20	2	264	23	2	567	44	2	244	11	0	–	–	–	–	–	–	–	–	–	–	–	–
5/17/23	–	–	–	–	–	–	–	–	–	–	–	–	–	–	–	–	–	–	1101	149	9	1857	237	18	1051	117	8
5/18/23	532	56	3	295	38	1	310	27	1	412	53	0	–	–	–	–	–	–	–	–	–	–	–	–	–	–	–

Table 8.6. Medford with rumble strips + longer taper

Date	Hour 0			Hour 1			Hour 2			Hour 3			Hour 21			Hour 22			Hour 23		
	F	E	LM	F	E	LM	F	E	LM	F	E	LM	F	E	LM	F	E	LM	F	E	LM
5/22/23	–	–	–	–	–	–	–	–	–	–	–	–	1527	164	30	1580	168	12	892	87	11
5/23/23	464	33	4	329	22	5	310	24	3	401	27	2	–	–	–	–	–	–	176	21	1
5/24/23	472	46	1	287	34	3	300	35	1	209	34	0	–	–	–	321	43	0	978	113	4
5/25/23	570	51	2	382	41	1	350	41	1	388	41	1	–	–	–	–	–	–	–	–	–

Appendix F. Sample Detections of Vehicles Traveling Too Close to the Work Zone Lane Closure Taper

(a) Id: 743, 05/31/2023, 22:14.

(b) Id: 954, 05/31/2023, 22:48.

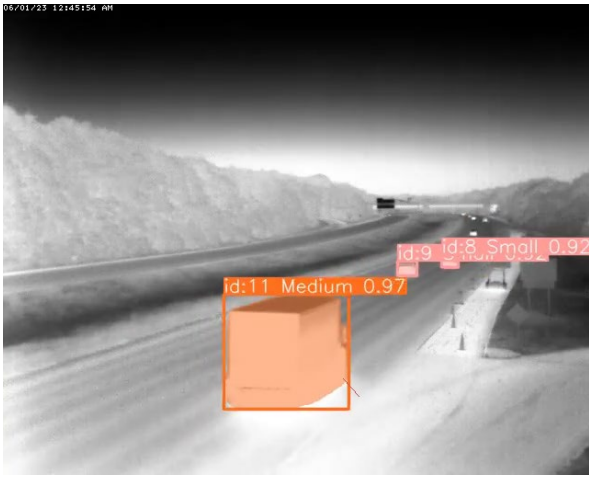

(c) Id: 11, 06/01/2023, 00:45.

(d) Id: 2300, 06/01/2023, 20:30.

Figure 8.44. Last-minute merges from the Danvers D2-downstream camera

(a) Id: 179, 06/01/2023, 02:10.

(b) Id: 11, 06/02/2023, 00:55.

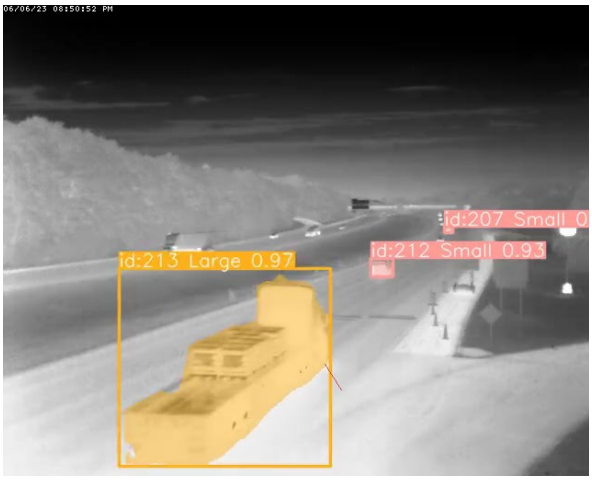

(c) Id: 11, 06/06/2023, 20:50.

(d) Id: 330, 06/07/2023, 00:21.

Figure 8.45. Additional last-minute merges from the Danvers D2-downstream camera

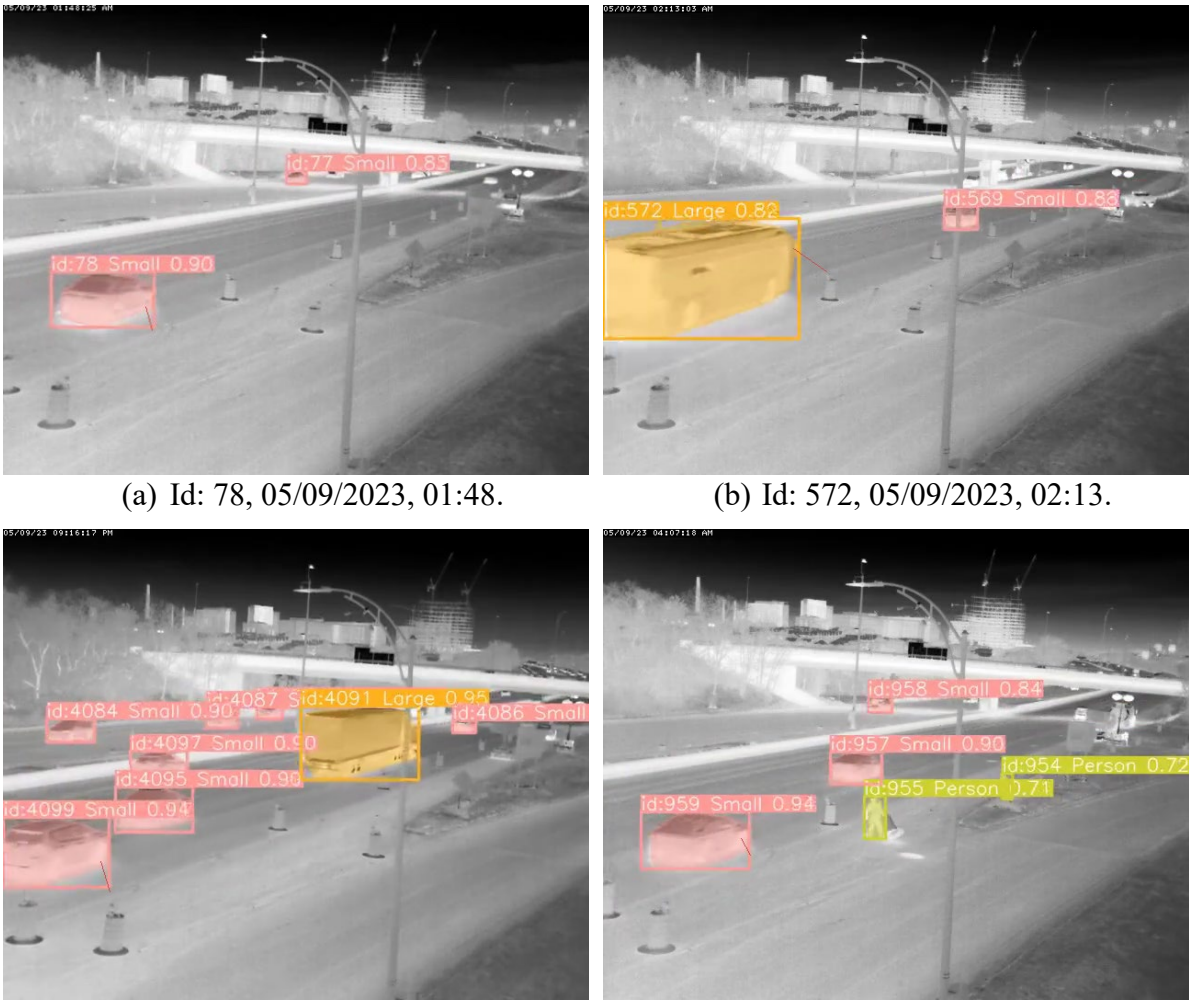

(a) Id: 78, 05/09/2023, 01:48.

(b) Id: 572, 05/09/2023, 02:13.

(c) Id: 4099, 05/09/2023, 21:16.

(d) Id: 959, 05/09/2023, 04:07.

Figure 8.46. Last-minute merges from the Medford M3-downstream camera

(a) Id: 66, 05/16/2023, 02:28.

(b) Id: 9053, 05/21/2023, 21:12.

(c) Id: 8935, 05/17/2023, 22:22.

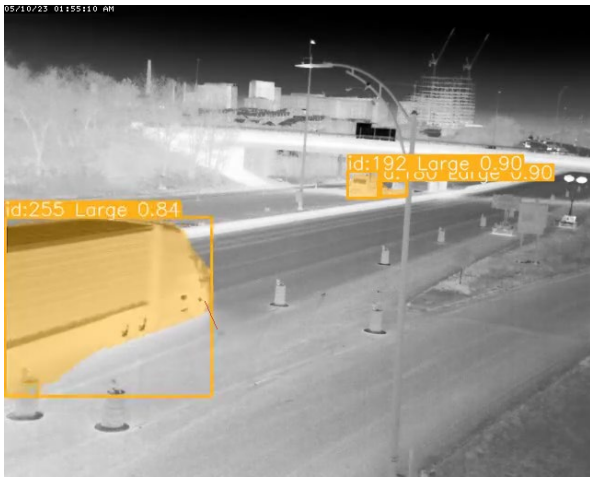

(d) Id: 255, 05/10/2023, 01:55.

Figure 8.47. Additional last-minute merges from the Medford M3-downstream camera